2009

Bottom boundary layer physics and sediment transport along a transgressive sand body, Ship Shoal, south-central Louisiana: implications for fluvial sediments and winter storms

Daijiro Kobashi
Louisiana State University and Agricultural and Mechanical College

BOTTOM BOUNDARY LAYER PHYSICS AND SEDIMENT TRANSPORT ALONG A TRANSGRESSIVE SAND BODY, SHIP SHOAL, SOUTH-CENTRAL LOUISIANA: IMPLICATIONS FOR FLUVIAL SEDIMENTS AND WINTER STORMS

A Dissertation

Submitted to the Graduate Faculty of the
Louisiana State University and
Agricultural and Mechanical College
in partial fulfillment of the
requirements for the degree of
Doctor of Philosophy

In

The Department of Oceanography and Coastal Sciences

By

Daijiro Kobashi
B.Sc. Tokai University, 1999
M.Sc. Tokai University, 2001

May, 2009

ACKNOWLEDGEMENTS

This dissertation would have been incomplete without dedicated help from numerous people as listed below.

First, I would like to express my sincere gratitude to my adviser, Dr. Gregory W. Stone, for his invaluable help that I needed to complete my doctoral degree. He has also given dedicated advice for my future career. I deeply appreciate his patience with my English. I thank my dissertation committee members, namely, Drs. S.A. Hsu, Masamichi Inoue, Felix Jose, Chunyan Li, Irving Mendelssohn, and Michael A. Dunn (Dean Representative) for dedicated commitments to my doctoral research. I acknowledge CSI field support group staff: Walker D. Winans, Steve Dartez, Ronald Stanford, Charlie Sibley, William J. Gibson, Rodney G. Fredericks, Floyd DeMers, Darren Depew, and Chris Cleaver for their assistance in the field deployments. In addition, oil and gas industries allowed us logistical supports. Valuable discussions were made with numerous researchers as well as with my committee members: Syed M. Khalil from Louisiana Department of Natural Resources, Barry Drucker, Geoffrey Wiekel, and Roger Amato from the U.S. Minerals Management Service, Department of the Interior, Dr. Richard Condrey, Dr. John Fleeger, Carey Gelpi, Mark Grippo, and Dr. Stan Dubois from LSU. The discussions significantly improved the quality of the dissertation. I appreciate discussions in the WAVCIS Laboratory and appreciate the help from the staff: Dr. Felix Jose, Dr. Baozhu Liu, Yixin Luo, Jian Li, Dana Watzke, Yuliang Chen, Seyed Mostafa StadatMousavi, Walter Guidroz, Julie D. Rosati, and Amy Spaziani. Finally, I would like to express my appreciation to my family and

my friends for the constant support during my overseas study in the US. Their assistance and more support significantly made my life much easier and more enjoyable.

This dissertation was completed under the financial supports from the U.S. Minerals Management Service, U.S. Department of the Interior (#1435-01-04-CA-35162) and Louisiana Department of Natural Resources (#2503-07-10). A part of my financial support was provided by the World Bank through the Joint Japan/World Bank Graduate Scholarship and also by the Theodore Ford Memorial Scholarship Award.

TABLE OF CONTENTS

ACKNOWLEDGEMENTS ii

LIST OF TABLES vi

LIST OF FIGURES vii

ABSTRACT xi

CHAPTER 1. GENERAL INTRODUCTION 1
1.1. Introduction 1
1.2. Conceptual Framework 2
1.3. References in Chapter 1 6

CHPATER 2. RESPONSE OF FLUVIAL FINE SEDIMENT DISPERSAL TO STORM WIND-CURRENT EFFECTS ON A HOLOCENE TRANSGRESSIVE SHOAL, ATCHAFALAYA SHELF, LOUISIANA, U.S.A: A NUMERICAL SIMULATION 9
2.1. Introduction 9
2.2. Experimental Setup 10
2.3. Results and Discussion 12
2.4. References in Chapter 2 19

CHAPTER 3. WIND-DRIVEN DISPERSAL OF FLUVIALLY-DERIVED FINE SEDIMENT FOR TWO CONTRASTING STORMS: EXTRA-TROPICAL AND TROPICAL STORMS, ATCHAFALAYA BAY/SHELF, SOUTH-CENTRAL LOUISIANA, U.S.A. 21
3.1. Introduction 21
3.2. Winter Storms and Tropical Storms in 2005 24
3.3. Louisiana Coastal Currents 26
3.4. Data Sources and Analytical Methods 28
3.5. Results and Discussion 32
3.6. References in Chapter 3 51

CHPATER 4. TWO CONTRASTING MORPHODYNAMICS OVER RECURRING SANDY AND MUDDY BOTTOMS OF A SHORE-PARALLEL HOLOCENE TRANSGRESSIVE SHOAL, SOUTH-CENTRAL LOUISIANA, USA 56
4.1. Introduction 56
4.2. Physical Setting 59
4.3. Data Acquisition 62
4.4. Data Analysis 65
4.5. Results 67
4.6. Discussion 83
4.7. References in Chapter 4 96

CHPATER 5. IMPACTS OF SAND REMOVAL FROM A SHORE-PARALLEL HOLOCENE TRANSGRESSIVE SHOAL ON HYDRODYNAMICS AND SEDIMENT TRANSPORT, SOUTH-CENTRAL LOUISIANA, U.S.A. 102
5.1. Introduction 102
5.2. Wave-Climate and Current Variability over the Inner Shelf 106
5.3. Model Experiment 107
5.4. Results and Discussion 117
5.5 References in Chapter 5 132

CHPATER 6. SYNTHESIS AND CONCLUSIONS 139
6.1. Fluvial Sediment Dispersal and Its Influence on Ship Shoal 139
6.2. Wave-Current-Bottom Sediment Interaction 140
6.3. Numerical Modeling 141

VITA 143

LIST OF TABLES

Table 2.1 Model cases....13

Table 2.2 Input parameters of river discharge, temperature, salinity and SSC 13

Table 3.1 Summary of 2005 hurricanes that made landfall along the northern Gulf of Mexico (Data source: Knabb (2005a; 2005b) 27

Table 4.1 Instrument configuration....64

Table 4.2 Number of winter storms for the 2006 and 2008 deployments. Type A is equivalent to AS storms and Type B is equivalent to MC storms by Pepper and Stone (2004)....72

Table 4.3 Mean (top) and Maximal (bottom) values of physical parameters (at the shoal crest) 75

Table 5.1 Louisiana barrier islands and restoration plans....105

Table 5.2 Ship Shoal Sand resources....105

Table 5.3 Case study A: Wind condition (Constant in domain)....114

Table 5.4 Case study A: Offshore wave boundary condition (South boundary)....114

Table 5.5 Ship Shoal sand mining scenarios 114

Table 5.6 Skill assessment of model results at CSI-15....118

Table 5.7 MIKE21 SW model result with shoal (left) and without shoal (right) 124

Table 5.8 M3 HD model result with shoal (left) and without shoal (right)....131

Table 5.9 Maximal difference in magnitude of hydrodynamic parameters between actual bathymetry and hypothetical bathymetry. Top low; Maximal difference in absolute magnitude of each parameter. Bottom low: Maximal values in magnitude of each parameter during model duration 134

LIST OF FIGURES

Figure 2.1 Map of study area and computational grids overlaid on the map. Ship Shoal and Tiger/Trinity shoals are shaded. 11

Figure 2.2 Distribution of sediment concentration: (a) Case 1 (No wind), (b) Case 2 (10 m s^{-1} SW wind), (c) Case 3 (10 m s^{-1} NW wind), and (d) Case 4 (No wind + 10 m s^{-1} NW wind) 14

Figure 2.3 MODIS satellite images and current profile of WAVCIS CSI-3 during a pre-frontal (upper) and a post-frontal (bottom) phase (Satellite images obtained from LSU Earth Scan Lab) 15

Figure 2.4 Time series of (a) wind stress (N m^{-2}) (u-component in solid line, v-component in red circles), (b) near surface currents (m s^{-1}) (u-component in solid line, v-component in red circles), (c) wave-induced shear stress (N m^{-2}), and (d) acoustic backscatter amplitude (decibel) during a winter storm. A triangle in (d) shows passage of a winter storm. The dashed line in (c) shows threshold for sediment suspension 18

Figure 3.1 Map of study area. Tracks of 2005 Hurricanes that made landfall on northern Gulf of Mexico are shown on bottom left. 23

Figure 3.2 MODIS satellite images and NOAA NARR wind field during (Hurricanes Katrina (left) and Rita (middle) and a cold front migrating from a polar region(right) (Images courtesy of MODIS Rapid Response Project at NASA/GSFC and Louisiana State University Earth Scan Lab) 25

Figure 3.3 Weekly-averaged (a) alongshore and (b) cross-shore wind stresses (N m^{-2}) and currents (m s^{-1}) of CSI-3 in 2005 29

Figure 3.4 (a) Atchafalaya River discharge at Simmesport, LA, between 1997 and 2006 and freshwater discharge, sediment load and SSC at (b) Morgan City, 2005, and (c) Wax Lake Outlet, 2005 34

Figure 3.5 MODIS Satellite images in (a) June 7, 2005, (b) April 2nd, 2005, (c) July, 6th, 2005, (d) March 28th, 2005 (e) September, 6th, 2005 (f) September 26th, 2005 36

Figure 3.6 Time series of (a) wind stress (N m^{-2}), (b) wave height (m) and water depth (m), (c) 24 hr moving-averaged current (m s^{-1}), (d) shear stress due to waves (N m^{-2}), and (e) SSC (kg m^{-3}) at WAVCIS CSI-14 between 2005/03/01-2005/09/30. Passage of winter storms and tropical cyclones are shown with shaded triangles in (e). 37

Figure 3.7 Time series of (a) wind stress (N m^{-2}), (b) significant wave height (m) and water depth (m), (c) 24 hr moving-averaged alongshore currents (m s^{-1}) (top3.75m, middle:2.03m, bottom:0.63m), (d) 24 hr moving-averaged cross-shore currents (m s^{-1}) (top:3.75m, middle:2.03m, bottom:0.63m), and (e) acoustic backscatter profile (decibel) at WAVCIS CSI-3 between 2005/03/01-2005/09/25. Passage of winter storms and tropical cyclones are shown with shaded triangles in (e). N.D. represents No Data. 37

Figure 3.8 Time series of (a) wind stress (N m^{-2}), (b) significant wave height (m) and water depth (m), (c) 24 hr moving-averaged alongshore currents (m s^{-1}) (top, middle:10.59m, bottom:1.49m), (d) 24 hr moving-averaged cross-shore currents (m s^{-1}) (top, middle:10.59m, bottom:1.49m), and (e) acoustic backscatter profile (decibel) at WAVCIS CSI-6 between 2005/03/01-2005/08/25. Passage of winter storms and tropical cyclones are shown with shaded triangles in (e). 38

Figure 3.9 Time series of (a) wind speed (m s^{-1}) and directions (degree), (b) wind stress (N m^{-2}) (alongshore/cross-shore), (c) 24 hr moving-averaged near surface currents (m s^{-1}) (alongshore/cross-shore), (d) significant wave height (m), and (e) SSC (kg m^{-3}) (left) and shear stress (N m^{-2}) (right) at WAVCIS CSI-14 between 2005/03/25 and 2005/04/08. 41

Figure 3.10 Time series of (a) wind speed (m s^{-1}) and directions (degree), (b) wind stress (N m^{-2}) (alongshore/cross-shore), (c) 24 hr moving-averaged near surface currents (m s^{-1}) (alongshore/cross-shore), (d) significant wave height (m), and (e) SSC (kg m^{-3}) (left) and shear stress (N m^{-2}) (right) at WAVCIS CSI-14 between 2005/08/25 and 2005/09/05. 42

Figure 3.11 Time series of (a) wind speed (m s^{-1}) (right) and direction (degrees) (left), (b) wind stress (N m^{-2}) (alongshore/cross-shore), (c) 24 hr moving-averaged near surface currents (m s^{-1}) (alongshore/cross-shore), (d) significant wave height (m), (e) SSC (kg m^{-3}) (left) and shear stress (N m^{-2}) (right) at WAVCIS CSI-14 between 2005/09/17 and 2005/09/29. 44

Figure 3.12 General sediment transport patterns for (a&b) winter storms, (c&d) hurricanes made landfall east of the study area, (e&f) hurricanes made landfall west of the study area 46

Figure 3.13 Frequencies of dispersal shift and the shifts that reached Ship Shoal between October, 2004 and May, 2005. 49

Figure 4.1 Map of study area 58

Figure 4.2 Variation of meteorological parameters during a winter storm 61

Figure 4.3 Schematic illustration of the PCADP system for 2008 deployment. Sensor heights of all instruments are listed in Table 4.1. 63

Figure 4.4 River discharge at Simmesport, Louisiana between 1997 and 2008 (Source: the U.S. Army Corps of Engineers, New Orleans District) 69

Figure 4.5 Grain size distribution for the 2006 (top) and 2008 deployments (bottom).....70

Figure 4.6 Sampled sediments: (upper) sand and (lower) fluid mud.....74

Figure 4.7 Time series of (a) wind stress, (b) wave height and peak period, (c) wave variance (high frequency (f>0.2 Hz) and low frequency (f<0.2Hz)), and (d) wave direction during the 2006 deployment.....76

Figure 4.8 Time series of (a) wind stress, (b) wave height and peak period, (c) wave variance (high frequency (f>0.2 Hz) and low frequency (f<0.2Hz)), and (d) wave direction for the 2008 deployment 77

Figure 4.9 Time series of (a) adjusted water level and cross-shore sea surface slope, (b) alongshore current, (c) cross-shore current, (d) OBS (0.3 m and 0.61 m above the bottom) and (e) SSC profile (2006 deployment).....79

Figure 4.10 Time series of (a) adjusted water level and cross-shore sea surface slope, (b) alongshore current, (c) cross-shore current, (d) OBS (0.35 m and 0.74 m above the bottom) and (e) turbidity profile (2008 deployment) 80

Figure 4.11 Time series of (a) wave orbital velocity and current speed (1m), (b) shear velocity, and (c) shear stress. The dashed line on the bottom figure shows the threshold for sediment suspension. Passage of winter storms is shown as shaded triangle on the bottom figure (2006 deployment).....81

Figure 4.12 Time series of (a) wave orbital velocity and current speed (1m), (b) shear velocity, and (c) shear stress. The dashed line on the bottom figure shows the threshold for sediment suspension. Passage of winter storms is shown as shaded triangle on the bottom figure (2008 deployment).....82

Figure 4.13 Satellite images during a pre-frontal phase (a) and a post-frontal phase (b) along with river discharge (c), bottom elevation at the SS06_2 (d), and SSC (f). Red line in (c) shows the border between high and low discharge suggested by Walker and Hammack (2000). The numbers, (1) and (3) represent passages of winter storms that accompany sediment supply from the Atchafalaya River. The number, (2) represent a passage of winter storms that does not accompany sediment supply from the river. 84

Figure 4.14 Time series of (a) wind speed and direction, (b) wave height, (c) horizontal current profile (d) vertical current profile (e) shear stress, (f) upper and lower SSC (g) sediment transport rates, (h) SSC profile (log scale), and (i)-(k) SSC profiles 88

Figure 4.15 Time series of (a) wind speed and direction, (b) wave height, (c) horizontal current profile (d) vertical current profile (e) shear stress, (f) upper and lower SSC (g) sediment transport rates, and (h) SSC profile (log scale) 91

Figure 4.16 Schematic illustration of sediment exchange on Ship Shoal during fluid mud regime.....94

Figure 4.17 Schematic illustration of sediment exchange on Ship Shoal during sand regime.....95

Figure 5.1 Proposed sand mining area: (A) South Pelto 13, (B) Ship Shoal Blocks 88/89, (C) Ship Shoal Blocks 84/85/98/99. Source: Khalil et al (2007).....105

Figure 5.2 Histogram of wave-climate parameters: (a) Wind speed, (b) Wind direction, (c) Wave height, and (d) Wave directions between 2007/01/01 and 2008/10/01, 639 days. The numbers in the figure show percentages. 108

Figure 5.3 Polar plots pertaining to (a) winds at Grand Isle, (b) waves at CSI-6, (c) surface currents at CSI-6, (d) near bottom currents at CSI-6, (e) near bottom currents at SS98_2, (f) near bottom currents at SS06_2, (g) near bottom currents at SS08_2 109

Figure 5.4 Map and computational grids 112

Figure 5.5 Bathymetry of model domain: with shoal (upper) and without shoal (lower).....112

Figure 5.6a Model validation of (a) wind speed, (b) wind direction, (c) wave height, (d) peak wave period, and (e) wave direction (MIKE 21 SW). 120

Figure 5.6b Model validation of (a) water level, (b) alongshore surface slope, (c) cross-shore surface slope, (d) alongshore current (surface), (e) cross-shore current (surface), (f)alongshore current (bottom), (g) cross-shore current (bottom), (h) water level during hurricane Lili (MIKE21/3 HD).....121

Figure 5.7 Wave height and vector distributions for case A study: (a, b) H_S=6m, T_P=11 s, Wave direction=135 (degree). (c, d) H_S=3 m, T_P=7s, Wave direction=135 (degree), (e, f) H_S=1m, T_P=5 s, Wave direction=135 (degree). Top figures represent the result with shoal and bottom figures the result without shoal.....123

Figure 5.8a Surface currents with shoal for various wind speeds and directions.....127

Figure 5.8b Bottom currents with shoal for various wind speeds and directions.....128

Figure 5.8c Surface currents without shoal for various wind speeds and directions....129

Figure 5.8d Bottom currents without shoal for various wind speeds and directions....130

Figure 5.9 Wave re-suspension Intensity (RI) for various cases. (a) Case A1, (b) Case A2, (c) Case A3, (d) Case A4, (e) Case A5 133

ABSTRACT

Ship Shoal, a shore-parallel sand body, was recently recognized as having a unique physical and biological environment and also as a potential sand resource for coastal restoration in coastal Louisiana. Little is known regarding such dynamics, in concert with fluvial sediments and winter storms, influenced in unique ecosystems, and likely in future potential sand mining. This dissertation addresses such the morphodynamics and sedimentary processes and their implications for the mining from the shoal using field measurements and numerical modeling studies.

During the winter-spring season, fluvial sediment plumes shifted from the prevailing west to southeast during the post-frontal phases, resulted in accumulation of fluid mud on the eastern flank of the shoal and consequent shoal sediment heterogeneity during the spring of 2006; this fluid mud layer strongly interacted with storm waves and currents through the processes of sediment re-suspension, vertical mixing, and hindered settling and redistribution. Studies during winter 2008 represented dynamics dominated by non-cohesive bottom material and hence followed the conventional approaches.

State-of-the-art numerical models for waves, currents and transport provided reasonably well estimation for the study area and showed changes in wave transformation, current variability, and sediment transport for various hypothetical post-dredging scenarios. Sediment re-suspension intensity showed spatial differences along the shoal: high on the western flank of the shoal and a decrease toward the eastern shoal due to the change in shoal bathymetry. The results indicated a favor for the fluid mud accumulation on the eastern flank of the shoal, corroborated by *in-situ* measurements.

Data suggest that Ship Shoal appears to have recurring sandy and muddy bottoms depending on the amount of storm-induced sediment reworking and fluvially-derived

sediments. The fluid mud on the shoal seems to be patchy and does not remain in place as permanently consolidated mud, given the frequency of winter storms and the dispersal shifts. Numerical simulations suggest that targeted small-scale mining would not significantly alter the hydrodynamics and sediment transport over the shoal. Dredging from the eastern flank of the shoal may give rise to lesser impacts than that from the middle and western flank of the shoal. This suggestion is consistent with that from our collaborative biological study.

CHAPTER 1

GENERAL INTRODUCTION

1.1. Introduction

In Louisiana, large portions of the coastal land have been facing severe land loss, particularly the retreat of Louisiana shorelines over the long-term rates of 6.1 m yr^{-1} and over short-term rates of 9.4 m yr^{-1} (NRC, 2006; Penland et al., 2005). The loss results from a mixture of natural processes including land subsidence and Mississippi River deltaic processes and anthropogenic activities including control of sediment discharge by engineered structures (cf. NRC, 2006). However, while there were little to no anthropogenic intervention, sediment supply from the Mississippi River through natural levees and regular flooding balanced high land subsidence, one of the highest rates in the U.S. (NRC, 2006); however, artificial levees and dams prevent natural sediment supply from the river. This, in turn, causes disequilibrium of the sediment budget, and further accelerates land loss (NRC, 2006). In addition, the northern Gulf coast is hurricane-prone and tropical storms and hurricanes strike the Louisiana coast approximately once every 3.0 year (Keim et al., 2007). The tropical cyclones contribute to and exacerbate land loss at alarming rates.

The Louisiana coast is characterized by the following; (1) shallow and broad shelf, (2) predominantly muddy seabed along with transgressive sand bodies and various reefs (Penland et al., 1988; Roberts, 1997; Kjerfve et al, 2003), (3) located along the mouth of Mississippi River basin, the largest drainage basin in the entire North America (Mossa, 1996), (4) high discharge of freshwater and sediments from the Mississippi River (Roberts, 1997), (5) the largest wetlands in contiguous 48 states, (6) wide varieties of wildlife habitats (Coast2050, 1998; LDWF, 2005), (7) important commercial fishery production (crabs,

shrimp, fish) (O'Connel et al., 2005), (8) low-energy environment, and (9) frequent passage of winter storms (i.e. extra-tropical storms which accompany cold fronts) and occasional hurricane landfalls or approaches (Hsu, 1988; Stone et al., 2004a).

1.2. Conceptual Framework

Recently, in response to rapid deterioration of the Louisiana barrier islands and beaches, and the demand to protect barrier islands and associated habitats in the Louisiana coastal zone, the U.S. Minerals Management Service (MMS), which administers mineral leases within U.S. Federal waters and conducts environmental studies under the National Environmental Policy Act, are seeking potential sand resources to aid in restoring the Louisiana coastal zone (Drucker et al., 2004).

In spite of limited sand resources in the immediate area landward of the coastal zone, there remain several sand resources along the coast of Louisiana: River channel, surrounding beaches, and offshore transgressive sand bodies (Kulp et al. 2005). The former two sources are not suitable for large-scale barrier island restoration because of insufficient sand volume. Thus, the sand resources from the outer continental shelf (OCS) have been considered as one of the plausible sand resources for re-nourishment of the barrier islands and beaches due to the available sand volume, proximity to target restoration areas and sand quality (Drucker et al. 2004; Khalil et al., 2007). Ship Shoal located approximately 20 km offshore of Isles Dernieres, has been a high priority target sand resource to restore the Isles Dernieres barrier chain, Caminada-Moreau headland and Timbalier Islands system, both of which are among the highest land loss regions in Louisiana (Williams et al., 1992; Drucker et al., 2004; Penland et al., 2005; Khalil et al., 2007). However, there are growing concerns with sand mining from the offshore sand bodies, particularly in terms of environmental impacts including hydrodynamic and sediment transport (Michel et al, 2001; Nairn et al., 2004; Palmer et al., 2008).

A significant number of studies have been undertaken to evaluate available sand volume and its sand quality in Ship Shoal (Penland et al., 1986; Kulp et al., 2001; Khalil et al., 2007), in addition to potential impacts of sand dredging on wave transformation and sediment transport (Stone and Xu, 1996; Pepper, 2000; Stone, 2000; Pepper and Stone, 2004; Stone et al., 2004b). In terms of the physical studies initiated first in 1994, perceived impacts were twofold: (1) modification in wave transformation and subsequent shoreface erosion of barrier islands, and (2) changes in circulation and sediment flux, and associated morphological changes due to sand dredging (Nairn et al., 2004). For (1), Stone and Xu (1996) and Stone et al. (2004b) implemented a spectral wave model to examine impacts of complete sand removal from the shoal on shoal wave transformation and consequent impacts on barrier islands based on a hypothetical bathymetric condition. For (2), Pepper (2000), and Pepper and Stone (2002; 2004) examined wave, current, bottom boundary layer (BBL), and sediment transport dynamics associated with winter storms on the western flank of Ship Shoal by deploying various arrays of the bottom boundary layer instruments in 1998 and 2000; some of the important results obtained from these studies are as follows.

(1) Hydrodynamics, bottom boundary layer and sedimentary processes on the Louisiana inner shelf during winter-spring seasons were characterized by quasi-periodic cycles of recurring passages of winter storms.

(2) Sediments were transported landward at the north edge of the shoal and seaward at the south edge of the shoal, suggesting the importance of the shoal regarding current modification

(3) Their analysis based on non-cohesive sediments concluded that sediment transport rates were significant mostly during winter storms, but high sediment transport also occasionally occurred during fair weather. This finding indicates the importance of winter storms on shoal BBL dynamics and morphological changes.

(4) The wave records showed that waves that propagated over the shoal were attenuated as much as 36 percent possibly as a result of frictional energy dissipation, suggesting that the shoal mitigates a significant amount of wave energy.

(5) Wave transformation significantly varied on comparing the model of a pre-sand mining configuration to that of a post-mining configuration. However, the effects of the wave transformation due to shoal removal along the barrier islands were negligible.

The above results produced the important cornerstone for studies of wave transformation and bottom boundary layer dynamics and sediment transport over the shoal as well as the low-energy Louisiana shelf; the studies also identified unique hydrodynamics over the shoal, both of which had been poorly understood (Pepper, 2000). However, some of the above results are still qualitative and preliminary studies suggest that the shoal physical environment is likely more complicated than previously recognized particularly regarding the following issues.

(1) Divers have often taken mud samples from Ship Shoal during deployments and satellite images also supported fluvial fine sediment transport to Ship Shoal during spring (Walker and Hammack, 2000); however, defining mechanisms remain unknown and all of the previous studies are limited to the dynamics pertinent to non-cohesive sediment (i.e. sand).

(2) Inner shelf shoals seem to have unique hydrodynamics and wave characteristics. These valuable functions were qualitatively addressed by Pepper (2000), but remain poorly understood, particularly wave dissipation effects and the response of wind to inner shelf currents and bathymetric modification.

(3) Potential impacts of sand dredging on physical process to date are limited to spectral wave model implementations (e.g., Stone et al., 2004b). Short-term impacts of sand dredging on waves, currents and sediment transport using pre- and hypothetical post-sand mining scenarios are very important for decision-making of potential sand dredging and implication for interplay between physical and biological processes.

Arrays of bottom boundary layer instruments, *in-situ* observing network, and state-of-the-art numerical modeling used in this study made it possible to examine the issues. This

dissertation was made through research efforts to a collaborative project jointly funded by the U.S. Minerals Management Service and Louisiana Department of Natural Resources as part of a large-scale coastal restoration project entitled "Long-Term Use of Ship Shoal Sand Resources for Restoration of Louisiana Barrier Islands and Beaches", which play a vital role to protect highly valuable habitats on the Louisiana coastal zone. Through the project, comprising of physical and benthic biological studies, unique, but complex physical processes and their interactions with benthic habitats have been revealed and potential impacts of sand mining on physical environments have been quantified. The focuses of the dissertation were given to demonstrate bottom boundary layer physics and sediment transport which may affect future potential sand mining, particularly the following issues: (1) impacts of fluvial sediments on the shoal physical environment, (2) wave-current-bottom sediment interactions, (3) coastal hydrodynamics associated with various storm winds, and (4) changes in hydrodynamic and sediment transport for various future sand mining scenarios.

This dissertation provides valuable information regarding physical processes over heterogeneous bottoms, which has little been reported in scientific literature. It also provides important implication for the interplay between physical processes and benthic biological habitat over the shoal, which is a primary concern of MMS for future potential sand mining and this collaborative study has enabled us to addresses the issue firsthand. Such comprehensive studies have little been reported in the scientific literature to date. Furthermore, most of the information obtained through this study can be transferrable to similar geological and physical settings worldwide and provides valuable case studies.

This dissertation consists of a series of manuscripts cohesively linked; Chapter 2 discusses fluvial sediment dispersal through numerical model implementations; chapter 3 discusses dispersal shifts of fluvial sediments and their influence on Ship Shoal bottom

sediments based on prolonged in-situ observational data and a series of satellite images. Chapter 4 discusses how those fluvial sediments influence shoal bottom boundary layer dynamics and sediment transport using in-situ data obtained from field deployments. Chapter 5 examines spatially-varying physical processes over the shoal and discusses potential impacts of sand mining on shoal physical environments by means of a-state-of-the-art numerical modeling. Finally the dissertation is closed by synthesis and conclusions in Chapter 6.

1.3. References in Chapter 1

Coast 2050 - Louisiana Coastal Wetlands Conservation and Restoration Task Force and the Wetlands and Conservation Authority. 1998. Coast 2050: Toward a Sustainable Coastal Louisiana. Louisiana Department of Natural Resources. Baton Rouge, LA.

Drucker, B. S., Waskes, W. and Byrnes, M.R., 2004. The U.S. Minerals Management Service Outer Continental Shelf Sand and Gravel Program: Environmental studies to assess the potential effects of offshore dredging operations in federal waters: *Journal of Coastal Research*, v. 20, no. 1, p. 1-5.

Hsu, S.A., 1988. Coastal Meteorology, Academic Press, 260pp.

Keim, BD, Muller, RA,, and Stone GW. 2007. Spatiotemporal Patterns and Return Periods of Tropical Storm and Hurricane Strikes from Texas to Maine. Journal of Climate 20(14): 3498.

Khalil, S.M., Finkl, C., Andrew, J.,Knotts, C.P., 2007. Restoration-quality sand from Ship Shoal, Louisiana: Geotechnical investigation for sand on a drowned barrier island. Proceedings of *Coastal Sediments '07*. New Orleans, Louisiana, 685-698.

Kjerfve. B., Perillo, G.M.E., Gardner, L.R., Rine, J.M., Dias, G.T.M. and Mochel, F.R., 2002. Morphodynamics of muddy environments along the Atlantic coasts of North and South America. In: T.R. Healy, Y. Wang and J.-A. Healy, Editors, *Muddy Coasts of the World: Processes, Deposits and Functions*, Elsevier, Amsterdam, 219–239.

Kulp, M., Penland, S., and Ramsey K., 2001, Ship Shoal: Sand Resource Synthesis Report, Coastal Research Laboratory, Dept. of Geology and Geophysics, Univ. of New Orleans, 70 p.

Kulp, M., Penland, S., Williams, S. J., Jenkins, C., Flocks, J., and Kindinger, J., 2005, Geological framework, evolution, and sediment resources for restoration of the Louisiana coastal zone: Journal Coastal Research, Special Issue No. 44, p. 56-71.

Louisiana Department of Wildlife and Fisheries (LDWF), 2005. Louisiana comprehensive wildlife conservation strategy, 455p.

Michel, J., Nairn, R., Johnson, J.A., and Hardin, D., 2001. Development and design of biological and physical monitoring protocols to evaluate the long-term impacts of offshore dredging operations on the marine environment: U.S. Department of Interior, Minerals Management Service, OCS Report MMS 2001-089, 116p.

Mossa, J., 1996. Sediment dynamics in the lowermost Mississippi River, Engineering Geology, 45, 457-479.

Nairn, R., Johnson, J.A., Hardine, D. and Michel, J., 2004. A biological and physical monitoring program to evaluate long term impacts from sand dredging operations in the United States outer continental shelf. *J. Coastal Res.*, 20, 126-137.

National Research Council (NRC), 2006. Drawing Louisiana's New Map, Addressing Land Loss in Coastal Louisiana, National Academies Press, Washington, DC, pp. 190.

O'Connel, M.T., Franze, C.D., Spalding, E.A., and Poirrier, M.A., 2005. Biological resources of the Louisiana coast: Part 2. Coastal animals and habitat associations. *Journal of Coastal Research*, SI 44, 146-161.

Palmer, T.A., Montagna, P.A., and Nairn, R.B. 2008. The effects of a dredged excavation pit on benthic macrofauna in offshore Louisiana. Environ. Manage., 41: 573-583.

Penland, S., Suter, J.R., and Moslow, T. F., 1986. Inner-shelf shoal sedimentary facies and sequences: Ship Shoal, Northern Gulf of Mexico, SEPM Core Workshop No.9, Modern and Ancient Shelf Clastics, 73-123.

Penland, S., Boyd, R., and Suter, J.R., 1988. Transgressive depositional systems of the Mississippi delta plain: A model for barrier shoreline and shelf sand development: *Journal of Sedimentary Petrology*, v. 58, no. 6, p. 932-949.

Penland, S., Connor, P.F., Beall, A., Fearnley, S., and Williams, S.J., 2005. Changes in Louisiana's shoreline, 1855-2002: Journal of Coastal Research, Special Issue no. 44, p. 7-39.

Pepper, D.A., 2000. Hydrodynamics, Bottom boundary layer processes, and sediment transport on the south-central Louisiana shelf: The influence of extra tropical storms and bathymetric modification. Unpublished *dissertation*, Louisiana State University, Baton Rouge, 159p.

Pepper, D.A. and Stone, G.W., 2002. Atmospheric forcing of fine sand transport on a low energy inner shelf: south-central Louisiana, USA. *Geo-Marine Letters*: 33-41

Pepper, D.A. and Stone, G.W., 2004. Hydrodynamics and sedimentary responses to two contracting winter storms on the inner shelf of the northern Gulf of Mexico, *Marine Geology*, 210, 43-62.

Roberts, H. H., 1997. Dynamic changes of the Holocene Mississippi River delta plain: The delta cycle: Journal of Coastal Research, v. 13, no. 3, p. 605-627.

Stone, G. W., 2000. Wave climate and bottom boundary layer dynamics with implications for

offshore sand mining and barrier island replenishment in south-central Louisiana. *OCS Study MMS 2000-53*. U.S. Dept. of the Interior, Minerals Mgmt. Service, Gulf of Mexico OCS region, New Orleans, LA, 90pp.

Stone, G.W. and Xu, J.P., 1996. Wave climate modeling and evaluation relative to sand mining on Ship Shoal, offshore Louisiana, for coastal and barrier island restoration, MMS OCS Study MMS96-0059. 170p.

Stone, G. W., Grymes, J.M., Dingler, J. R., Pepper, D. A., 1997. Overview and significance of hurricanes on the Louisiana coast, U.S.A., Journal of Coastal Research, 13 (3), 591-710

Stone, G.W., Liu, B., Pepper, D. A., and Wang, P., 2004a. The importance of extra-tropical and tropical cyclones on the short-term evolution of barrier islands along the northern Gulf of Mexico, *Marine Geology*, 210, 64-78.

Stone, G.W., Pepper, D.A., Xu, J. and Zhang, X., 2004b. Ship Shoal as a Prospective Borrow site for barrier island restoration, Coastal south-central Louisiana, USA: Numerical wave modeling and field measurements of hydrodynamics and sediment transport. *Journal of Coastal Research*, 20(1), 70-89.

Walker, N.D. and Hammack, A. B., 2000. Impacts of Winter Storms on Circulation and Sediment Transport: Atchafalaya-Vermilion Bay Region, Louisiana, U.S.A., *Journal of Coastal Research*, 16(4), 996-1010. West Palm Beach (Florida), ISSN 0749-0208.

Williams, S. J., Penland, S. and Sallenger, A.H., 1992. Louisiana Barrier Island Erosion Study, Atlas of Shoreline Changes in Louisiana from 1853 to 1989, 1-2150-A., U.S. Department of Interior and US Geological Survey, 103p.

CHPATER 2

RESPONSE OF FLUVIAL FINE SEDIMENT DISPERSAL TO STORM WIND-CURRENT EFFECTS ON A HOLOCENE TRANSGRESSIVE SHOAL, ATCHAFALAYA SHELF, LOUISIANA, U.S.A: A NUMERICAL SIMULATION

2.1. Introduction

River plumes (both positive and negative buoyancy currents) are important forcing for local hydrodynamics and consequent linking to coastal ecosystem (e.g., Chao, 1987; Wright and Nittrouer, 1995; Murray, 1997). It has long been known that Atchafalaya River sediments are transported westward during most of the year (cf. Wells and Kemp, 1981), following the prevailing wind and consequent coastal circulation pattern. However, recent studies show that during high river discharges, sediment dispersal often shifts in direction from westward to southeastward (cf. Walker and Hammack, 2000; Kobashi et al., 2007a). Although not all the storms contribute to it, this shift likely accompanies the cold front-induced extra-tropical storms, which frequent the Louisiana coast every 3 to 10 days between October and May (DiMego et al., 1976; Hsu, 1988). A Holocene transgressive shoal, Ship Shoal, which is on the pathway of the shifted dispersal and is predominantly characterized as having a sandy bottom, could be covered with fluid mud and dramatically alter its bottom sediment characteristics from sand to heterogeneous bottom sediments, which in turn alter its diverse benthic habitat and local sediment dynamics (Stone et al., 2006; Kobashi et al., 2007a; 2007b). However, not all post-frontal winds trigger the dispersal shift and the impacts on the shoal have not been understood (Kobashi et al., in review, 2008).

The purpose of this paper is preliminarily to show the response of the fluvial fine sediment dispersal to extra-tropical storms by implementing a three dimensional numerical model with varying wind fields. Such an effort has not been undertaken to date in this environment and has an important implication for the shoal ecosystem and hydrodynamics

including potential wave-current attenuation over cohesive sediment on the shoal and inner shelf.

2.2. Experimental Setup

A coupled three dimensional hydrodynamic and advection-dispersion model, MIKE 3 HD/TR was implemented for the study. The HD/TR model solves incompressible Reynolds-averaged Navier-Stokes equation and advection-dispersion equation, respectively (DHI, 2005). The model uses the unstructured triangular mesh grid and finite volume method; vertical discretization was equidistant and the number of the vertical layers was selected as 10. Detailed model description is elaborated on in DHI (2005). The model domain covered the Atchafalaya Bay and Shelf and three transgressive shoals, Ship Shoal and Tiger/Trinity shoals (Figure 2.1). The computational grid consisted of fine-resolution meshes near the Atchafalaya River mouth (maximal grid area as 6.1 x 10^5 m^2) and coarser-resolution meshes for the rest of the domain (maximal grid area as 4.9 x 10^6 m^2) (Figure 2.1).

Four model cases were selected, representing the wind pattern associated with fair weather and extra-tropical storms: (1) no wind, (2) 10 m s^{-1} constant wind from the southeast (135 degrees), (3) 10 m s^{-1} constant wind from the northwest (315 degrees), and (4) 10 days with no wind followed by 3 days of 10 m s^{-1} northwest wind (see Table 2.1). The model duration is 20 days for all cases except case 4, which is 13 days. River discharges at the mouths of the Lower Atchafalaya River and Wax Lake Outlet (Figure 2.1) were selected as constant 3,000 m^3 s^{-1} and 1,500 m^3 s^{-1}, respectively. Suspended sediment concentration (SSC) was selected as constant 140 mg l^{-1} and 45 mg l^{-1} at the mouths of the Lower Atchafalaya River and Wax Lake Outlet, respectively (Figure 2.1). Sediments debouched from both rivers comprise primarily of fine-grained silt and clay; according to Wells and Kemp (1981), the fluvial sediment composition is comprised of montmorillonite, illite and kaolinite.

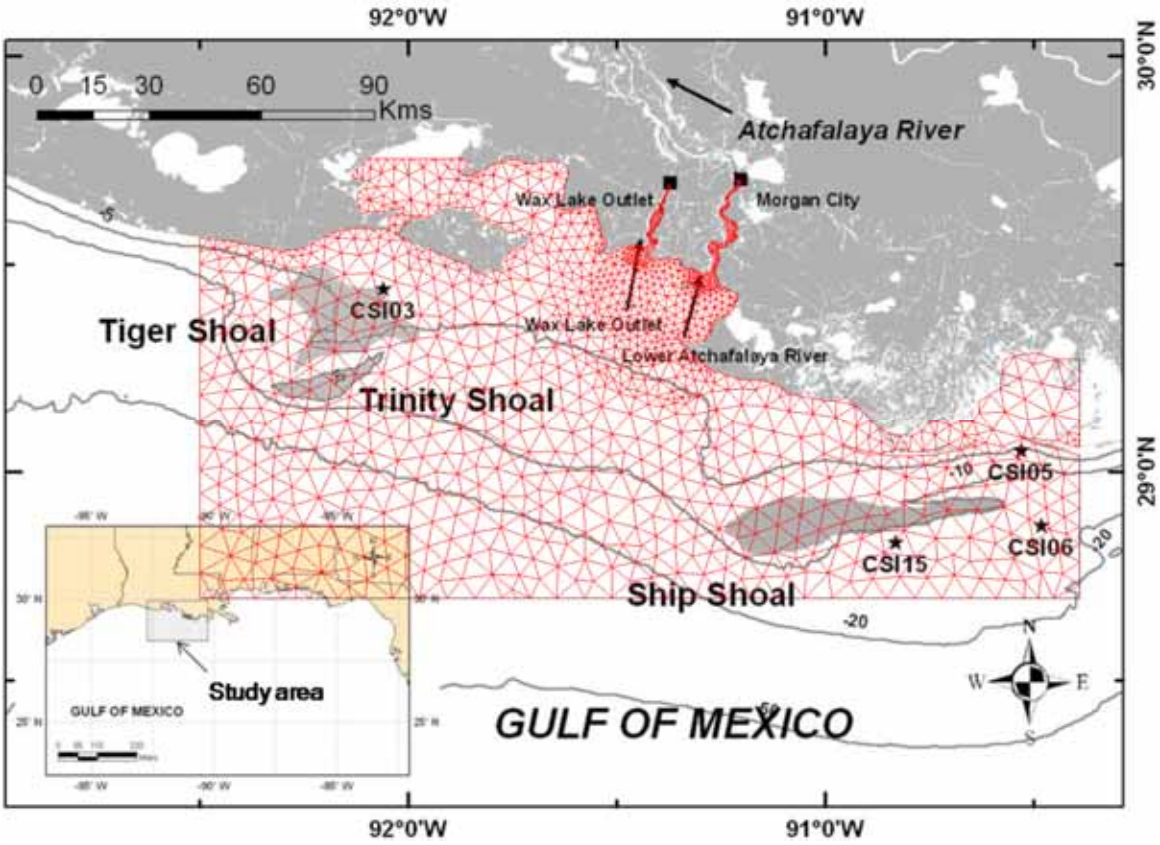

Figure 2.1 Map of study area and computational grids overlaid on the map. Ship Shoal and Tiger/Trinity shoals are shaded.

Those input parameters were determined with reference to *in-situ* data from the U.S. Geological Survey national water data reports at Morgan City and Wax Lake Outlet (e.g. Baumann et al., 2006) and considered as moderately high discharge of the lower Atchafalaya River mouths during spring. Initial temperature, salinity, and the SSC were set up as 25^{o} C, 35 PSU, and 0 mg l^{-1}, respectively. Input parameters including river point sources are summarized in Tables 2.1 and 2.2. The purpose of this preliminary study is to examine the response of fluvial sediment dispersal to varying storm winds. Therefore, waves, water level fluctuations, and the Coriolis force were not included in the modeling. The concepts presented here will be tested using comprehensive numerically-derived and *in situ* data.

2.3. Results and Discussion

In Figure 2.2, model results pertaining to the SSC distribution for each scenario after 20 days (13 days for case 4) of simulations are shown. All of the figures clearly showed the effects of wind on fluvial sediment dispersal.

For case 1, which was run with no wind input, the plume abruptly lost its momentum once discharged into the Atchafalaya bay/nearshore and was dispersed over approximately the 5 m isobath and was laterally distributed (Figure 2.2a).

For case 2, with the uniform southeast wind of 10 m s^{-1}, the sediment plume was dispersed toward the west, in consistent with satellite imagery presented for general dispersal patterns (Figures 2.2b, and 2.3 (top left)) as well as results of previous studies (e.g., Wells and Kamp, 1981; Walker and Hammack, 2000).

For case 3 with the uniform northwest wind of 10 m s^{-1}, the fluvial sediment path was shifted from the west and dispersed toward the southeast along the coast and offshore to Ship Shoal, located approximately 50 km southeast of the river mouth (Figures 2.1 and 2.2c). Though the prevailing wind is southeasterly during most of the year along the Louisiana coast (Murray, 1997), this shift in direction of the plume dispersion often occurs during post-frontal

Table 2.1 Model cases

Cases	Wind Speed	Wind Direction	Duration
Case 1	NA	NA	20 days
Case 2	10 m s^{-1}	135 degrees	20 days
Case 3	10 m s^{-1}	315 degrees	20 days
Case 4	NA	NA	10 days
	10 m s^{-1}	315 degrees	3 days

Table 2.2 Input parameters of river discharge, temperature, salinity and SSC

Parameters	LAR*[1]	WLO*[2]	Domain
River discharge	3000 m^3 s^{-1}	1500 m^3 s^{-1}	NA[*3]
Temperature	20 °C	20 °C	25 °C
Salinity	0 PSU	0 PSU	35 PSU
SSC	145 mg l^{-1}	45 mg l^{-1}	0 mg l^{-1}

[*1]LAR: Lower Atchafalaya River mouth
[*2]WLO: Wax Lake Outlet mouth
[*3]NA: Not applicable

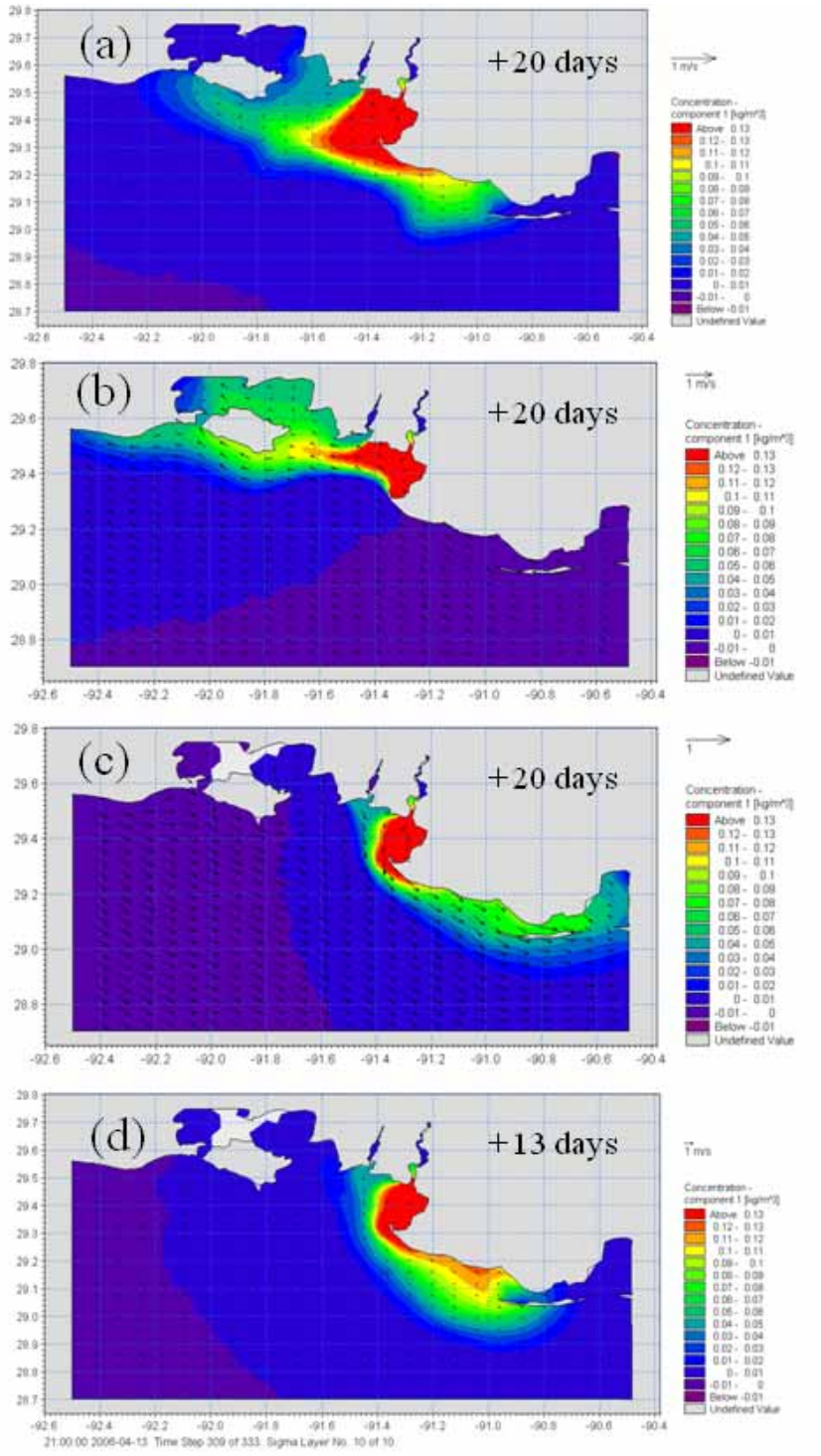

Figure 2.2 Distribution of sediment concentration: (a) Case 1 (No wind), (b) Case 2 (10 m s^{-1} SW wind), (c) Case 3 (10 m s^{-1} NW wind), and (d) Case 4 (No wind + 10 m s^{-1} NW wind)

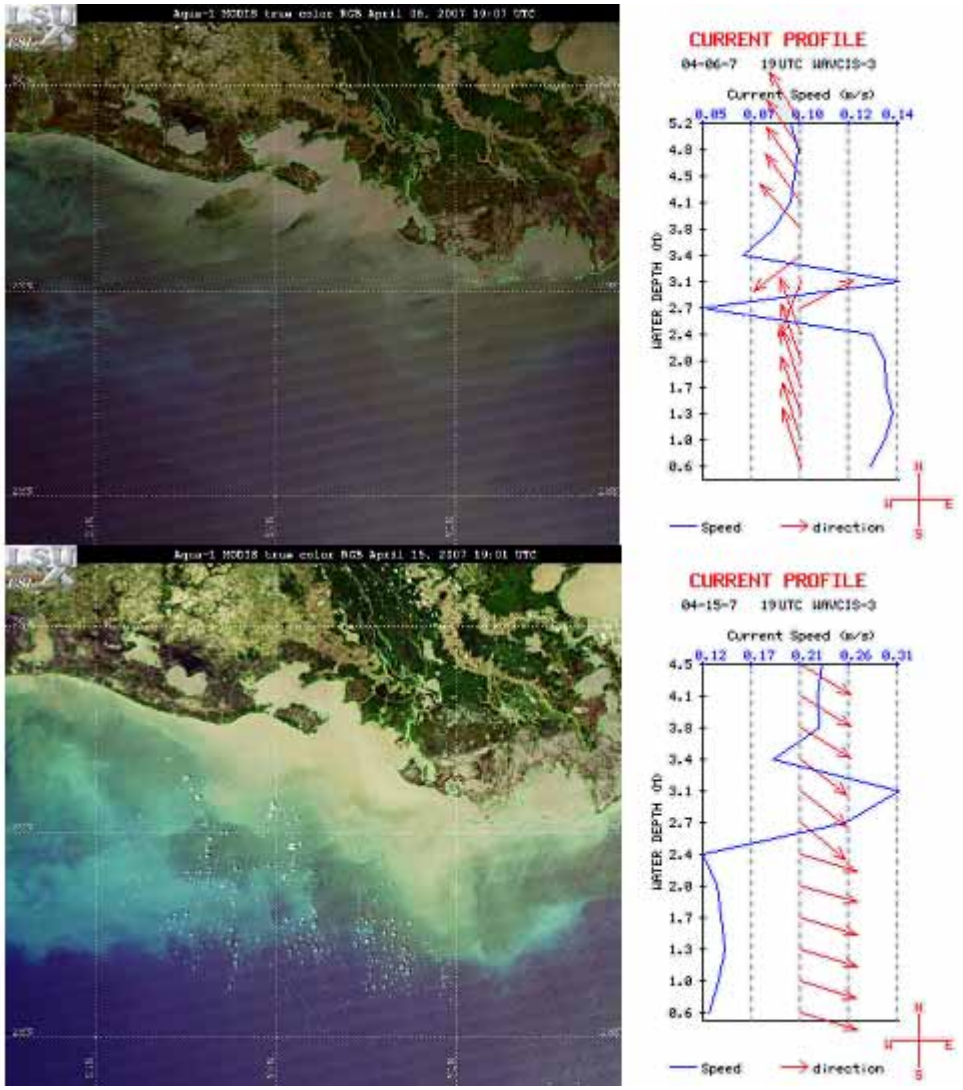

Figure 2.3 MODIS satellite images and current profile of WAVCIS CSI-3 during a pre-frontal (upper) and a post-frontal (bottom) phase (Satellite images obtained from LSU Earth Scan Lab)

phase of winter storms, during which wind direction is predominantly from the northern quadrant (Walker and Hammack, 2000; Kobashi et al., 2007a).

The post-frontal regime lasts for 1 to 3 days depending on the nature and intensity of the storm (Pepper and Stone, 2004). The current velocity over the Atchafalaya Bay for all model cases ranged from 0.15 to 0.25 m s^{-1}, which was in general agreement with the current velocity observed at CSI-14 (West Cote Blanche Bay, 91º 33.41' W, 29º 30.96' N) located west of the bay, during winter weather. Since the post-frontal northerly wind lasts for roughly up to 3 days, the sediment plume freshly debouched from the river mouths was not able to reach the shoal during the post-frontal phase (~ 3 days window), as shown in Figure 2.2c, and hence not in conformity with data obtained from satellite imagery (Kobashi et al., 2007a). A possible reason is that the source of the fine sediments dispersed southeastward may not be directly dispersed from the river mouths, rather advected and dispersed from the sediments already transported over the Atchafalaya bay/nearshore as illustrated in Figure 2.3 (top left). In order to prove this hypothesis, the case 4 was implemented.

Case 4 was divided into two wind regimes during the 13 day model duration; for the first 10 days the model was run with no wind to determine the initial SSC distribution and was followed by the 3 day simulation with the northwesterly wind (i.e. a total of 13 day model duration) (Table 2.1). The model result showed that the sediments that were already debouched from the river and transported over the bay/nearshore reached the shoal after three days of persistent northwesterly wind (Figure 2.2d). Similar results were obtained from the model results for different wind speeds (20 m s^{-1}, 15 m s^{-1}, and 12 m s^{-1}) though different were the periods which took for the fluvial sediments to reach the shoal. Additionally, the model result generally agreed with the satellite imagery of a typical dispersal pattern during post-frontal phases, obtained from Louisiana State University, Earth Scan Laboratory, as shown in Figure 2.3 (bottom left). *In-situ* observational data from WAVCIS CSI-3 (Stone et

al., 2001; http://www.wavcis.lsu.edu) during a pre-frontal (Figure 2.3 top right) and post-frontal phase (Figure 2.3, bottom right) showed a complete shift of current profile from northwestward to southeastward throughout the entire water column during the period.

Time series of met-ocean data from CSI-3, during the period under study clearly indicated strong storm-wind stress (Figure 2.4a) and associated current shifts (Figure 2.4b) from the northwest to southeast during a storm, supporting our model outputs. In addition, this dispersal shift illustrated in Figure 2.3 likely accompanied wave-induced sediment re-suspension. Wave-induced shear stress above the threshold for sediment suspension (Figure 2.4c, dash line) and the acoustic backscatter signal amplitude (Figure 2.4d), which is a proxy for sediment concentration, clearly illustrated significant re-suspension during the storm, suggesting the importance of sediment suspension and associated dispersal due to storm waves and currents. A similar result was obtained from CSI-14 data during winter storms in 2005 (Kobashi et al., in review, 2008) It should be noticed that this model study did not include bottom sediment re-suspension and deposition; therefore, these effects, which are also important as shown in Figure 2.4 and are clearly captured by the satellite image over Tiger and Trinity shoals in Figure 2.3 (bottom left) (see location in Figure 2.1), have to be considered for future model implementation, particularly during severe weather such as extra-tropical and tropical storms, the two primary weather events capable of causing bottom sediment re-suspension over the low-energy Louisiana coast (Kobashi et al. in review, 2008).

Overall, the model results illustrated strong response of fluvial fine sediment dispersal to wind-driven currents associated with the extra-tropical storms and the model simulated plume shifts, as supported by *in-situ* observing data and satellite images. This simplified model implementation is preliminary; however, the MIKE3 HD/TR model has the ability to simulate Atchafalaya River sediment dispersal reasonably well if accurate input parameters of wind, sediment sources, and hydrodynamic parameters are included, except for the small

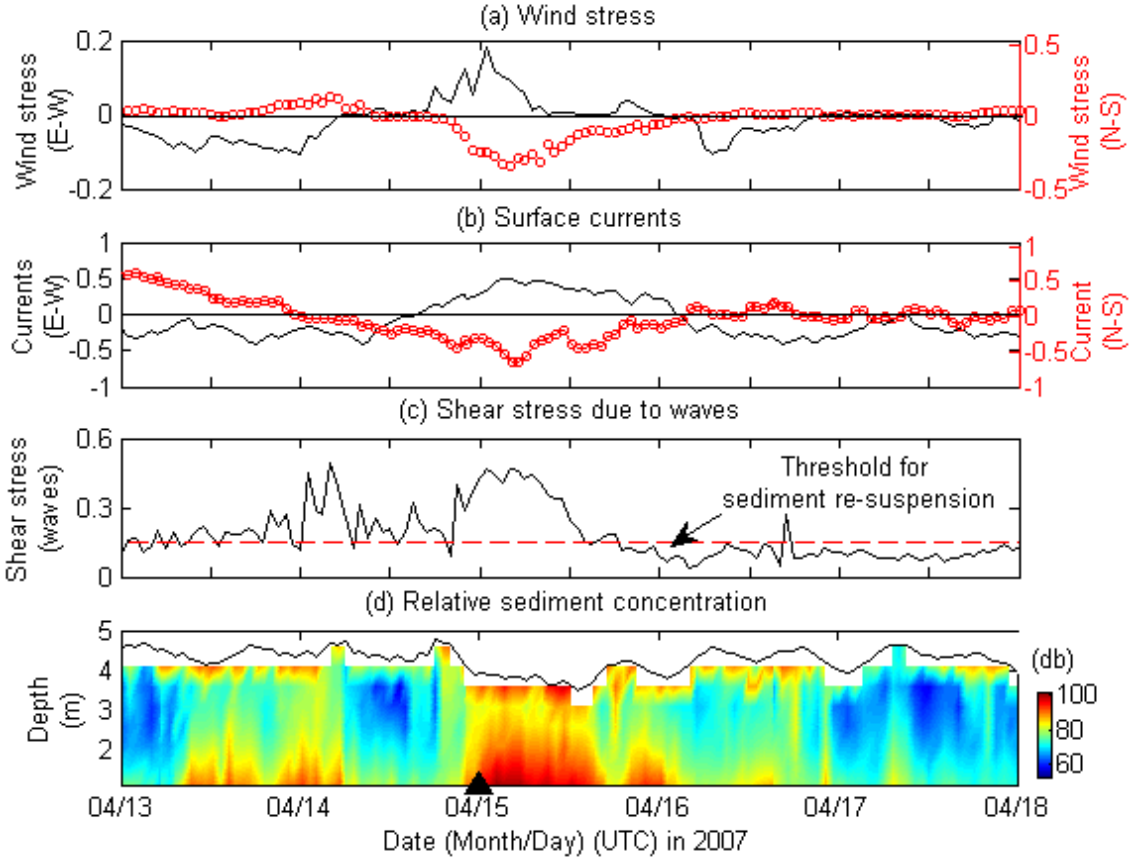

Figure 2.4 Time series of (a) wind stress (N m^{-2}) (u-component in solid line, v-component in red circles), (b) near surface currents (m s^{-1}) (u-component in solid line, v-component in red circles), (c) wave-induced shear stress (N m^{-2}), and (d) acoustic backscatter amplitude (decibel) during a winter storm. A triangle in (d) shows passage of a winter storm. The dashed line in (c) shows threshold for sediment suspension.

scale eddies as seen in the satellite images (Figure 2.3), a consequence of the selected computational grid size. Modeling hydrodynamics and sediment transport, including sediment re-suspension and depositional effects, is currently being pursued.

2.4. References in Chapter 2

Baumann, T., Goree, B.B., Lovelace, W.M., Montgomery, P.A., Ross, G.B., Walter, D.J., Ward, A.N., 2006. Water Resource Data Louisiana Water Year 2005, Water Data Report USGS-WDR-LA-05-1, 913pp.

Chao, S-Y., 1987. River-forced estuarine plumes. *J. of Phys. Oceanogr.* 18. 72-88.
DHI, 2005. MIKE21&3 Flow Model FM. Hydrodynamics and Transport Module Scientific Documentation, 42p.

DiMego, G.J., Bosart, L.F., and Endersen, G.W., 1976. An examination of the frequency and mean conditions surrounding frontal incursions into the Gulf of Mexico and Caribbean Sea. *Monthly Weather Review*, 104,709-718.

Hsu, S.A., 1988. Coastal Meteorology, Academic Press, 260pp, New York.

Kobashi, D., Jose, F. and Stone, G.W., 2007a. Impacts of fluvial fine sediments and winter storms on a transgressive shoal, off south-central Louisiana, U.S.A., *Journal of Coastal Research*, SI 50, 858-862.

Kobashi, D., Jose, F. and Stone, G.W., 2007b. Heterogeneity and dynamics of sediments on a shoal during spring-winter storm season, south-central Louisiana, USA.. Proceedings of *Coastal Sediments* '07, New Orleans, Louisiana, 921-934.

Kobashi, D., Jose, F., Luo, Y., and G.W. Stone, 2008. Wind-driven Dispersal of Fluvially-derived Fine Sediment for Two Contrasting Storms: Extra-tropical and Tropical Storms, Atchafalaya Bay/Shelf, south-central Louisiana, U.S.A. Submitted.

Murray, S., 1997. An observational study of the Mississippi-Atchafalaya coastal plume: Final report. OCS Study MMS 98-0040 U.S. Dept. of the Interior, Minerals Mtmt. Service, Gulf of Mexico OCS Region, New Orleans, LA. 513pp.

Pepper, D.A. and Stone, G.W., 2004. Hydrodynamics and sedimentary responses to two contracting winter storms on the inner shelf of the northern Gulf of Mexico, *Marine Geology*, 210, 43-62.

Stone, G.W., Zhang, X.P., Gibson, W., and Fredericks, R., 2001. A new Wave-Current online information system for oil spill contingency planning (WAVCIS), Proceedings of 24th Arctic and Marine Oil spill Program Technical Seminar 2001, Edmonton, Alberta, Canada, 401-425.

Stone, G.W., Liu, B., Pepper, D. A., and Wang, P., 2004. The importance of extra-tropical and tropical cyclones on the short-term evolution of barrier islands along the northern Gulf of Mexico, *Marine Geology*, 210, 64-78.

Stone, G.W., Condrey, R., Fleeger, J., 2006. Environmental investigation of long-term use of Ship Shoal sand resources. Year 2 annual report, MMS/LDNR, 62pp.

Walker, N.D. and Hammack, A.B., 2000. Impacts of Winter Storms on Circulation and Sediment Transport: Atchafalaya-Vermilion Bay Region, Louisiana, U.S.A., *Journal of Coastal Research*, 16(4), 996-1010. West Palm Beach (Florida), ISSN 0749-0208.

Wells, J.T., and Kemp, P., 1981. Atchafalaya mud stream and recent mudflat progradation: Louisiana chenier plain. *Transaction*, Gulf Coast Association of Geological Society, v.31, 409-416.

Wright, L.D. and Nittrouer, C.A., 1995. Dispersal of river sediments in coastal seas: Six contrasting cases. *Estuaries*, Vol. 18, No. 3, 494-508.

CHAPTER 3

WIND-DRIVEN DISPERSAL OF FLUVIALLY-DERIVED FINE SEDIMENT FOR TWO CONTRASTING STORMS: EXTRA-TROPICAL AND TROPICAL STORMS, ATCHAFALAYA BAY/SHELF, SOUTH-CENTRAL LOUISIANA, U.S.A.

3.1. Introduction

It has long been known that Atchafalaya River fine sediments have been transported westward during most of the year, following Louisiana coastal currents (Wells and Kemp, 1981; Cochrane and Kelly, 1986; Murray, 1997). Dispersal of the fine sediments from the Atchafalaya River, whose sediment load is estimated as approximately 80 million tons yr^{-1} (Milliman and Meade, 1983), has contributed to the seaward progradation of the Chenier plain at the rate of 5 to 10 m yr^{-1} (Wells and Kemp, 1981; Kemp, 1986; McBride et al., 2007). Moreover, the westward mud transport and deposition cause unique hydrodynamic behavior including strong wave dissipation over the muddy bottom along the western Louisiana shelf (cf. Kemp, 1986; Sheremet and Stone, 2003). However, recent studies have shown that during winter-spring season sediment dispersal often shifts the direction from westward to south/southeastward, especially during the spring flood regime (Walker and Hammack, 2000; Kobashi et al., 2007a). This conspicuous shift in the fine sediment dispersal pattern during spring accompanies winter storms driven by cold front passages across the coast. In addition, tropical cyclones also help to re-distribute inner-shelf sediments further onshore and offshore, even to the continental shelf boundary, as seen from satellite imagery.

River plumes from both the Mississippi River and its main distributary, the Atchafalaya River, have been examined by numerous studies because of their importance on the coastal ecosystem (e.g. water quality, nutrient load, contaminant transport) and also sediment management for restoration (cf., Walker and Rouse, 1993; Murray, 1997; Walker and Hammack, 2000). Walker (2001) and Walker and Hammack (2000) examined the

responses of the sediment plume from the Atchafalaya River during storms, based on satellite images and *in-situ* data, for different winter storm and tropical storm events. Their study showed the response of river-borne sediments to varying storm winds. However, the analysis was solely based on satellite imagery interpretation and limited to short-term *in-situ* observations of water level, currents and sediment concentration. As a result, the dispersal and transport mechanisms of the fine sediments that originated from the Atchafalaya River and associated coastal hydrodynamics and bottom boundary layer characteristics, are not yet fully understood. Kobashi and Stone (in review, 2008) suggested, based on their numerical model study, that wind-induced south-easterly currents during post-frontal phases are a dominant factor for south/southeastward sediment dispersal during winter storms; however, they also suggested that local sediment re-suspension needs to be considered.

A major motivation for this study has come from the fact that the intermittent sediment dispersal shifts to a south/southeasterly direction strongly alter bottom sediment characteristics of a Holocene transgressive shoal, Ship Shoal, located approximately 50 km southeast of the Atchafalaya River mouth. This shoal was previously considered as having a sandy bottom year-round, and is in fact intermittently heterogeneous bottoms (i.e. mixture of sand and fluid mud), which in turn likely alters local sediment dynamics and its benthic biological environment (Stone et al., 2006; Kobashi et al., 2007a; 2007b) (Figure 3.1). In addition, during tropical cyclones, substantial sediment re-distribution can be expected, given the shallow bathymetry of the shoal.

This paper addresses this unique wind-driven dispersal and transport mechanisms of the fluvial sediments associated with hydrodynamics and bottom boundary layer characteristics during two contrasting storms, tropical and extra-tropical storms. The paper also addresses the impact of fine sediment depositions on the shoal, based on extended *in-situ* observations and analysis of satellite imagery for the period between October 2004 and

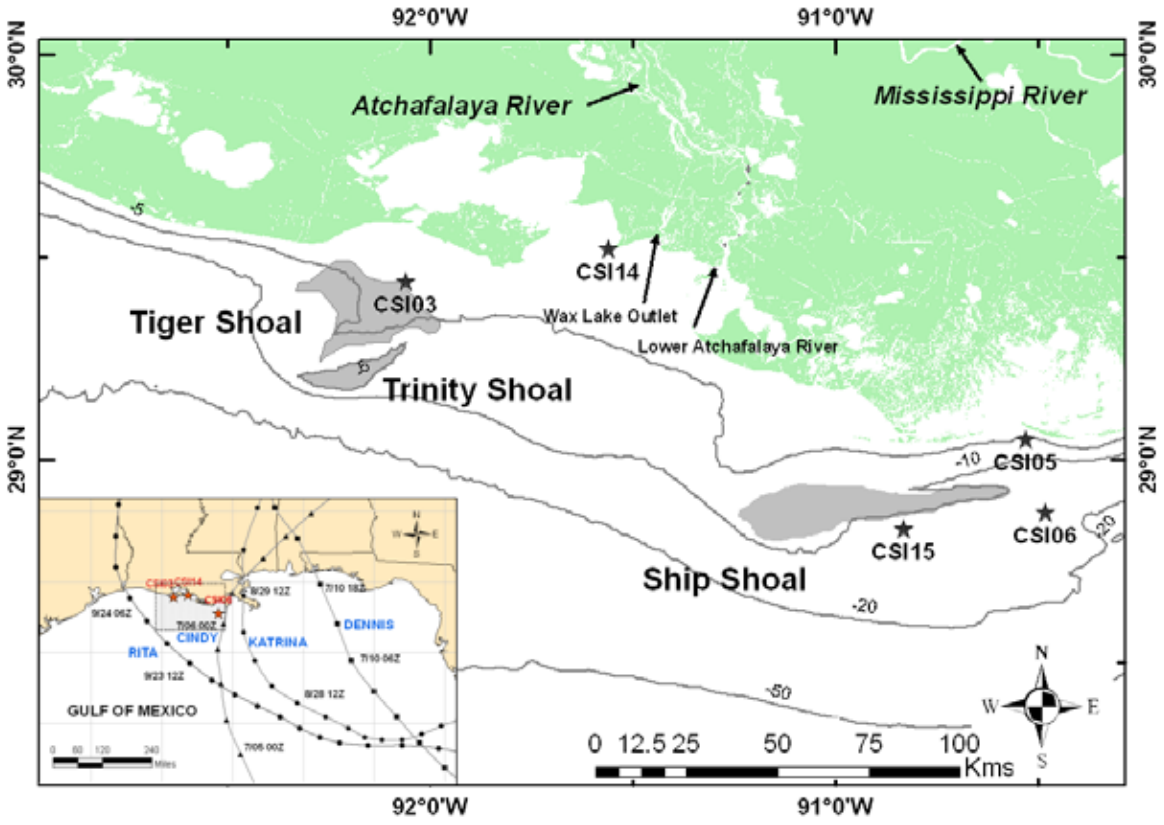

Figure 3.1 Map of study area. Tracks of 2005 Hurricanes that made landfall on northern Gulf of Mexico are shown on bottom left.

September, 2005.

3.2. Winter Storms and Tropical Storms in 2005

3.2.1. Winter Storms

Winter storms are low pressure systems which originate in the arctic polar region (polar frontal zone). The low pressure accompanies atmospheric fronts (i.e. cold fronts and warm fronts), moving from west to east following westerly; the fronts eventually pass the northern Gulf coast every 3 to 10 days between October and May (DeMego et al., 1976; Hsu, 1988). Before the cold fronts pass the Gulf, relatively strong winds blow from the southeast; during post-frontal events, wind direction strongly shifts from the southern quadrant to the northern quadrant and air temperature and barometric pressure abruptly decrease (Figure 3.2, bottom right) (cf. Hsu, 1988).

These strong wind fields and the rapidly fluctuating wind directionality cause a unique hydrodynamic behavior off the Louisiana shelf. Cold fronts are one of two major driving forces along with tropical cyclones, and significantly affect wave-climate, hydrodynamics and sediment transport along this low-energy shelf (e.g., Stone, 2000; Kobashi et al., 2005; Keim et al., 2007). In 2005, approximately 40 cold fronts passed the Louisiana coast. In addition, the year 2005 was the transition period of El Nino to neutral and La Nina. During the El Nino, jet streams shift further to the south and more winter storm activities are expected; while, during La Nina, winter storm activities are expected to be less frequent. On the other hand, tropical cyclones are known to be intensified during neutral or La Nina period (Manty, 1993). When Hurricanes Katrina and Rita made landfall, the climatological condition was the neutral to weak La Nina. Discussing the influence of El Nino/La Nina on storm activities is beyond the scope of this paper. More detailed information regarding impacts of El Nino on storm activities is elaborated on in Manty (1993).

3.2.2. Tropical Cyclones

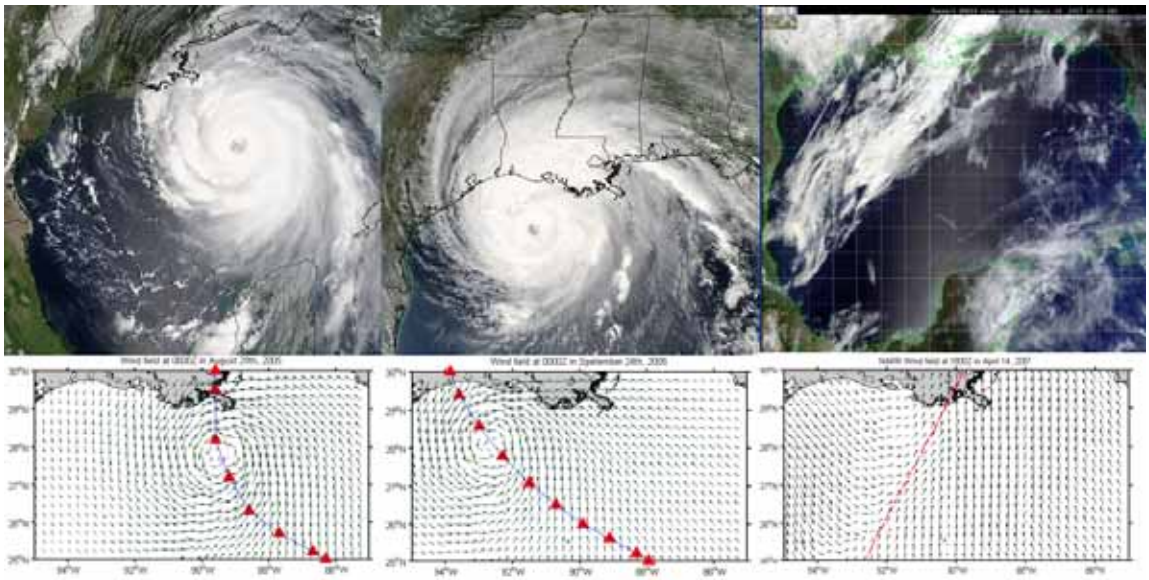

Figure 3.2 MODIS satellite images and NOAA NARR wind field during (Hurricanes Katrina (left) and Rita (middle) and a cold front migrating from a polar region(right) (Images courtesy of MODIS Rapid Response Project at NASA/GSFC and Louisiana State University Earth Scan Lab)

During the 2005 hurricane season, 27 named tropical storms were generated in the Atlantic Basin and out of which 15 developed into hurricanes. The season was the most active in recorded history (NCDC, 2006). Three of the season's seven major hurricanes – Dennis, Katrina and Rita- along with Hurricane Cindy caused considerable damage along the coastal Louisiana. Three of them, namely, Katrina, Rita and Cindy, made landfall along the Louisiana coast causing wide spread destruction due to hurricane-forced winds, waves and significant storm surges (Figures 3.1 and 3.2; Table 3.1). The barrier island chains along the coast were either totally eroded due to hurricane waves and storm surges or sustained multiple breaches and overwash (Stone et al., 2004). Freshwater marshes also sustained heavy damage due to the intrusion of salt water, which was accentuated by the presence of dredged channels all along the coastal marshes (Stone et al., 2004). Even though Hurricane Dennis made landfall along Santa Rosa Island in Florida, hurricane-induced winds and waves caused conspicuous damage to the barrier islands along the eastern Louisiana. Table 3.1 shows a brief summary of the hurricanes which made landfall over the northern Gulf of Mexico. More detailed information regarding each hurricane is provided by Knabb et al., (2005a; 2005b).

3.3. Louisiana Coastal Currents

Along the Louisiana/Texas (LA-TX) shelf, the dominant force to drive coastal currents is the prevailing wind, particularly during storms, given the fact that waves and tidal currents are generally low (i.e. low-energy micro-tidal environment) (Cochrane and Kelly, 1986; Murray, 1997). During most of the year, the wind blows from the southeast and hence, the coastal current direction is mostly westward. Cochrane and Kelly (1986) first showed the strong response of coastal currents to seasonal wind patterns over the LA-TX shelf. Their study revealed that current direction over the LA-TX inner shelf is westward during most of the year; while, the current over the LA-TX shelf in summer reverses from westward to

Table 3.1 Summary of 2005 hurricanes that made landfall along the northern Gulf of Mexico (Data source: Knabb (2005a; 2005b)

Name	Max wind speed	Max storm surge	Min pressure	Time of landfall	Landfall location
Cindy	34 m/s	6 ft (1.8 m)	956 mb	0300UTC, July 6th	Grand Isles, LA
Dennis	64 m/s	7 ft (2.2 m)	946 mb	1930 UTC, July 10th	Santa Rosa Islands, FL
Katrina	73 m/s	28 ft (8.5 m)	902 mb	1110 UTC, August 29th	Buras, LA
Rita	78 m/s	15 ft (4.6 m)	897 mb	0740 UTC, September 24th	Johnson's Bayou, LA

eastward, following a wind reversal from the southeast to west in summer. This seasonal current pattern along the LA-TX shelf was also reported by the Louisiana-Texas Shelf Circulation and Transport Processes Study (LATEX), based on the deployment of numerous meteorological sensors and acoustic Doppler current profilers over the LA-TX shelf (cf. Murray, 1997; Nowlin et al., 1998). The weekly-averaged wind stress and current velocities (top, middle, and bottom layers) at the WAVCIS CSI-3 station in a depth of approximately 5 m (Figure 3.1) in 2005 have similar results, showing a strong correlation between the wind and current fields (Figure 3.3). The current velocities at top, middle and bottom layers show the same trend and are mostly westward except during April, June, July and August (Figure 3.3). A detailed discussion of current variation is included in a later section of this paper.

3.4. Data Sources and Analytical Methods

Data sources used for analysis include data from *in-situ* observing stations, WAVCIS (Wave-Current-Surge Information System) CSI's-3, 6, and 14 (see locations in Figure 3.1) and satellite images from the Louisiana State University Earth Scan Laboratory (hereafter referred to as ESL), and hydrological data from the U.S. Geological Survey National Water Information System (Walker and Rouse, 1993; Stone et al., 2001; Baumann et al., 2006). WAVCIS CSI-14 provided hourly directional wave parameters, single-point current, water quality (temperature, salinity and turbidity) all at 1.6 m above the bottom as well as meteorological data. CSI-3 and 6 provided hourly wave parameters, water level, and current profile; water quality data (temperature, salinity, and turbidity) over 1, 2, and 3 m above the bottom were also provided. Detailed information regarding WAVCIS is provided by Stone et al. (2001) and Zhang (2003). Satellite imagery of MODIS (Moderate Resolution Image Spectrometer) true color was obtained from the ESL (Walker and Rouse, 1993).

Data analysis is mainly based on time series analysis of the *in-situ* data. Directional wave parameters for CSI-14 and CSIs 3 and 6 were computed using the PUV method

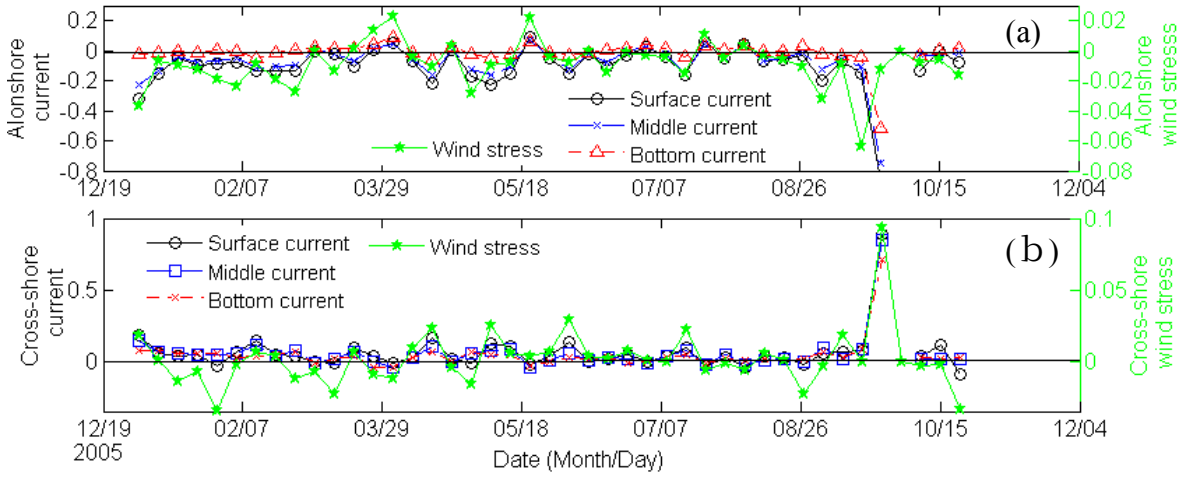

Figure 3.3 Weekly-averaged (a) alongshore and (b) cross-shore wind stresses (N m^{-2}) and currents (m s^{-1}) of CSI-3 in 2005.

(Gordon and Lohmann, 2001) and the standard spectral method developed by the U.S. Army Corps of Engineers Field Wave Gauging Program with the orbital velocity spectrum algorithm developed by RD Instruments Inc (Earle, et al., 1995; RD Instruments Inc., 2004), respectively. From the meteorological data, wind stress (τ) was calculated from the following balk equation.

$$\tau = \rho_a C_f U_{10}^2 \quad \text{..... (3-1)}$$

where ρ_a is air density (1.3 kg m^{-3}), C_f is surface drag coefficient, and U_{10} is wind speed at 10 m above the surface. The drag coefficient (C_f) was computed based on Wu (1982), Holthuijsen (2007), and Hsu (2003; 2006).

$$C_f = \begin{cases} 1.2875\times10^{-3} & U_{10} < 7.5(ms^{-1}) \\ (0.8+0.065\times U_{10})\times10^{-3} & 7.5\,(\mathrm{m\,s^{-1}}) \le U_{10} < 20.0(ms^{-1}) \\ 2.5\times10^{-3} & U_{10} \ge 20.0(ms^{-1}) \end{cases} \quad \text{..... (3-2)}$$

Suspended sediment concentration (SSC) at CSI-14 (located at West Cote Blanche Bay, see Figure 3.1) was estimated based upon the calibration of the turbidity sensor (optical backscatter sensor, OBS) with sediments and water sampled from the site. A detailed calibration procedure is given in Sheremet et al. (2005). The resultant conversion from the OBS to the SSC was obtained as follow (r^2=0.998) (Liu, B. Personal communication, 2007).

$$SSC = 0.001\times OBS - 0.0114 \quad \text{..... (3-3)}$$

For CSI's-3 and 6, acoustic backscatter signal amplitude (ABS) from ADCP (Acoustic Doppler Current Profiler) was given as a proxy for the SSC profile (cf. SonTek, 1997).

Except for a few isolated sand bodies, bottom sediments of our study area are mainly silt and clay, due to the influx of fine-grained sediments primarily from the Atchafalaya River. Routines for computing the bottom boundary layer parameters (hereafter referred to as BBLP) for many previous studies are applicable for clear water and sandy bottom (cf.,

Nielsen, 1992). For a cohesive bed, which is applicable for our study area, it is known that the algorithms to compute the BBLP for cohesive sediments rely on empirical formulae, which are largely site-specific (e.g. Mehta et al., 1989; McAnally et al., 2007). Moreover, for turbid waters, bottom drag is strongly reduced and the BBLP using conventional methods such as the von-Karman Plandlt equation, is overestimated (cf. Li and Gust, 2000). In addition, waves and currents are interacted with each other and for this reason the BBLP for combined wave-current is not simply the sum of individual BBLP (cf. Grant and Madsen, 1986; Nielsen, 1992). In this paper, the BBLP for cohesive sediments, namely the bottom shear velocity and stress due to waves ($u_{*w,}$ τ_w) and due to currents ($u_{*c,}$ τ_c) were estimated using linear wave theory from Madsen (1976) (Equation 3-4) and using the quadratic stress law (Thompson et al., 2006) (Equation 3-5), respectively. The wave shear stress was applied to CSIs-3, 6, and 14 data, and the current shear stress was applied to CSI-14 data. Solutions are provided as follows.

$$\tau_w = \rho_f u_{ob} \sqrt{\nu \frac{2\pi}{T_P}}\,,\; u_{*W} = \sqrt{\frac{\tau_w}{\rho_f}} \quad \text{..... (3-4)}$$

$$\tau_c = \rho_f C_D U_{100}{}^2\,,\; u_{*C} = \sqrt{\frac{\tau_C}{\rho_f}} \quad \text{..... (3-5)}$$

$$u_{ob} = \left(\frac{\pi H_S}{T_P \sinh(kh)} \right)^{-1} \quad \text{..... (3-6)}$$

$$\left(\frac{2\pi}{T_P} \right)^2 = gk \tanh(kh) \quad \text{..... (3-7)}$$

where ρ_f is fluid density (kg m^{-3}), ν is viscosity (1.34 x 10^{-6} m^2 s^{-1}), g is gravitational acceleration (9.8 m s^{-2}), C_D is bottom drag coefficient, U_{100} is mean current velocity at 1 m above the bottom in m s^{-1}, H_S is significant wave height in m, T_P is peak wave period in seconds, u_{ob} is near-bottom wave orbital velocity in m s^{-1} (Equation 3-6), k is wave number in

m^{-1} estimated by the dispersion relation (Equation 3-7), and h is water depth in m. Pressure and current sensors at CSI-14 were installed at 1.6 m above the seabed; we extrapolated the current to that at the conventional height, 1 m above the bottom, by logarithmic method, assuming flow at the bottom is zero. For the bottom drag coefficient (C_D), several studies used a constant drag coefficient to estimate the bed shear stress (e.g., Sternberg, 1972; Adams et al., 1987); however, the coefficient depends on shear velocity, which varies with turbidity in same physical conditions (Li and Gust, 2000; Thompson et al., 2006). We preliminarily estimated C_D corresponding to sediment concentration (C) based on the result of Thompson et al (2006) using a third order polynomial fit (r^2=0.76). By comparing τ_c for varying C_D to that for the constant C_D for a smooth bed, it is found that both results were almost identical. As a result, the constant C_D of 0.0022, following Soulsby (1997), was used in this study.

Fluid density (ρ_f) for saline turbid water (10˚C and 30 PSU) was estimated from the result of Thompson et al. (2006) using linear regression (r^2=1.0) (Equation 3-8).

$$\rho_f = 0.65 \times C + 1020 \quad \text{..... (3-8)}$$

The critical shear stress for erosion of 0.15 N m^{-2} was selected as the threshold for cohesive sediment re-suspension with reference to Wright et al (1997). This value is also the same as the maximum threshold value used by the DHI Water and Environment Inc., based on their extensive numerical model studies (Kerper, D.R. personal Communication, 2006).

3.5. Results and Discussion

3.5.1. Atchafalaya River Freshwater Discharge and Sediment Load

In Figure 3.4a, we present mean, maximum, and minimum river discharge at Simmesport, upstream Atchafalaya River, between 1997 and 2006, obtained from the U.S. Army Corps of Engineers, New Orleans District. The Atchafalaya freshwater discharge was maximal in spring (April) due to ice melting from Rocky and Appalachians mountains, and

minimum in summer (September). The maximum discharge in spring exceeded 600,000 cubic feet per seconds (cfs) (≈ 17,000 m^3 s^{-1}). Walker and Hammack (2000) suggest the discharge higher than 200,000 cfs (≈ 5,662 m^3 s^{-1}) at Simmesport as a high discharge event. Freshwater discharge, sediment load, and the SSC of Morgan City and Wax Lake Outlet obtained from the U.S. Geological Survey (USGS) are shown in Figures 3.4b and 3.4c (Baumann et al., 2006). In spring, the freshwater discharge reached 300,000 cfs (≈ 8,493 m^3 s^{-1}) and 200,000 cfs (≈ 5,662 m^3 s^{-1}) at Morgan City and Wax Lake Outlet. The sediment load and the SSC during this period were also high, during which significant quantities of fluvial sediments were debouched down to the receiving basin (see Figures 3.4b and 3.4c). One of the noticeable characteristics of the data for both Morgan City and Wax Lake Outlet was that the SSC was abnormally high in summer in spite of low river discharge and low wind energy regime. During this time, freshwater and sediment load in addition to the SSC had no correlation. More discussion is provided in a later section of this paper.

3.5.2. Atchafalaya River Fine Sediment Dispersal Patterns

As mentioned in a previous section, the Atchafalaya River fine sediment dispersal and transport are influenced by the prevailing wind and associated coastal currents. The wind-induced westerly currents, during fair weather conditions, transport the sediments westward, and are referred to as the mud stream by Wells and Kemp (1981), as also seen from a MODIS true color image obtained from the ESL (Figure 3.5a). With the onset of a winter storm over the basin, abrupt change of wind direction occurs, which deflects the direction of current and the sediment plumes along the shelf. During spring, concurrent with winter storms, this westward transport occasionally shifts the direction from the west to south/southeast, during the post-frontal northerly wind regime. Such a situation can be clearly seen in Figures 3.5b and 3.5d. It should be noted that not all post-frontal winds yielded this substantial shift in the plume. During tropical cyclones, the transport is dependent upon storm tracks and its

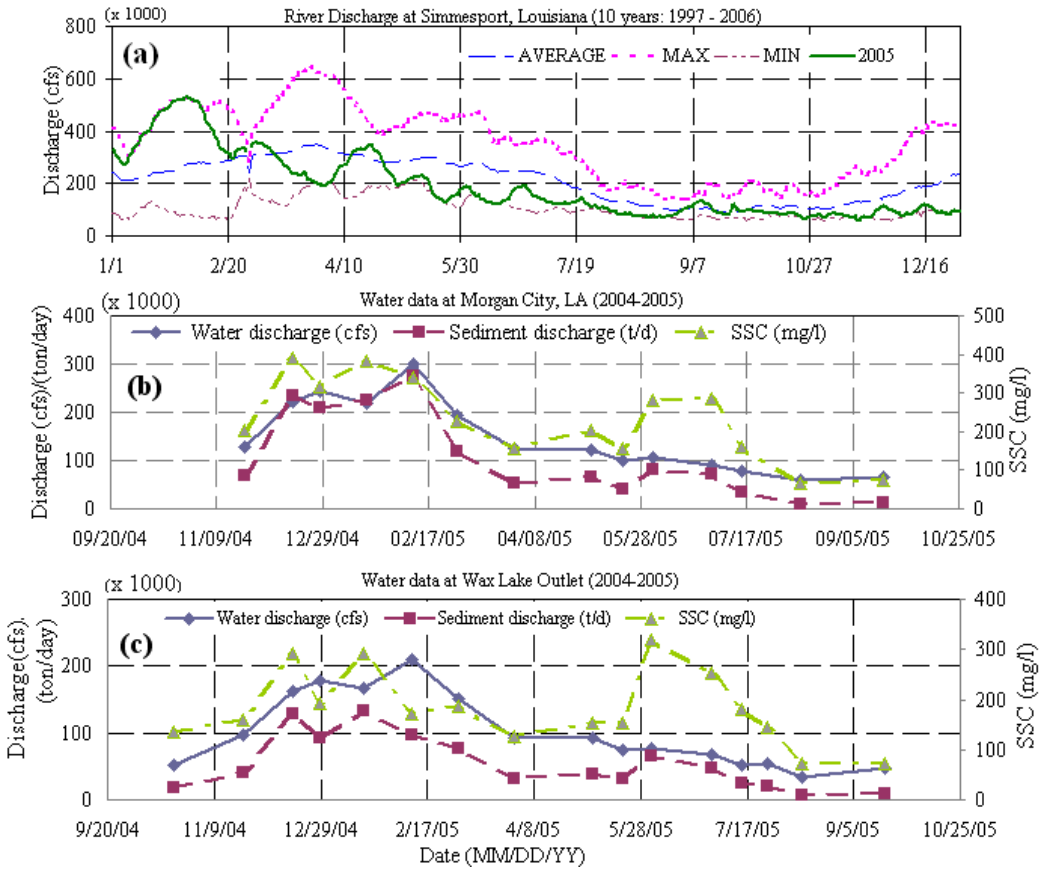

Figure 3.4 (a) Atchafalaya River discharge at Simmesport, LA, between 1997 and 2006 and freshwater discharge, sediment load and SSC at (b) Morgan City, 2005, and (c) Wax Lake Outlet, 2005

intensity. Preliminary analysis of satellite images during the 2005 hurricane season exhibits strong contrasts with respect to sediment dispersal and transport.

During Hurricanes Cindy (Figure 3.5c), Katrina (Figure 3.5e), and Rita (Figure 3.5f), sediment dispersal patterns driven by the hurricane-induced winds can be clearly seen in spite of low river discharge during summer, implying the importance of local sediment re-suspension. The mechanism of fluvially-derived sediment dispersal and transport is discussed in the following sections.

3.5.3. Wave-climate and Associated Hydrodynamics over the Louisiana Inner Shelf

In Figures 3.6, 3.7 and 3.8 are presented time series of wave-climate, 24 hour moving-averaged currents and SSC (and ABS) at CSI's-3, 6, and 14, respectively. Wave-climate, hydrodynamics and bottom sediment interaction over the Atchafalaya Bay/Shelf are strongly associated with meteorological conditions and river discharge from the Atchafalaya River. As shown in Figure 3.3, alongshore currents at CSI-3 were westward during most of the year 2005, except April, June, July and August during which the prevailing current direction was eastward and the north component was almost zero. The eastward currents in April were associated with the passage of winter storms and the persistent easterly coastal currents during June, July and August were attributed to the reversal in the wind direction to the east, as also reported by Cochrane and Kelly (1986). Cross-shore currents were negative in winter and spring due to strong post-front wind stress and were positive during summer. High positive cross-shore wind stress in late September was associated with Hurricane Rita (Figure 3.3). During fair weather, wave-induced bottom shear stress at CSI-14 was generally lower than the threshold for sediment suspension (Figure 3.6d); while during winter storms and tropical cyclones, shown as shaded triangles in Figure 3.6e, the shear stress due to waves exceeded the critical value, which corresponded to an increase in the sediment re-suspension and in the SSC (Figures 3.6d and 3.6e).

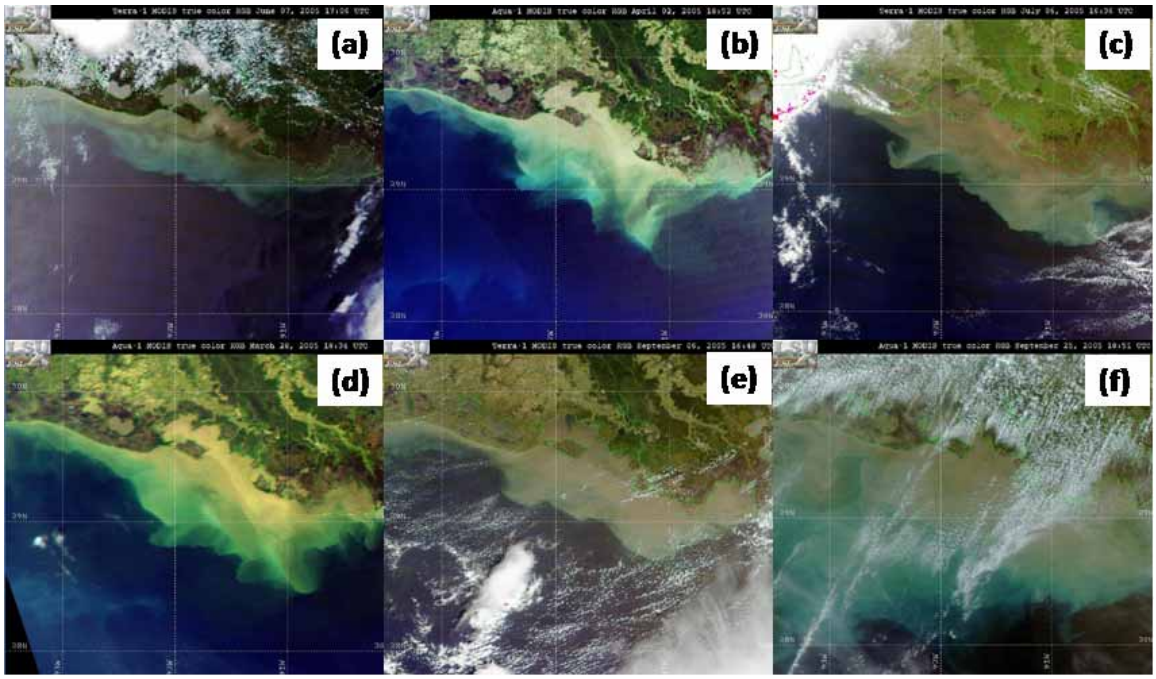

Figure 3.5 MODIS Satellite images in (a) June 7, 2005, (b) April 2nd, 2005, (c) July, 6th, 2005, (d) March 28th, 2005 (e) September, 6th, 2005 (f) September 26th, 2005.

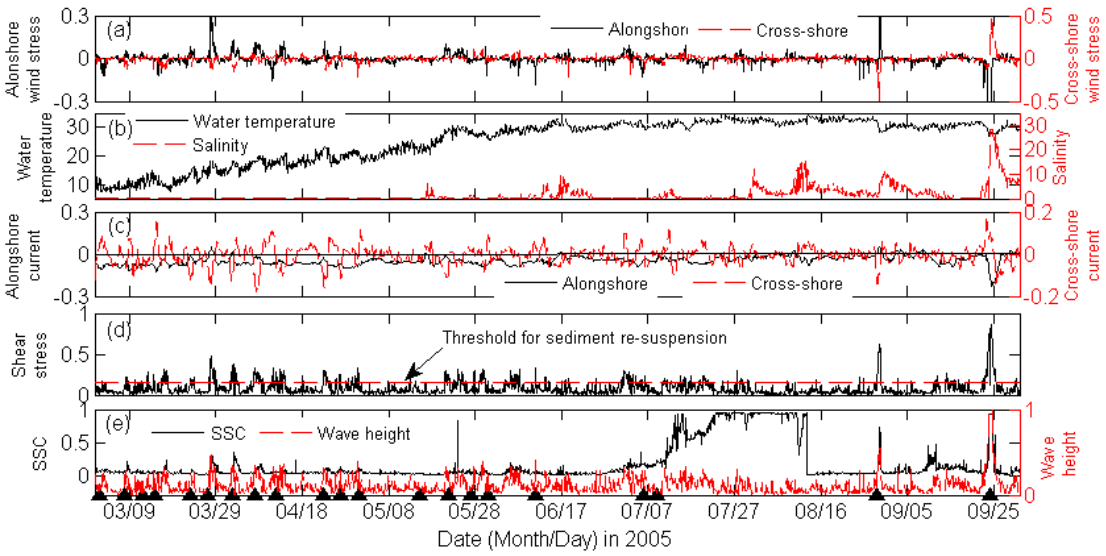

Figure 3.6 Time series of (a) wind stress (N m^{-2}), (b) wave height (m) and water depth (m), (c) 24 hr moving-averaged current (m s^{-1}), (d) shear stress due to waves (N m^{-2}), and (e) SSC (kg m^{-3}) at WAVCIS CSI-14 between 2005/03/01-2005/09/30. Passage of winter storms and tropical cyclones are shown with shaded triangles in (e).

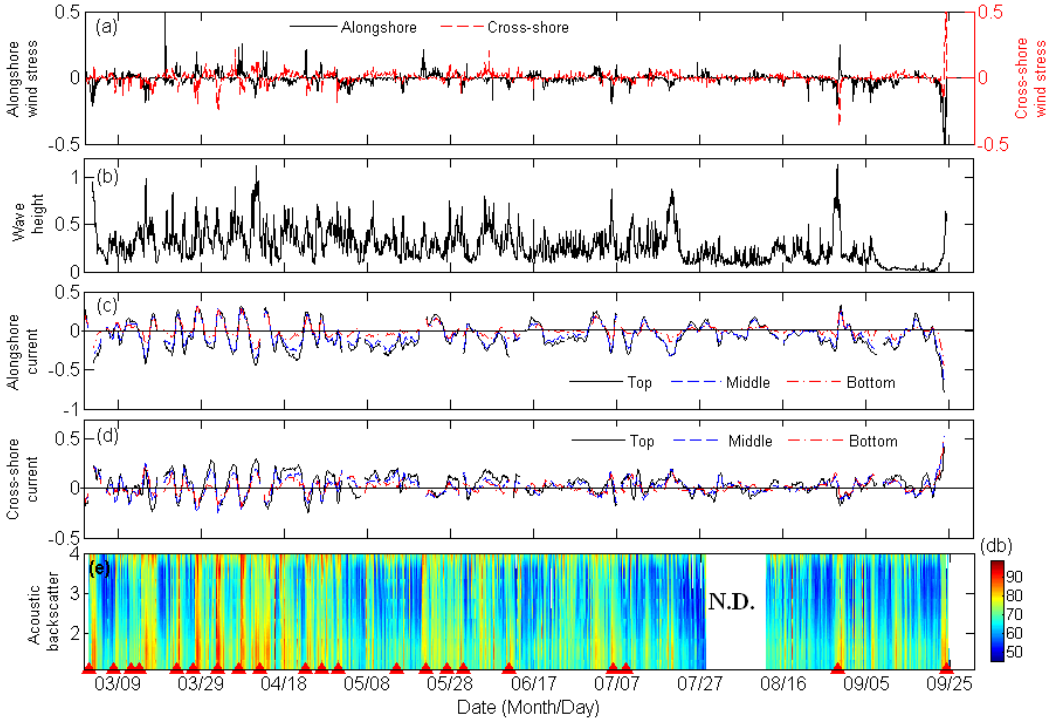

Figure 3.7 Time series of (a) wind stress (N m^{-2}), (b) significant wave height (m) and water depth (m), (c) 24 hr moving-averaged alongshore currents (m s^{-1}) (top3.75m, middle:2.03m, bottom:0.63m), (d) 24 hr moving-averaged cross-shore currents (m s^{-1}) (top:3.75m, middle:2.03m, bottom:0.63m), and (e) acoustic backscatter profile (decibel) at WAVCIS CSI-3 between 2005/03/01-2005/09/25. Passage of winter storms and tropical cyclones are shown with shaded triangles in (e). N.D. represents No Data.

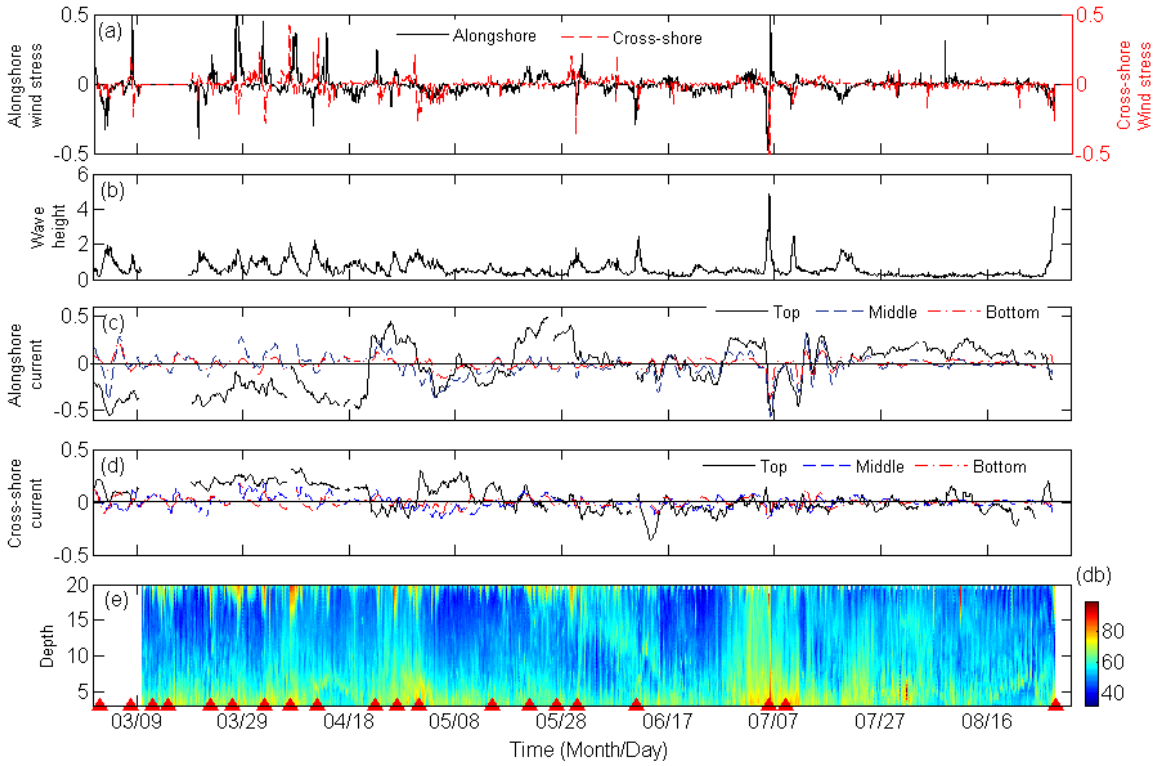

Figure 3.8 Time series of (a) wind stress (N m^{-2}), (b) significant wave height (m) and water depth (m), (c) 24 hr moving-averaged alongshore currents (m s^{-1}) (top, middle:10.59m, bottom:1.49m), (d) 24 hr moving-averaged cross-shore currents (m s^{-1}) (top, middle:10.59m, bottom:1.49m), and (e) acoustic backscatter profile (decibel) at WAVCIS CSI-6 between 2005/03/01-2005/08/25. Passage of winter storms and tropical cyclones are shown with shaded triangles in (e).

For CSI-3 located at approximately the 5 m isobath, alongshore and cross-shore currents were oscillated with a period of 3 to 10 days (Figures 3.7c and 3.7d). This oscillation corresponded to variation of wind stress as a result of periodic wind shift due to winter storms (Figures 3.7a and 3.7c). High ABS, thus high SSC, was strongly associated with enhanced wind stress and consequent wave-induced sediment re-suspension. The high SSC was noticed throughout the water column during storms due to sediment suspension and vertical mixing. Significant wave height (hereafter referred to as wave height) at CSI-3 was mostly less than 1 m, which is usually lesser than that of CSI-5 (not in Figure 3.7), in spite of the same isobaths and thus comparable wave energy, but with different bottom sediment configurations (i.e. cohesive bottom). This suggests the significance of wave energy dissipation over muddy bottom as reported by Sheremet and Stone (2003) as well as frictional dissipation over two sand shoals. For CSI-6 located at approximately 20 m isobaths, similar hydrodynamic characteristics can be deciphered. The wave height reached up to 2 m during winter storm period and approximately 5 m during tropical cyclones Cindy and Katrina (Figure 3.8b). There was no wave record during Hurricane Rita at CSI-6 as the station was partially damaged due to high waves and storm surge sustained from Hurricane Katrina. The ABS, a proxy for the SSC, showed higher values during both winter storms and tropical cyclones. Bottom sediment re-suspension and subsequent mixing events were mostly limited to approximately 10 m above the bottom during winter storms (Figure 3.8e); while, during hurricanes Cindy and Dennis, in early July, the re-suspended sediment clearly reached water surface (around 20 m isobaths) due to strong sediment re-suspension and storm-induced turbulence (vertical velocity over 0.1-0.15 m s^{-1}, not in Figure 3.8).

3.5.4. Response of the Sediment Dispersal to Two Contrasting Storms

Preliminary satellite image analysis shows the unique response of fluvially-derived sediments to storms (Figure 3.4). The response of the sediment transport to two contrasting

storms was examined using *in-situ* ocean observing data from WAVCIS CSI-14 (Figures 3.9–3.11) as well as from CSI's-3 and 6 (Figures 3.7-3.8). Since hurricanes Cindy, Dennis and Katrina had similar dispersal patterns, only the result during Hurricane Katrina was provided.

3.5.4.1. Winter Storms

In Figure 3.9, the time series data at CSI-14 between March 25th and April 8th are shown. During the period, two winter storms crossed the study area: one was on March 27th and the other on April 1st. During each storm, the wind speed exceeded 10 m s^{-1} and the direction of wind strongly shifted from the southeast to north (Figure 3.9c). Wave height reached 0.5 m in March 28th when the bottom shear stress due to waves (τ_w) exceeded the threshold for sediment suspension and was consistent with an increase in the SSC, indicating the sediment re-suspension during the period. Whereas, the shear stress due to currents (τ_c) was not correlated with the SSC during this period which suggests that the waves are a primary factor for sediment re-suspension and the currents contribute to the transport of the suspended sediments. Wind stress was high during post-frontal phases, directing southeastward in consistent with the current direction. As a result, the fine sediments from the river along with re-suspended sediments from the bottom were transported southeastward during this period, as supported by the satellite image in Figure 3.5b and d.

3.5.4.2. Tropical Cyclones

3.5.4.2.1. Hurricane Katrina

Time series data at CSI-14 during Hurricane Katrina are shown in Figure 3.10. Hurricane Katrina made landfall at approximately 200 km east of our study area on August 29th, 2005. Wind speed reached 20 m s^{-1} and wave height exceeded 0.5 m at CSI-14, in spite of the fetch-limited wave generation (station was located at the front left quadrant of the hurricane path). Shear stress due to waves reached 0.7 N m^{-2} during this time, which was

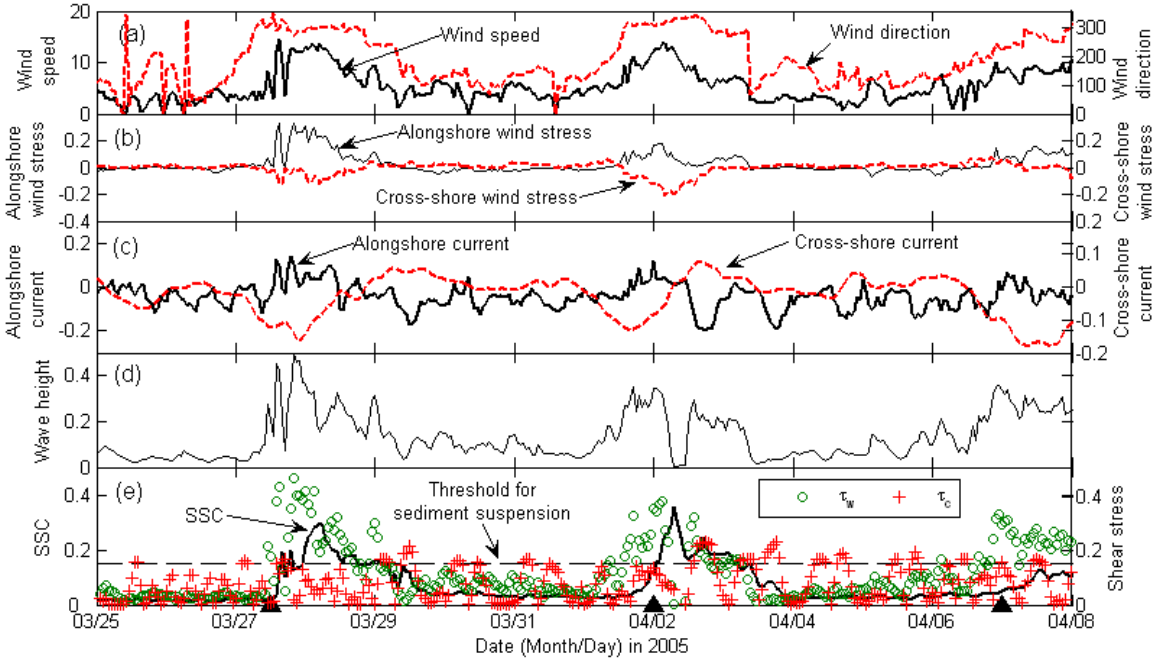

Figure 3.9 Time series of (a) wind speed (m s^{-1}) and directions (degree), (b) wind stress (N m^{-2}) (alongshore/cross-shore), (c) 24 hr moving-averaged near surface currents (m s^{-1}) (alongshore/cross-shore), (d) significant wave height (m), and (e) SSC (kg m^{-3}) (left) and shear stress (N m^{-2}) (right) at WAVCIS CSI-14 between 2005/03/25 and 2005/04/08.

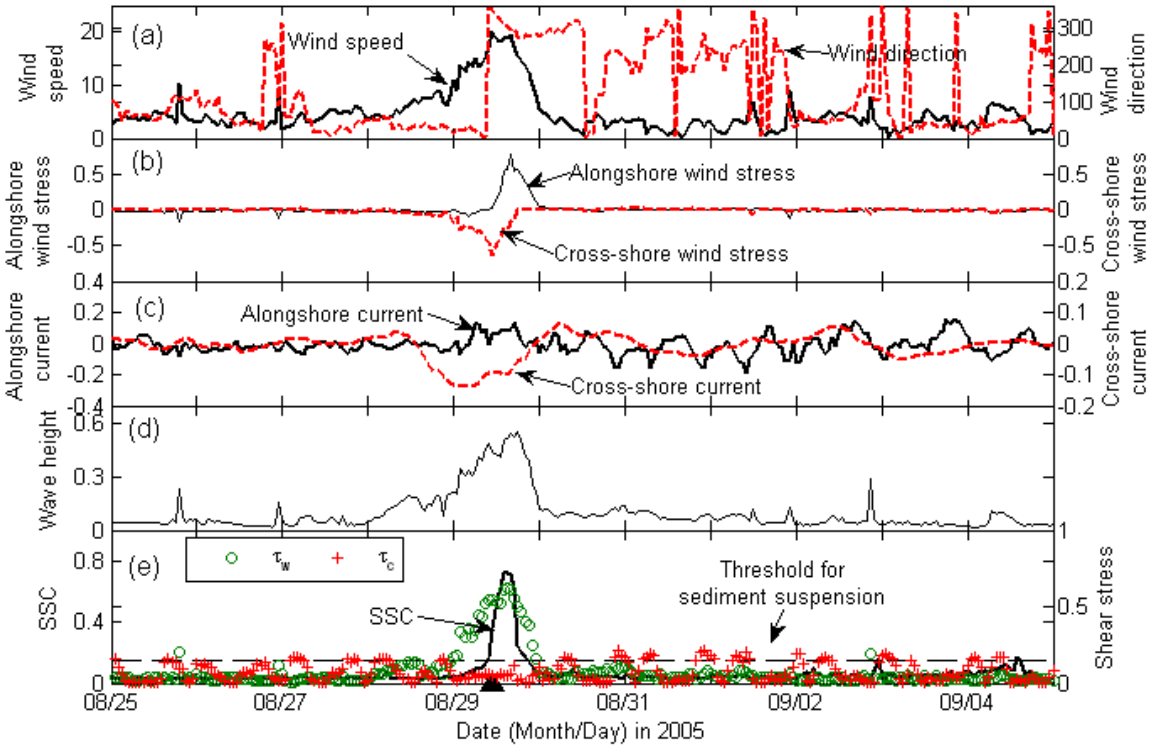

Figure 3.10 Time series of (a) wind speed (m s^{-1}) and directions (degree), (b) wind stress (N m^{-2}) (alongshore/cross-shore), (c) 24 hr moving-averaged near surface currents (m s^{-1}) (alongshore/cross-shore), (d) significant wave height (m), and (e) SSC (kg m^{-3}) (left) and shear stress (N m^{-2}) (right) at WAVCIS CSI-14 between 2005/08/25 and 2005/09/05.

more than 4 times higher than the estimated threshold for sediment suspension. While, the stress due to currents was closer to or slightly higher than the threshold, it had no correlation to SSC. The SSC recorded a maximum of 0.7 kg m^{-3} during the landfall and was associated with high wave-induced shear stress, clearly indicating strong sediment re-suspension and mixing during the post-storm phase, given the fact that turbidity sensor was installed at about 1.6 m above the bottom over approximately 3.0 m isobaths. Both alongshore and cross-shore wind stresses during the hurricane landfall were more than 10 times higher than those during fair weather. This high wind stress, whose direction is toward southeast, generates southeast currents and transports the re-suspended and well-mixed sediments toward southeast, validating the dispersal pattern identified from the satellite imagery obtained after the landfall. Hurricanes Cindy and Dennis, both of which made landfall east of the study area, had a similar dispersal pattern to that of Hurricane Katrina.

3.5.4.2.2 Hurricane Rita

In Figure 3.11, we present time series data at CSI-14 during Hurricane Rita, which made landfall at approximately 250 km west of the study area, near the LA-TX border on September, 24th, 2005. Data showed that maximal sustained wind speed at CSI-14 reached 24.4 m s^{-1} and wave height attained 1.8 m, approximately 10 times higher than the height during fair weather, due to wave setup by southerly hurricane-force wind. The extremely high waves caused strong sediment re-suspension; the shear stress due to waves reached 0.9 N m^{-2}, 6 times higher than the threshold; while stress due to currents was less than the threshold and had poor correlation to the SSC. The SSC reached 1.0 kg m^{-3}, the saturation level and lasted for about a day. During the pre-hurricane landfall, wind direction progressively changed from east, southeast and south as Rita approached the landfall site. Current variation followed the wind pattern. During the approaching phase of the storm, northwesterly currents transported the re-suspended fine sediments towards onshore over most of the Atchafalaya Shelf (Figures

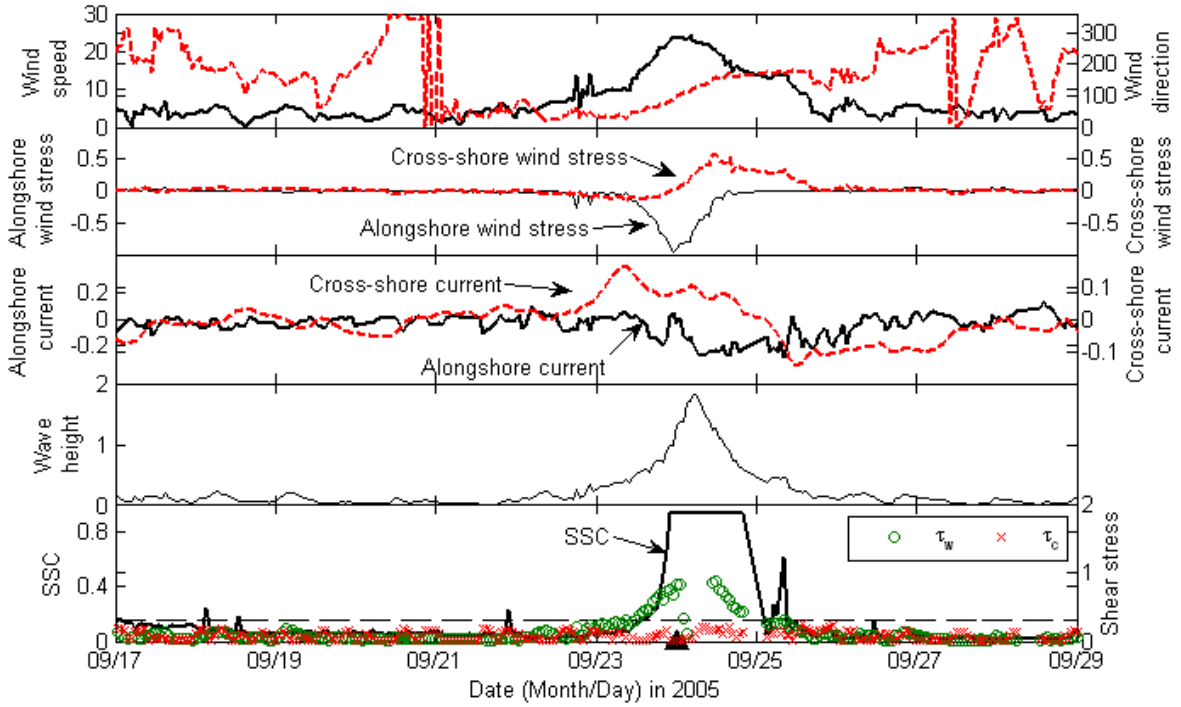

Figure 3.11 Time series of (a) wind speed (m s^{-1}) (right) and direction (degrees) (left), (b) wind stress (N m^{-2}) (alongshore/cross-shore), (c) 24 hr moving-averaged near surface currents (m s^{-1}) (alongshore/cross-shore), (d) significant wave height (m), (e) SSC (kg m^{-3}) (left) and shear stress (N m^{-2}) (right) at WAVCIS CSI-14 between 2005/09/17 and 2005/09/29.

3.5f and 3.11c); while, during the post-landfall phase, southerly return flow was dominated, transporting the sediments back offshore (Figure 3.11).

3.5.4.2.3 Generalized Dispersal Patterns during Cold Fronts and Tropical Cyclones

Analysis of the *in-situ* data and satellite imagery showed unique hydrodynamics and sediment dispersal patterns for the two contrasting storms, namely, extra-tropical storms (i.e. cold fronts) and tropical cyclones (i.e. tropical storms and hurricanes) that are the two dominant forces to drive sediment transport along the low-energy Louisiana inner shelf (Figure 3.2). Figure 3.12 illustrates typical sediment transport patterns during (i) winter storms (Figures 3.12a and 3.12b), (ii) tropical cyclones which strike east of the study area (Figures 3.12c and 3.12d), and (iii) tropical cyclones which strike west of the study area (Figures 3.12e and 3.12f), respectively.

During fair weather and pre-frontal phases of winter storms, southeasterly wind-induced currents transport the fine sediment westward; while, post-frontal wind shifts current direction from the west to south/southeast and further transport the sediment offshore (Figure 3.12a and b). Sediment sources are likely from both the lower Atchafalaya River and Wax Lake Outlet and also from locally re-suspended sediments in the bay.

During the period when tropical cyclones approach the coast or make landfall in the vicinity, along the northern Gulf of Mexico, the dispersal and transport patterns depend on the intensity of the storm and the storm track. For tropical cyclones, which make landfall east of the study area such as Katrina, Cindy and Dennis, strong easterly wind-induced currents transport sediment westward during the pre-hurricane phases and currents due to northerly post-hurricane winds transport sediment south/southeastward (i.e. offshore) (Figure 3.5e and 3.10). This dispersal is likely to accompany strong bottom sediment suspension due to high bottom shear stress and vertical mixing. During the post-hurricane phase, despite relatively lower wind speeds when compared to those east of the right front quadrant of the storm and

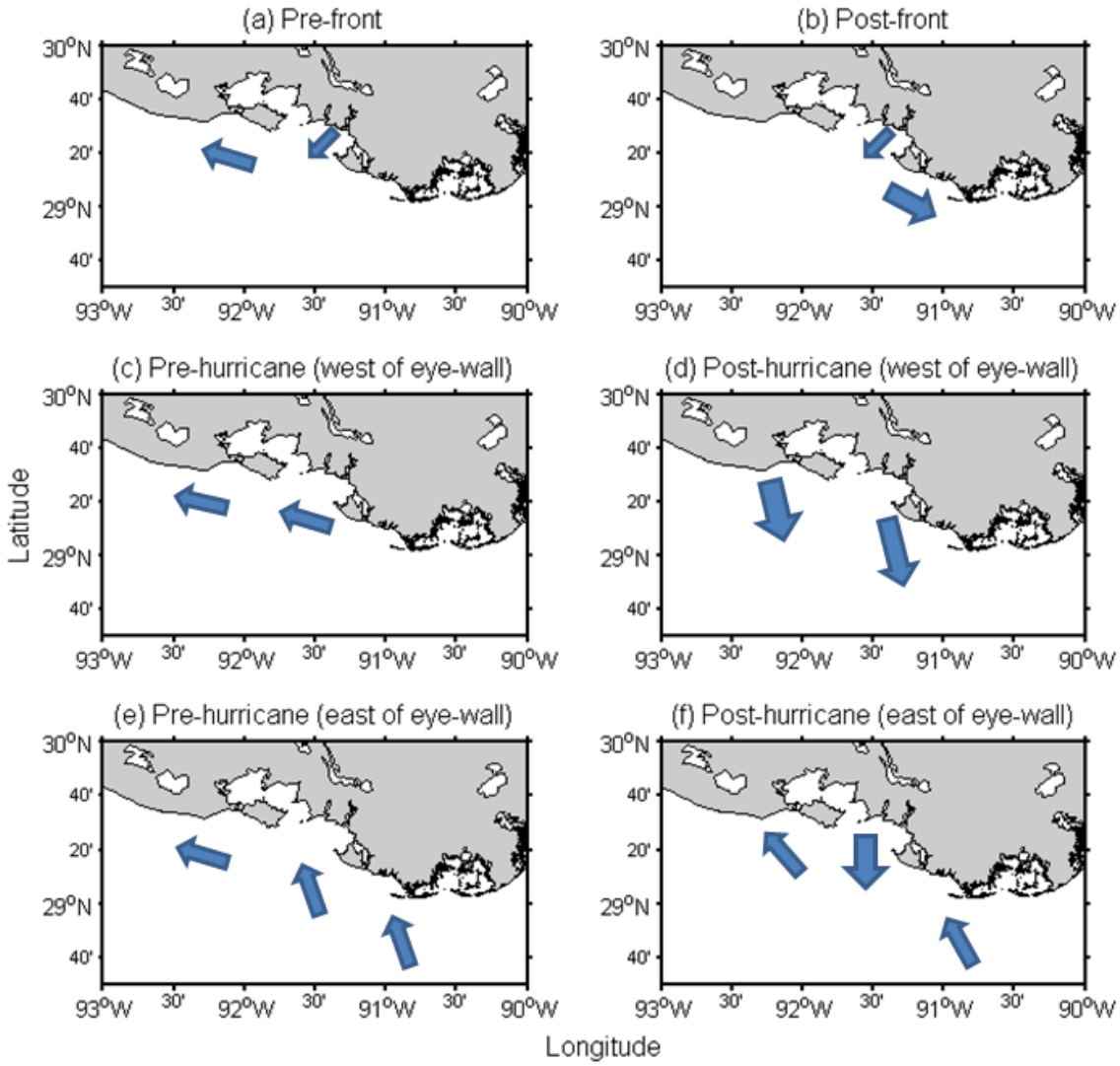

Figure 3.12 General sediment transport patterns for (a&b) winter storms, (c&d) hurricanes made landfall east of the study area, (e&f) hurricanes made landfall west of the study area

also fetch-limited onshore waves, sediment re-suspension becomes substantial (Figure 3.10).

During tropical cyclones that make landfall farther west of the study area, such as Hurricane Rita, extremely high waves due to high southerly winds east of the eye-wall strongly re-suspend and mix bottom sediments throughout the entire water column likely over the entire inner shelf, and storm currents subsequently transport the sediments onshore (west/northwest). During the post-landfall phase, the sediments that are already transported to the Atchafalaya Bay/nearshore would be flushed offshore with strong return flow, and are re-distributed onto the Louisiana continental shelf (Figure 3.11).

During spring, when high river discharge coincides with the passage of a cold front across the region, southerly currents during post-frontal phases are capable of transporting fine sediments to the south/southeast. During relatively low river discharge, especially during the summer hurricane season, local re-suspension seems to be the main source of sediment for the dispersal. Thus it is concluded that the sediment dispersal characteristics of the Atchafalaya Bay/Shelf result from either the seasonal existence of high fluvial sediment discharge, local sediment re-suspension or a combination of the two. Kobashi and Stone (in review, 2008), based on their preliminary numerical model study, demonstrated that under varying storm winds from northwest along with a moderately high freshwater and sediment discharge from the lower Atchafalaya River and Wax Lake Outlet, sediments originated from the Atchafalaya River and transported over the bay/nearshore can reach up to Ship Shoal, which is located roughly 50 km southeast of the river mouth, in approximately three days during the post-frontal phase.

In spite of low river discharge and generally low wind forcing during summer, the SSC from both lower Atchafalaya River and Wax Lake Outlet as well as at CSI-14 was abnormally high. This high SSC is often measured in summer according to the USGS water data records (Figure 3.4). Strong correlation existed with river discharge during certain years

(e.g. 2000, 2003, and 2004); whereas there was no correlation at all in the succeeding year (e.g., 2002, 2005). We have not yet confirmed why the SSC along the river course during summer was so high. Possible reasons may be due to upstream dredging activities, agricultural activities, land clearing etc. Upstream sediment transport from the receiving basin seems not to be realistic since both USGS stations are situated at the significant distance from the mouth of the rivers and also the direction of stream flow was downstream during summer (Walter, D. Personal Communication, 2007). Localized sediment re-suspension along the rivers appears not to occur given the fact that river sediment transport is mainly bed load rather than suspended load during low discharge.

3.5.5. Frequencies of Dispersal Shifts and Their Impacts on a Transgressive Shoal

The fluvially-derived sediment transport significantly alters bottom sediment configurations on a Holocene transgressive shoal (Kobashi et al., 2007a). As already mentioned, the fine sediment supply from the Atchafalaya River during post-frontal phases and sediment re-distribution during tropical cyclones are likely the major sources of fine sediments onto the shoal since the frequency of winter storms is much higher than those of tropical cyclones. The sediment supply of river-borne sediments mostly occurs during winter and spring. Based on *in-situ* observing data from WAVCIS CSI-14 and satellite images from the ESL between October 2004 and May 2005, we have investigated how often such dispersal shifts and the shifts which reached Ship Shoal occurred during the period. Figure 3.13 shows a summarized result from the analysis. We define here the dispersal shifts as persistent changes of current direction from west/northwest to south/southeast during post-frontal phases and are sustained for a few days. The number of the shifts which reached Ship Shoal was determined based on satellite images from the ESL. The figure shows that the number of dispersal shifts was maximal in spring with a total of 5 shifts in a month. The average number during the 8 month period was 0.125 times per day (i.e. once every 8 days).

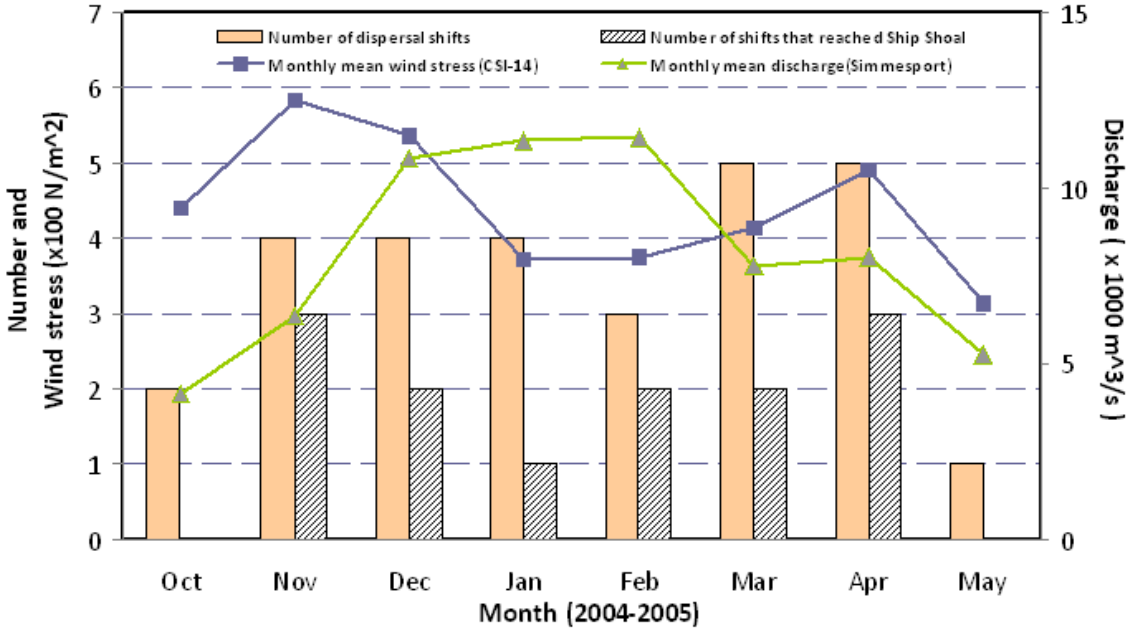

Figure 3.13 Frequencies of dispersal shift and the shifts that reached Ship Shoal between October, 2004 and May, 2005.

However, not all fluvial sediment associated with dispersal shifts reached the shoal, but the sediment reached the shoal once every 19 days on average compared to once every 6.05 days for the frequency of cold fronts. The number of the shifts had no correlation with monthly mean Atchafalaya river discharge at Simmesport (Figure 3.13, triangle marks); however, it had a strong correlation with monthly mean wind stress (Figure 3.13, square marks). As mentioned in the previous sections, the strong post-frontal winds trigger this dispersal shift; therefore, the correlation between the wind stress and the number of the shifts is reasonable. In spite of relatively cloud-free satellite imagery during post-frontal phases, the analysis was significantly affected by cloud conditions and hence some dispersal shifts were not confirmed from the satellite images although the *in-situ* data showed the shifts of currents; thus, the result is still qualitative.

Ship Shoal has been found as having diverse benthic habitats and unique sedimentary environment (Stone et al., 2006). Distribution of benthic organisms on the shoal is strongly affected by bottom sediment types (Palmer et al., 2008) and the species sampled from the entire shoal during biological cruises in spring as well as in summer and fall were generally inhabitable on the bottom in the sandy range and cannot inhabit in and/or on bottoms buried by fluid mud for over a week (Fleeger J., Personal communication, 2007). Possible reasons for this information gap may be because (i) benthic organisms dwelling on unconsolidated fluid mud may have been inadvertently removed due to the sampling technique (Winans, W., Personal Communication, 2007), (ii) sediment distribution may have been patchy so that fine sediment supply may not have significantly affected the benthic communities or, (iii) sediment reworking associated with winter storms was more frequent than fine sediment supply and therefore, fine sediment (i.e. fluid mud) seems to remain temporarily on the bottom and benthic organisms may have been capable of adapting to such intermittent lithological change. In summer and fall when the dispersal shifts are infrequent, shoal bottom

sediments seems to be exposed to sand and shells, particularly on the shallower middle and western flank of the shoal unless fine sediments are not flushed out during storms, and/or fine sediments are supplied, for instance, during tropical cyclones. The relationship between benthic habitats and fluvial and bottom boundary layer processes is currently being studied.

3.6. References in Chapter 3

Adams, C. E., Swift, D.J., Coleman, J.M., 1987. Bottom currents and fluviomarine sedimentation on the Mississippi prodelta shelf: February-May 1984, J. Geophys. Res., Vol.92(C.13),14,595-14,609.

Allison, M.A., Sheremet, A., Goñi, M.A., Stone, G.W., 2005. Storm layer deposition on the Mississippi-Atchafalaya subaqueous delta generated by Hurricane LILI. Cont. Shelf Res., 25, 2213-2232.

Baumann, T., Goree, B.B., Lovelace, W.M., Montgomery, P.A., Ross, G.B., Walter, D.J., Ward, A.N., 2006. Water Resource Data Louisiana Water Year 2005, Water Data Report USGS-WDR-LA-05-1, 913pp.

Cochrane and Kelly, 1986. Low-frequency circulation on the Texas-Louisiana continental shelf. J. Geophys. Res., 91 (C9), 10645-10659.

DiMego, G.J., Bosart, L.F., and Endersen, G.W., 1976. An examination of the frequency and mean conditions surrounding frontal incursions into the Gulf of Mexico and Caribbean Sea. Mon. Weather Rev., 104,709-718.

Earle, M.D. and McGehee, D. and Tubman, M., 1995. Field wave gaging program, wave data analysis standard, Instruction report CERC-95-1,U.S. Army Corps of Engineers, Waterways Experiment Station, 46p.

Gordon, L. and Lohrmann, A., 2001, Near-shore Doppler current meter wave spectra, Proceedings of Waves 2001, ASCE.

Grant, W. D. and Madsen, O. S., 1986, The Continental-Shelf Bottom Boundary Layer, Ann. Rev. Fluid Mech., 18:265-305.

Holthuijsen, L.H. 2007. Waves in Oceanic and Coastal Waters. Cambridge University Press. 404pp.

Hsu, S.A., 1988. Coastal Meteorology, Academic Press, 260p.

Hsu, S.A., 2003. Estimating overwater friction velocity and exponent of power-law wind profile from gust factor during storms. Journal of Waterway, Port, Coastal and Ocean Engineering, vol.129, No.4, 174-177.

Hsu, S.A., 2006. Measurements of Overwater Gust Factor From NDBC Buoys During Hurricanes, NWA Electric Journal of Operational Meteorology, 2006-EJ2.

Keim, B. D., Muller, R.A., and Stone, G.W., 2007. Spatiotemporal patterns and return periods of tropical storm and hurricane strikes from Texas to Maine. J. Climate, 20, 3498-3509.

Kemp, P.G., 1986. Mud deposition at the shoreface: wave and sediment dynamics on the Chenier plain of Louisiana. Unpublished Ph.D. dissertation, Louisiana State University, Baton Rouge, Louisiana, USA, 147p.

Khalil, S.M., Finkl, C., Andrew, J.,Knotts, C.P., 2007. Restoration-quality sand from Ship Shoal, Louisiana: Geotechnical investigation for sand on a drowned barrier island. Proceedings of *Coastal Sediments '07*. New Orleans, Louisiana, 685-698.

Knabb, R.D., Rhome, J.R. and Brown, D.P., 2005a. Tropical cyclone Report Hurricane Katrina, National Hurricane Centre, National Oceanographic and Atmospheric Administration, Miami, Florida, 43p.

Knabb, R.D., Brown, D.P. and Rhome, J.R., 2005b. Tropical cyclone Report Hurricane Rita, National Hurricane Centre, National Oceanographic and Atmospheric Administration, Miami, Florida, 33p.

Kobashi, D., Jose, F., and G. W. Stone, 2005. Hydrodynamics and sedimentary responses within bottom boundary layer: Sabine Bank, western Louisiana, *Transaction*, Gulf Coast Association of Geological Societies, v.55, 392-399.

Kobashi, D., Jose, F., and Stone, G.W., 2007a. Impacts of fluvial fine sediments and winter storms on a transgressive shoal, off south-central Louisiana, U.S.A., *Journal of Coastal Research*, SI 50, 858-862.

Kobashi, D., Jose, F., and Stone, G.W., 2007b. Heterogeneity and dynamics of sediments on a shoal during spring-winter storm season, south-central Louisiana, USA.. Proceedings of *Coastal Sediments* '07, 921-934.

Kobashi, D., and Stone, G.W. 2008. Response of fluvial fine sediment dispersal to storm wind-current effects on a Holocene transgressive shoal, Atchafalaya Shelf, Louisiana, USA: A numerical simulation. In review.

Li, M.Z. and Gust, G. 2000. Boundary layer dynamics and drag reduction in flows of high cohesive sediment suspensions. Sedimentology 47, 71-86.

Madsen, O.S., 1976, Wave climate of the continental margin: Elements of its mathematical description., In: Stanley and Swift, eds, Chapter 6, Marine Sediment Transport and Environmental Management, 65-87.

Manty, R.E., 1993. Effect of the El Nino/Southern Oscillation on Gulf of Mexico, winter, frontal-wave cyclones: 1960-89. Volume 1. Unpublished Ph.D. dissertation, Louisiana State University, Baton Rouge, Louisiana, USA, 397p.

McAnally, W. H., Friedrichs C., Hamilton, D., Hayter, E. Shrestha, P., Rodriguez, H., Sheremet, A., and Teeter, A., 2007. Management of fluid mud in estuaries, bays and lakes. I: Present state of understanding on character and behavior. J. Hydraul. Eng.-ASCE, 133 (1), 9-22.

McBride, R., Taylor, M.J., and Byrnes, M.R., 2007. Coastal morphodynamics and Chenier-Plain evolution in southwestern Louisiana, USA: A geomorphic model. Geomorphology, 88, 367-422.

Mehta, A.J., Hayter, E.J., Parker, W.R., Krone, R.B., Teeter, A.M., 1989. Cohesive sediment transport. I: Process Description. J. Hydraul. Eng.-ASCE, Vol. 115, No. 8, 1076-1093.

Milliman, J.D., Meade, R.H., 1983. World–wide delivery of river sediment to the oceans. J. Geol., Vol.91, No.1, 1-21.

Murray, S., 1997. An observational study of the Mississippi-Atchafalaya coastal plume: Final report. OCS Study MMS 98-0040 U.S. Dept. of the Interior, Minerals Mtmt. Service, Gulf of Mexico OCS Region, New Orleans, LA. 513pp.

National Climatic Data Center, 2006. Climate of 2005 Atlantic Hurricane Season. http://www.ncdc.noaa.gov/oa/climate/research/2005/hurricanes05.html

Nielsen, P., 1992. Coastal bottom boundary layer and sediment transport. Advanced Series on Ocean Engineering, vol.4 (eds.: Liu, P. L-F), World Scientific Publishing Co. Pte. Ltd., 324p.

Nowlin, W.D. Jr., A.E. Jochens, R.O. Reid, and S.F. DiMarco. 1998 . Texas-Louisiana Shelf Circulation and Transport Processes Study: Synthesis Report, Volume I: Technical Report. OCS Study MMS 98-0035. U.S. Dept. of the Interior, Minerals Mgmt Service, Gulf of Mexico OCS Region, New Orleans, LA. 502 pp.

Palmer, T.A., Montagna, P.A., and Nairn, R.B. 2008. The effects of a dredged excavation pit on benthic macrofauna in offshore Louisiana. Environ. Manage., 41: 573-583.

RD Instruments Inc., 2004. WAVES PRIMER: Wave Measurements and the RDI ADCP Waves Array Technique, 1-22 pp., RD Instruments Inc., San Diego CA.

Sheremet, A, and Stone, G. W., 2003, Observations of nearshore wave dissipation over muddy sea bed, J. Geophys. Res., 108(C11), 2257, doi: 10.1029/2003JC001885, 2003.

Sheremet, A., A.J. Mehta, B. Liu, G.W. Stone, 2005, Wave–sediment interaction on a muddy inner shelf during Hurricane Claudette, Estuar., Coastal Shelf S., v.63, p.225–233.

SonTek Inc., 1997. SonTek Doppler Current Meters – Using Signal Strength Data to monitor Suspended Sediment Concentration, SonTek Application Notes, San Diego, California, 7p.

Soulsby, R., 1997. Dynamics of marine sands, Thomas Telford Ltd, 272p.

Sternberg, R.W., 1972, Predicting Initial Motion and Bedload Transport of sediment particles in the shallow marine environment. In:Swift, Duane, and Pilkey, eds., Shelf sediment

transport: Process and Pattern. Stroudsburg, PA: Dowden, Hutchinson, and Ross, Inc., p. 61-82.

Stone, G. W., 2000, Wave climate and bottom boundary layer dynamics with implications for offshore sand mining and barrier island replenishment in south-central Louisiana. *OCS Study MMS 2000-53*. U.S. Dept. of the Interior, Minerals Mgmt. Service, Gulf of Mexico OCS region, New Orleans, LA, 90pp.

Stone, G.W., Zhang, X.P., Gibson, W., and Fredericks, R., 2001. A new Wave-Current online information system for oil spill contingency planning (WAVCIS), Proceedings of 24th Arctic and Marine Oil spill Program Technical Seminar 2001, Edmonton, Alberta, Canada, 401-425.

Stone, G.W., Liu, B., Pepper, D. A., and Wang, P., 2004, The importance of extratropical and tropical cyclones on the short-term evolution of barrier islands along the northern Gulf of Mexico, Mar. Geol., 210, 64-78.

Stone, G.W., Condrey, R., Fleeger, J., 2006. Environmental investigation of long-term use of Ship Shoal sand resources. Year 2 annual report, MMS/LDNR, 62pp.

Thompson, C.E.L., Amos, C.L., Angelaki, M., Jones, T.E.R, and Binks, C.E., 2006. An evaluation of bed shear stress under turbid flows, J. Geophys. Res., 111, C04008, doi:10.1029/2005JC003287.

Walker, N.D., and Rouse, L.J. Jr. 1993. Satellite assessment of Mississippi River discharge plume variability. OCS Study MMS 93-0044. U.S . Dept. of the Interior, Minerals Management
Service, Gulf of Mexico OCS Regional Office, New Orleans, La. 50 pp.

Walker, N.D. and Hammack, A. B., 2000. Impacts of Winter Storms on Circulation and Sediment Transport: Atchafalaya-Vermilion Bay Region, Louisiana, U.S.A., J. Coast. Res, 16(4), 996-1010. West Palm Beach (Florida), ISSN 0749-0208.

Walker, N.D., 2001. Tropical storm and hurricane wind effects on water level, salinity, and sediment transport in the river-influenced Atchafalaya-Vermilion Bay system, Louisiana, USA. Estuaries, 24(4), 498-508.

Wells, J.T. and Kemp, P., 1981. Atchafalaya mud stream and recent mudflat progradation: Louisiana chenier plain. *Transactions*, Gulf Coast Association of Geological Society, v.31, 409-416.

Whitehouse, R.J.S., Soulsby, R., Roberts, W., Mitchener, H., 2000. Dynamics of Estuarine Muds. Thomas Telfort Ltd. and HR Wallingford.

Wright, L.D., Nittrouer, C.A., 1995. Dispersal of river sediments in coastal seas: Six contrasting cases. Estuaries, Vol. 18, No. 3, 494-508.

Wright, L.D., Sherwood, C.R. and Sternberg, R.W., 1997. Field measurements of fair-weather bottom boundary layer processes and sediment suspension on the Louisiana inner continental shelf, Mar. Geol., 140, 329-345.

Wu, J. 1982. Wind-stress coefficients over sea surface from breeze to hurricane. J. Geophys. Res., 87, C12, 9704-9706.

Zhang, X.P., 2003. Design and implementation of an ocean observing system: WAVCIS (Wave-current-surge information system) and its application to the Louisiana coast. Unpublished Ph.D. dissertation, Louisiana State University, Baton Rouge, USA, 194p.

CHAPTER 4

TWO CONTRASTING MORPHODYNAMICS OVER RECURRING SANDY AND MUDDY BOTTOMS OF A SHORE-PARALLEL HOLOCENE TRANSGRESSIVE SHOAL, SOUTH-CENTRAL LOUISIANA, USA

4.1. Introduction

Bottom boundary layer dynamics (BBLDs) over the Louisiana shelf are characterized by low-energy regime; waves and current fields are known to be not strong enough to disturb bottom sediments and cause transport (Adams et al, 1987; Wright et al, 1997). However, two energetic weather events, namely tropical and quasi-periodic extra-tropical storms (i.e. winter storms that accompany cold fronts), significantly affect bottom boundary layer (BBL) and sediment transport over this low-energy shelf (Pepper and Stone, 2004; Allison et al, 2005; Kobashi et al., 2005; Sheremet et al., 2005; Stone et al., 2005; Kobashi et al., 2007a). Several field studies have been conducted in order to understand the BBLDs on various parts of the U.S. continental shelves. Particular attention was paid to investigating the BBLDs during storms during which the BBLDs are reported to be significant across the coasts (e.g. Cacchoine and Drake, 1982; 1990; Wright et al., 1991; Green et al., 1995; Li et al., 1997; Pepper and Stone, 2004; Kobashi et al., 2005). Adams et al (1987) studied bottom currents and associated sediment transport over the Louisiana inner shelf near the Southwest Pass in Louisiana in 60 m of water where bottom sediment was predominantly fine-grained silt and clay. Their study revealed that sediment re-suspension was less important on evaluating sediment transport processes. Wright et al. (1997) studied bottom boundary layer characteristics and sediment transport by deploying a tripod off the Louisiana coast along 15.5 and 20.5 m isobaths during summer non-storm conditions in 1992 and 1993. The study concluded that bottom currents were typically weak during fair weather and bed shear stress during fair weather was too weak to re-suspend bottom sediments.

Stone (2000) conducted a detailed BBL study in 1998 and 2000 by deploying various arrays of the BBL instruments on the western flank of Ship Shoal which is also known as a potential offshore sand resource. A strong response of bottom boundary layer processes (BBLPs) for sandy bottoms to winter storms were quantified. In addition, the study qualitatively documented unique flow modulations associated with complex shoal bathymetry. Despite such studies, it was recently revealed that the fluvial sediments from the Atchafalaya located approximately 50 km northwest from the shoal, has a decisive impact on the shoal morphodynamics which has not previously been recognized (Kobashi et al., 2007a). Walker and Hammack (2000) investigated the Atchafalaya River sediment plume structure using satellite imagery and limited *in-situ* data and showed a strong response of the plume to varying wind fields. Kobashi et al (In review, 2008a) and Kobashi and Stone (In review, 2008a) further investigated mechanisms of Atchafalaya sediment plume shifts with respect to rapidly varying wind, particularly during post-frontal phases, based on numerical simulations and prolonged *in-situ* observational data from stations near Atchafalaya Bay and in deeper water off the Louisiana coast. Both studies led to the conclusion that strong post-frontal northwesterly wind stress generates strong offshore currents, which in turn transport fluvial sediments to the southeast in concert with the sediment re-suspension associated with storm waves. The results were further corroborated using satellite imagery analysis. In the early Spring of 2006, instrument arrays including a pulse-coherent acoustic Doppler profiler (PCADP) and acoustic Doppler velocimeters (ADV) were deployed at the eastern flank of Ship Shoal in depths ranging from 12-13 m (Figure 4.1); the study unveiled complex interactions of winter storms and fluvial fine sediments from the Atchafalaya River with shoal morphodynamics for the first time (cf. Kobashi et al., 2007a; 2007b; 2008). In order to bolster our findings, further deployments were conducted in winter 2008 along a transect across the middle of the shoal in depths ranging from 7-8 m (Figure 4.1).

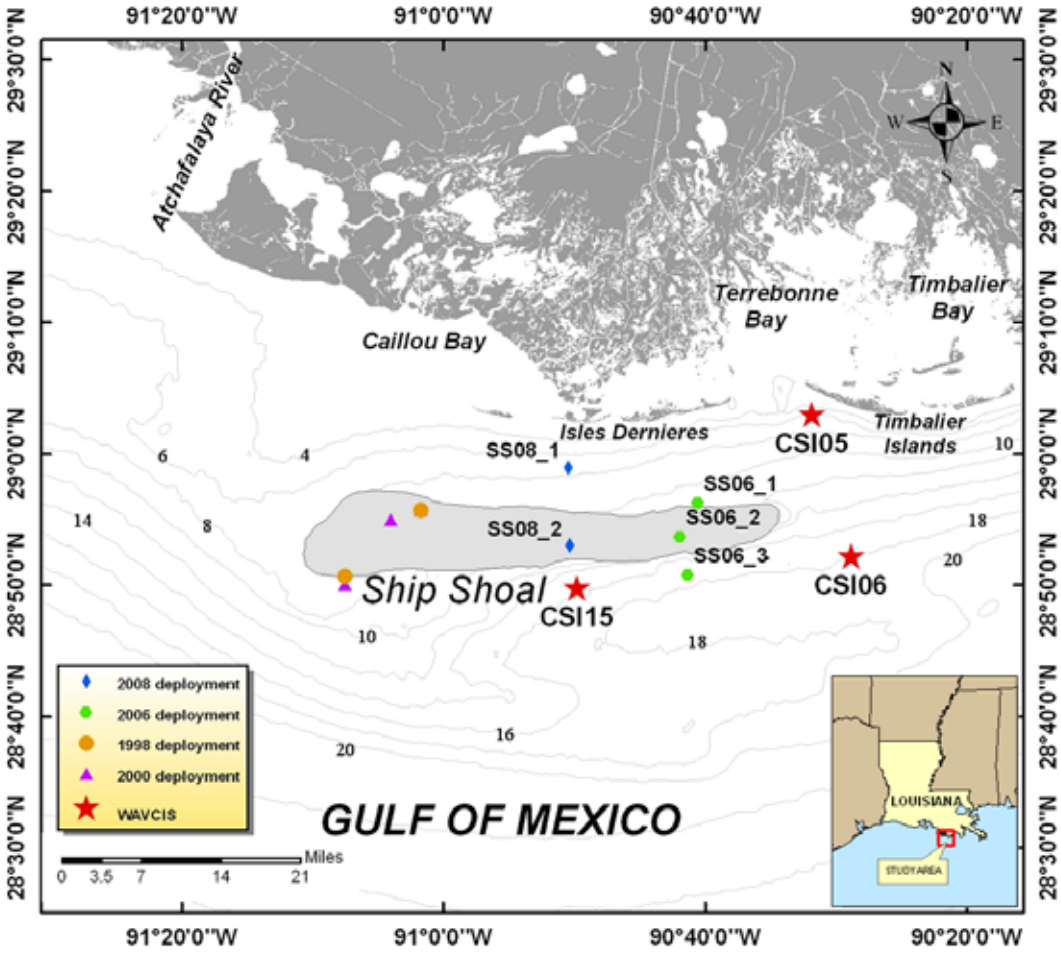

Figure 4.1 Map of study area

These transect data represented sand-dominated morphodynamics and were in contrast with the 2006 deployments, which represented a low-energy fine sediment environment. Our collaborative study revealed that the shoal may play an important role in commercial fisheries as well as in the life cycle of benthic organisms, for instance, by providing blue crabs with a hatching and foraging ground (Condrey and Gelpi, 2008) and also for benthic micro-algae to provide oxygen and food sources (Grippo et al., submitted). The benthic habitat distribution strongly correlates with types of sediments and physical parameters such as waves, currents as well as temperature, salinity, and dissolved oxygen at the bottom (Michel et al., 2001; Palmer et al., 2008). It has been hypothesized that the morphodynamic features of the shoal has a critical role on the bio-physical interaction of the shoal and consequently on the shoal ecosystem. Such extensive research efforts have little been reported in the scientific literature.

In this paper, an attempt has been made to compare and contrast morphodynamics of two contrasting shoal bottom settings, namely, fluid mud and fine sand, and further to discuss such unique dynamics over the shoal. Implications associated with the morphodynamics for potential impacts on future sand dredging is also briefly discussed.

4.2. Physical Setting

The Louisiana shelf is characterized as very low gradient, a recipient of substantial quantities of fluvial sediments from both the Mississippi and Atchafalaya rivers, and also a low-energy micro-tidal environment: these are characteristics ideal for the accumulation of fluvial fine sediments onto the continental shelf. In such a low-energy shelf environment, stratification prevails, particularly during summer, when bottom water often demonstrates hypoxic conditions (Rabalais et al., 2002). In winter, the recurring passage of extra-tropical storms can break stratification and water density tends to be homogeneous throughout the water column (DiMego et al., 1976; Wiseman et al., 1986; Kobashi et al., 2007a; Rabalais et

al., 1994). In winter, quasi-periodic passage of winter storms accompanies cold fronts along with sudden veering of the wind from southern to northern quadrants as well as sharp drops in air temperature and barometric pressure (Kobashi et al., 2005; see also Figure 4.2).

During summer, the coast is exposed to tropical storms. Keim et al. (2007) estimated that the return period of tropical storms and hurricanes in southern Louisiana was 3 years. During fair weather conditions, prevailing southeast wind and consequent waves and currents transport materials (sediments and other passive materials) westward (alongshore) (Cochrane and Kelly, 1986; Murray, 1997; Cipriani and Stone, 2001); while, during the post-frontal phase, cross-shore currents generated by persistent cross-shore winds are often dominant (Chuang and Wiseman, 1983; Pepper, 2000; Kobashi et al., 2007b).

The cyclic nature of the Mississippi River delta formation have formed large offshore sand bodies, drowned paleo-barrier islands off Louisiana, on the end phase of the delta cycle (Penland et al., 1986; 1988; Roberts, 1997). Ship Shoal, a shore-parallel elongated sand shoal, located approximately 20 km off the Isles Dernieres, 50 km long and 15 km wide and surrounded by the 10 m isobath, is known as a remnant of the abandoned Maringouin delta that was active approximately 7500 years BP (Penland et al, 1986). Bathymetry data show that the western part of the shoal is significantly shallower than the eastern part (Figure 4.1). Historical survey data suggest that Ship Shoal is migrating landward at a rate of 10 to 15 m yr^{-1} under present sea level conditions. This migratory trend of the shoal can be attributed to recurring storm impacts and predominant wave action from the southeast (Kulp et al., 2001). In addition, literature and recent bathymetric data suggest that Ship Shoal has been "deepening", given the fact that the shoal has been re-worked extensively during intense storms. Also, the entire Louisiana coast is subsiding in response to the rapid rise in relative sea level (Roberts, 1997; Kulp et al., 2001).

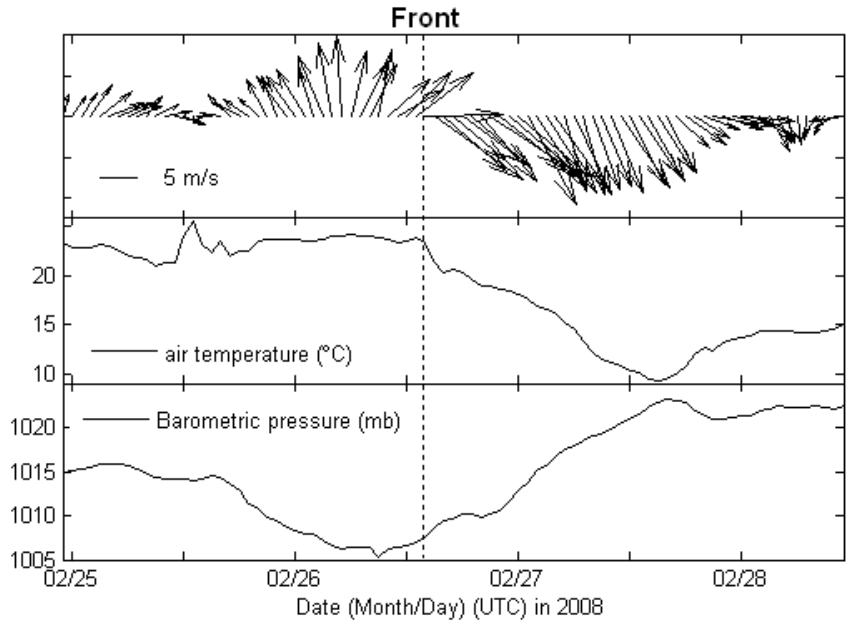

Figure 4.2 Variation of meteorological parameters during a winter storm

4.3. Data Acquisition

Field measurements were carried out off south-central Louisiana during 2006 and 2008. Various BBL arrays were deployed in spring 2006 on the eastern flank of the shoal (SS06_1 – SS06_3 in Figure 4.1) over a period of 45 days and in winter 2008 on the middle of the shoal (SS08_1 and SS08_2 in Figure 4.1) over a period of 52 days. Three different arrays of oceanographic instruments were deployed on offshore, crest and onshore of the shoal (Figure 4.1). Two ADV tripods and a PCADP system were used for the surveys. In 2006, two ADV systems deployed on the onshore and offshore of the shoal consisted of a pressure sensor and a downward-looking acoustic Doppler velocimeter. For one of the ADV systems deployed on the inshore station, two optical backscatter sensors (OBSs) were also equipped. The PCADP system deployed on the crest in 2006 comprised of a downward-looking pulse-coherent acoustic Doppler profiler, two optical backscatter sensors and a pressure sensor. In 2008, one ADV system with two OBSs was deployed north of Ship Shoal (SS08_1, see location in Figure 4.1) and one ADV system without OBSs and the PCADP system on the crest (SS08_2). The PCADP system deployed in 2008 consisted of a downward looking PCADP, two OBS sensors, two CTD sensors and upward-looking ADCP (Figure 4.3). The above instrument arrays have been widely used to investigate BBL characteristics all over the world (Cacchoine et al., 2006). All instruments recorded *in-situ* data discontinuously (i.e. burst mode) to maximize survey duration. Every hour, the instruments recorded 2048 bursts with sampling frequencies of 2 Hz for the PCADP system, 4 Hz for the ADV system with the OBSs and 10 Hz for the ADV system without the OBSs. Detailed instrument configurations are listed in Table 4.1. Bottom sediments and bottom water samples were collected during all deployment and retrieval cruises. In addition, more

sediment samples, plexiglass cores, and underwater camera images (SPI) were taken during collaborative benthic survey cruises.

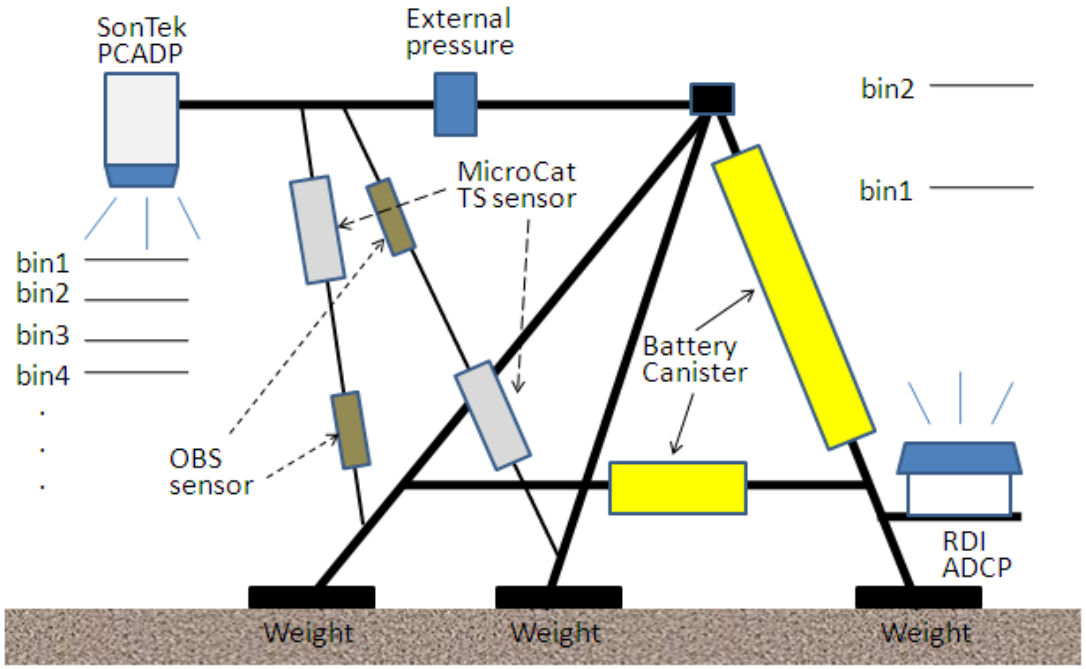

Figure 4.3 Schematic illustration of the PCADP system for 2008 deployment. Sensor heights of all instruments are listed in Table 4.1.

Table 4.1 Instrument configuration

Year	System	Instruments	Locations	Survey period	Sensor height
2006	**ADV (SS06_1)**	Druck™ Pressure Sensor D&A™ Optical Backscatter SonTek™ Acoustic Doppler Velocimeter	28º 56.284'N 90º 40.523'W	04/06 00:00 - 05/20 09:00 " "	90 cm 19, 78 cm 48 cm
	PCADP (SS06_2)	SonTek™ Pulse-Coherent Doppler Profiler D&A™ Optical Backscatter Druck™ Pressure Sensor	28º 53.701'N 90º 41.893'W	04/06 00:00 – 05/23 02:01 " "	116 cm 30, 61 cm 116 cm
	ADV (SS06_3)	ParoScientific™ Pressure Sensor SonTek™ Acoustic Doppler Velocimeter	28º 50.808'N 90º 41.307'W	04/06 00:00 -05/25 18:00 "	68 cm 47 cm
2008	**ADV (SS08_1)**	Druck™ Pressure Sensor D&A™ Optical Backscatter SonTek™ Acoustic Doppler Velocimeter	28 º 58.950' N 90 º50.406' W	02/10 00:00 - 03/23 13:30 " "	78 cm 41, 78 cm 47 cm
	PCADP (SS08_2)	SonTek™ Pulse-Coherent Doppler Profiler D&A™ Optical Backscatter Druck™ Pressure Sensor RDI™ ADCP Workhorse 1200 kHz MicroCat™ TS sensors	90 º 50.298' W, 28 º 53.018' N	02/10 00:00 -03/09 04:00 " " 02/10 00:00 -04/03 14:20 "	120 cm 35, 74 cm 120 cm 45 cm 30, 63 cm
	ADV (SS08_2)	ParoScientific™ Pressure Sensor SonTek™ Acoustic Doppler Velocimeter	28 º 53.023' N, 90 º50.302' W	02/10 00:00 03/30 11:30 "	66 cm 45 cm

4.4. Data Analysis

Prior to data analyses of *in-situ* measurements, all data were inspected regarding QA/QC. For the ADV and PCADP systems, the following criteria were used: (1) mean near bottom current velocity higher than 1.0 m/s were removed since such values are not realistic for the low-energy Louisiana coast even during severe winter storms; (2) all data with less than a 70% correlation (30% for mean currents) were removed; (3) data less than 15 decibel (db) signal-noise ratio (SNR) were removed. Criteria (2) and (3) are recommended by an instrument manufacturer (SonTek, 1997b; 2004). In addition to the automatic screening, all data were visually inspected and apparent outliers were removed.

Bulk wave parameters, spectra of waves and currents, and the BBLPs were computed from field data. Wave parameters and directional waves were computed based on the PUV method (Gordon and Lahmann, 2001). Current signals less than a 40 hour period were filtered out by using the 10^{th} order butterworth filter in order to examine sub-tidal (i.e. wind-induced) currents. The OBSs were calibrated to estimate suspended sediment concentration (SSC) using sampled bottom sediments and water following the procedure by Sheremet et al. (2005). Acoustic backscatter amplitude (ABS), a by-product of acoustic current meters, is known to be related to the SSC (e.g. SonTek, 1997) and the SSC profile was estimated from the ADV and PCADP ABS by comparing the ABS to the calibrated SSC results (Kobashi et al., 2007b). This method contains inevitable noises since the backscatter is corresponding not only to the SSC but also to sediment composition, grain size etc. (e.g. Gartner, 2002); however, this method has been widely used to estimate the SSC despite such disadvantages because of a cost-effective method and less influence on bio-fouling than the OBS (Garner, 2002; Kobashi et al. 2007a). Sediment grain size was analyzed by granulometric analysis and sedigraph (cf. Stone et al., 2006).

The BBLPs were calculated based on various algorithms. For the 2006 deployment in which the bottom sediment was predominantly silt and clay, the BBLP, namely shear velocity (u_*) and shear stress (τ), due to (1) waves, (2) currents, and (3) combined wave-currents were computed based on (1) linear wave theory (Madsen, 1976, equation 4-1), (2) the von-Karman Plandlt equation (equations 4-2&4-3) and quadratic stress law (Sternberg, 1972, equation 4-4), and (3) an empirical formulae proposed by Whitehouse et al. (2000) (equation 4-5), respectively. For the von-Karman equation, the following criteria were applied: (1) linear regression coefficient (r^2) for currents against depth (in log scale) needs to be higher than 0.98 (Wright et al., 1997); (2) maximal differences in current direction between velocity profiles need to be less than 20 degrees (Drake and Cacchoine, 1992). For stratified water, the BBLP from the von-Karman equation is overestimated and needs to be corrected using a stability parameter (Grant and Madsen, 1986; Glenn and Grant, 1987). However, because of a lack of available data, in this study, equation (4-2) was used to estimate the BBLPs. Under highly turbid water, it is reported that the bottom drag coefficient reduces significantly, which may cause shear stress to be overestimated (e.g., Li and Gust, 2000; Whitehouse et al., 2000; Thompson et al., 2006). In this study, the drag coefficient at 100 cm above the seabed (C_{D100}) for a muddy bottom (i.e. smooth bed) was selected as 0.0022 following Soulsby (1997) and Kobashi et al (In review, 2008a).

$$\tau_w = \rho_f u_{ob}\left(\nu\frac{2\pi}{T}\right)^{1/2}, u_* = \sqrt{\frac{\tau_W}{\rho}} \tag{4-1}$$

$$u(z) = \frac{u_*}{\kappa}\ln\left(\frac{z}{z_0}\right) \tag{4-2}$$

$$\tau_{cl} = \rho_f {u_*}^2 \tag{4-3}$$

$$\tau_{cq} = \rho_f C_{D100} {u_{100}}^2 \tag{4-4}$$

$$\tau_{wc\_m} = \tau_c \left[1 + 9.0 \left(\frac{\tau_w}{\tau_w + \tau_c} \right)^{9.0} \right] \quad (4\text{-}5)$$

For the 2008 deployment in which the sediment was predominantly sand, the following methods were used: (1) linear wave theory for wave shear stress (equation 4-1), (2) log-linear method (equations 4-2&4-3) and quadratic stress law (equation 4-4) for current shear stress, (3) Reynolds stress method (Green, 1992; Pepper, 2000) and an empirical formulae proposed by Soulsby (1997) (equation 4-6) for combined wave-current. The bottom drag coefficient at 100 cm above the seabed (C_{D100}) for ripple sand was selected as 0.0061 (Soulsby, 1997).

$$\tau_{wc\_s} = \tau_c \left[1 + 1.2 \left(\frac{\tau_w}{\tau_w + \tau_c} \right)^{3.2} \right] \quad (4\text{-}6)$$

Critical shear stress, above which bottom sediments are expected to be suspended, for non-cohesive sediments was calculated from grain size data based on the modified Yalin parameter (Li et al, 1997; Pepper, 2000) and was estimated as 0.153 Pa (Pascal) (=N m^{-2}) for the 2008 deployment. Maximum critical shear stress for cohesive sediments in this paper was determined as 0.15 Pa with reference to Wright et al. (1997) and Kerper, D. (personal communication, 2006); this value was used in Kobashi et al. (2007a), Kobashi et al. (2008) and Kobashi et al. (in review, 2008a) and shows reasonable results as Kobashi et al (in review, 2008a) suggest.

4.5. Results

4.5.1. Atchafalaya River Hydrology

The Mississippi River system is currently discharging freshwater and fluvial sediments mainly through two rivers, the Mississippi and Atchafalaya rivers. The main stream, Mississippi River discharges 70 percent of total freshwater and another 30 percent

from a distributary, the Atchafalaya River (Mossa, 1996; Roberts, 1997). Twelve-year records of river discharge at Simmesport, upstream on the Atchafalaya River as illustrated in Figure 4.4, showed high discharge in spring and low discharge during summer. There were two peaks of discharge: one in January and the other in April. High discharge in April was associated with ice melting in both the Rocky and Appalachian mountains with maximal discharge that exceeded 600,000 cubic feet per second (cfs) (=16,990 m^3 s^{-1}), which was more than three times higher than the threshold of high river discharge, 200,000 cfs (=5,663.4 m^3 s^{-1}) reported by Walker and Hammack (2000). While in the summer dry season, discharge was characterized as low.

In 2006, high river discharge occurred in late March and mid May (Figure 4.4). In winter 2008, river discharge was higher than the threshold between February and July with maximal discharge of 626,000 cfs (=17,726.3 m^3 s^{-1}) in mid April (Figure 4.4). Such high river discharge likely gives rise to debouching large quantity of fluvial sediments down to the receiving basin in spring (Kobashi et al, in review, 2008a).

4.5.1. Bed Characteristics

Bed characteristics for both deployments were analyzed based on bottom sediments sampled on site and plexi-glass cores taken in a 2005 biological cruise (Stone et al., 2005b) and sub-surface images from an underwater camera (SPI) taken during a biological cruise in 2006 as well as reports from divers (Stone et al., 2006). Figure 4.5 shows grain size distributions during the pre- and post-deployments in spring 2006 and winter 2008. Grain size distributions were remarkably different between the deployments. Sediments sampled when the arrays were deployed in spring 2006, were predominantly clay with the median grain diameter of 1.11 microns (1.11×10^{-6} m) (Figs 4.5 top and 4.6 bottom); while, sediments during post-deployment were fine sand with a median diameter of 127 microns (127×10^{-6} m) (Figures 4.5 top and 4.6 bottom). In the 2008 deployment, sediments for both pre- and

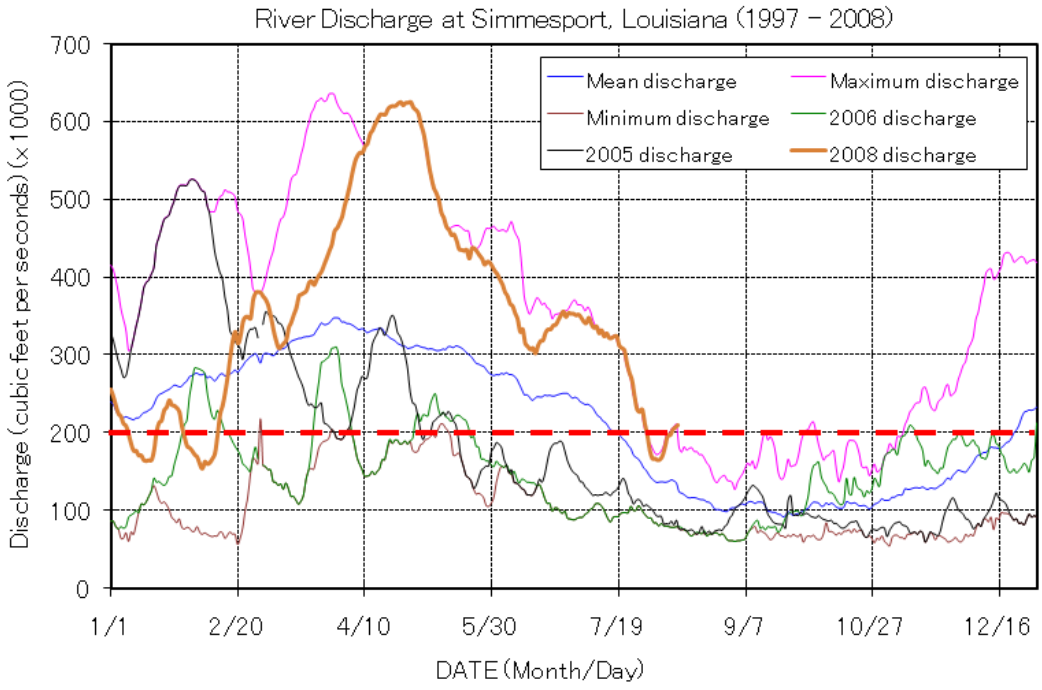

Figure 4.4 River discharge at Simmesport, Louisiana between 1997 and 2008 (Source: the U.S. Army Corps of Engineers, New Orleans District)

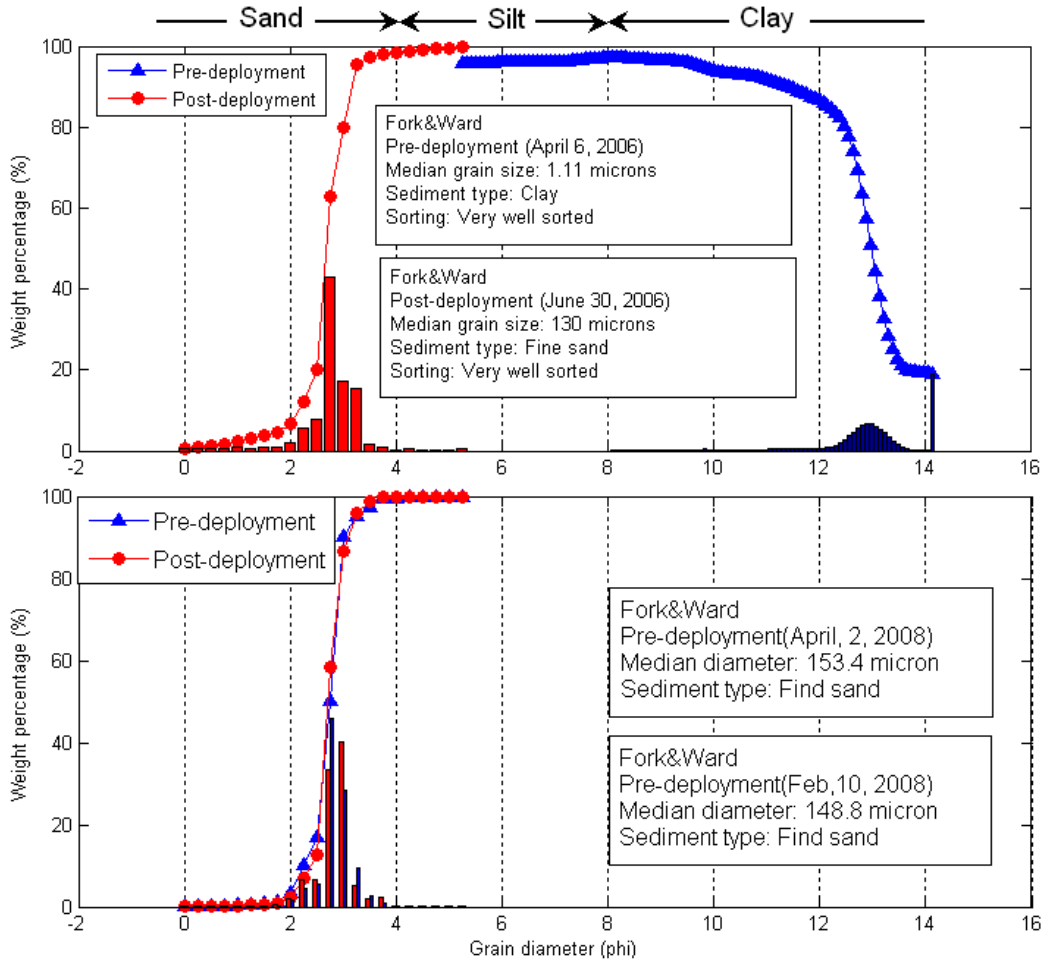

Figure 4.5 Grain size distribution for the 2006 (top) and 2008 deployments (bottom)

post-deployments were predominantly sandy with a median diameter of 153.4 microns (153.4 x 10^{-6} m) during the pre-deployment and 148.8 microns (148.8 x 10^{-6} m) during the post-deployment (Figure 4.5 bottom). However, sediments obtained from post-deployments in 2006 and 2008 also included a small amount of unconsolidated fluid mud on nearby survey locations. Sediments were obtained using plexiglass cores on the western shoal and were predominantly sandy; borrows, shells, and mud lens were evident (not shown). The images from the SPI showed distinct ripple formation and the geometry was determined as approximately 5 cm high and 15 cm long (i.e. ripple steepness ≈ 0.33).

4.5.2. Wave-Climate, and Variability of Currents and Sediment Concentration

In spring 2006 and winter 2008, over the deployment periods, a total of five and eleven winter storms passed over the study area (Table 4.2). Pepper and Stone (2004) discussed two distinct cold front types: AS storms (type A in Table 4.2) and MC storms (type B in Table 4.2). The AS storms are characterized by weak pre-frontal winds and strong post-frontal winds from northeast. The MC storms are characterized by fairly strong southerly winds during pre-frontal phases followed by strong northwesterly winds (Pepper and Stone, 2004). Of the storms, four and six storms were associated with the AC storms and one and five with the MC storms in the 2006 and 2008 deployments, respectively (Table 4.2). Predominant wind and wave direction was from the southeast during both deployments (Table 4.3); during storms, strong wind stress directed to the southeast, prevailed (Figures 4.7 and 4.8). Maximal wind speed attained 22 m s^{-1} and 19 m s^{-1} during the 2006 and 2008 deployments, respectively. Mean significant wave height was less than 1 m during both deployments; wave height increased as storms approached, exceeding 2 m over the shoal and the inner shelf (Table 4.3); however, the wave height on the inshore station was significantly lower than the height over the crest and offshore (55% and 46% for mean and maximum wave heights in the winter 2008, respectively; see Table 4.3).

Table 4.2 Number of winter storms for the 2006 and 2008 deployments. Type A is equivalent to AS storms and Type B is equivalent to MC storms by Pepper and Stone (2004)

	Total number	Type A	Type B
2006 deployment	5	4	1
2008 deployment	11	6	5

Low frequency swells (f < 0.2 Hz) were dominant during most of the deployment period; however, during the onset of storms and post-frontal phases, wind-induced high frequency seas (f > 0.2 Hz) responded quickly to storm winds as illustrated in Figures 4.7 and 4.8 (see also Sheremet et al., 2005; Stone et al., 2005a; Jose et al., 2007).

Sea surface slope and currents over the shoal were highly variable, but showed strong response to varying wind directions associated with winter storms for both 2006 and 2008 deployments (Figures 4.9 and 4.10). During the 2006 deployment, the storms passed on April 8th and May 10th and changed sub-tidal water level by 20 cm and 10 cm, respectively; the storm passed in late April and increased the water level by approximately 15 cm. During the former two storms, cross-shore currents (offshore and onshore) were generated. During the storm in late April, cross-shore near bottom currents were generated and yielded total net flux directed offshore. During the 2008 deployment, the sub-tidal water level decreased as fronts passed over the study area. Reduction in the water level was maximal when wind blew alongshore with a maximal change of 40 cm during the winter storm on March 7th and strong offshore currents were generated. This trend was also reported along the Gulf Coast (e.g. Cragg et al., 1983; Walker et al., 2001). Cross-shore sea surface slope estimated by water level differences between SS06_3 and CSI-5 in 2006 and between CSI-6 and CSI-5 in 2008, showed an influence of surface slope on wind and cross-shore currents. Pepper and Stone (2002) suggested that, based on bottom current data, that cross-shore sediment flux was offshore and onshore at an offshore and onshore stations, respectively; the net sediment flux during winter storms were directing offshore (Pepper and Stone, 2002). Such trends were detected from the data for the 2008 deployment; however, bottom currents varied depending on storm wind direction and consequent sea surface slope as well as due to the bottom topography (Kobashi and Stone, in prep, 2008b). Turbidity data (and SSC) for both deployments also varied with passages of winter storms.

Figure 4.6 Sampled sediments: (upper) sand and (lower) fluid mud

Table 4.3 Mean (top) and Maximal (bottom) values of physical parameters (at the shoal crest)

Year	Wind speed ($m\ s^{-1}$)	Wind direction (degree)	H_S (m) Off, Crest, In	T_P (sec) Off, Crest, In	Wave direction (degree) Off, Crest, In	Bottom C_{spd} ($m\ s^{-1}$) Off, Crest, In	Bottom C_{dir} (degree) Off, Crest, In	U_{orb} ($m\ s^{-1}$) Off, Crest, In
2006	5.9	166.6	0.46, 0.58, ND*	6.2, 6.0, ND*	- , 129.6, ND*	0.04, 0.02, 0.05	142.9, 145.3, 159.2	0.09, 0.13, ND*
	22.0	-	2.19, 2.32, ND*	9.8, 10.2, ND*	-	0.23, 0.26, 0.23	-	0.57, 0.81, ND*
2008	7.3	149.8	0.87, 0.83, 0.39	6.0, 6.3, 6.6	167.5,185.3,167.5	0.10,0.05,0.07	140.6, 180.3, 159.5	0.15,0.22,0.21
	19.1	-	3.42,2.96, 1.85	10.7,16.0, 12.8	-	0.31,0.30,0.43	-	1.02,1.38,1.12

*ND: No data. H_S: significant wave height, T_P: peak wave periods, C_{SPD}: Current speed, C_{dir}: Current direction, U_{orb}: bottom wave orbital velocity

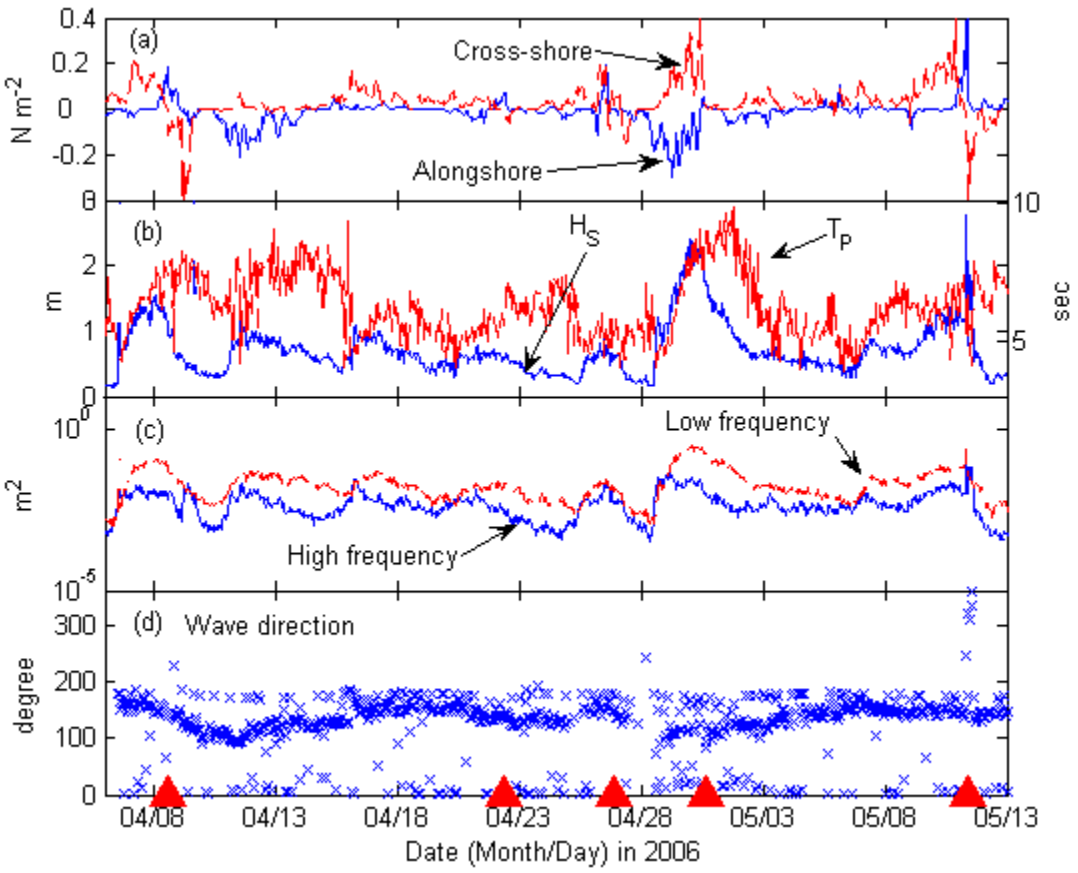

Figure 4.7 Time series of (a) wind stress, (b) wave height and peak period, (c) wave variance (high frequency (f>0.2 Hz) and low frequency (f<0.2Hz)), and (d) wave direction during the 2006 deployment

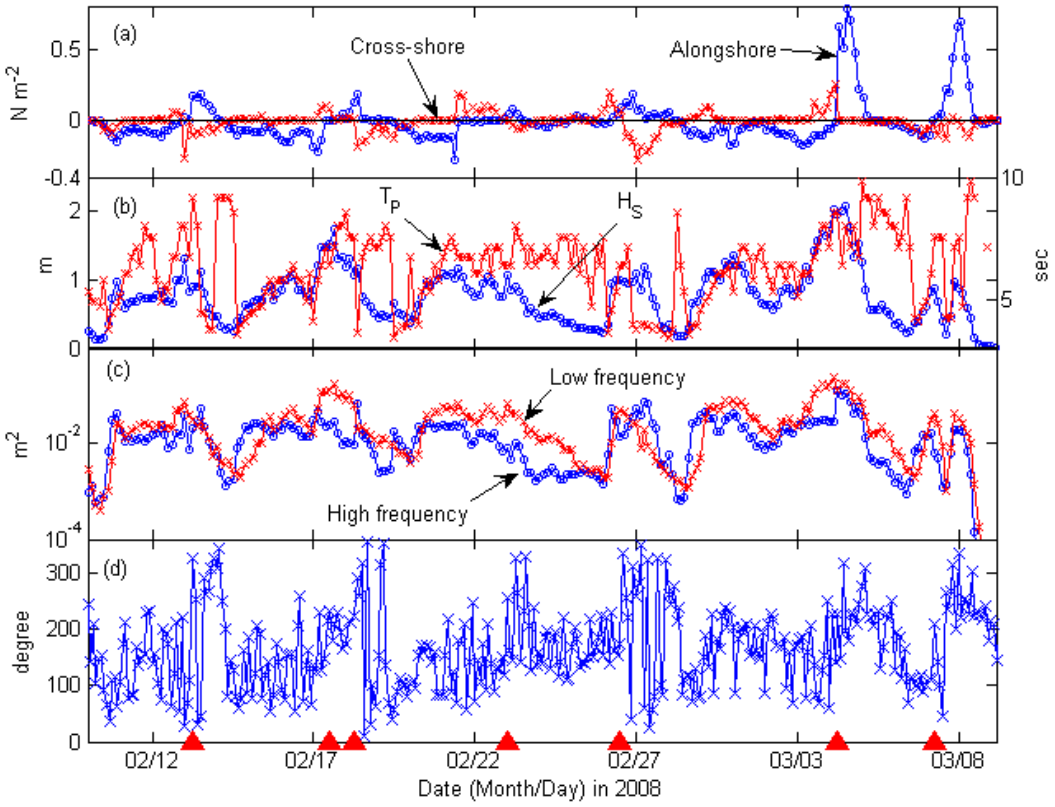

Figure 4.8 Time series of (a) wind stress, (b) wave height and peak period, (c) wave variance (high frequency (f>0.2 Hz) and low frequency (f<0.2Hz)), and (d) wave direction for the 2008 deployment

Turbidity increased during the onset of the storms and decreased in the wake of the storms; however, variations in the turbidity (and SSC) were different between the 2006 and 2008 deployments. For the 2006 deployment, a large portion of the bottom OBS sensor recorded values approaching zero during fair weather. This is likely attributed to the sensor burial into fluid mud as discussed in detail in section 4.6.2.1. The upper turbidity concentrations were usually higher than those recorded lower in the water column: for the 2008 deployment, on the other hand, the upper turbidity was almost always lower than lower turbidity levels.

Bed elevation change was also be directly related to winter storms; increase in the bed elevation corresponded to high river discharge or a post river discharge phase. Decreases in the elevation of approximately 20 cm followed by a 30 cm increase in the elevation, recorded during a storm in late April, 2006. The bed elevation change in winter 2008 was small except on March 5th, 2008 (Figure 4.10). A detailed discussion is presented in section 4.6.1.

4.5.3. Bottom Boundary Layer Characteristics

Variations in the BBLPs correspond to the passage of winter storms. Compared to Figures 4.9 and 4.11 and Figures 4.10 and 4.12, there is a strong correlation between changes in the shear stress, particularly wave-induced shear stress (τ_w), and turbidity (and SSC). When the storms passed the study site, shear stress increased as wave height, wave period, and bottom currents increased, and finally reached the threshold value (i.e. critical shear stress) above which bottom sediment was suspended; waves and currents began to re-suspend the bottom sediments. Increase in the shear stress above the threshold value was consistent with increase in the SSC. Shear stress during fair weather in spring 2006 was largely lower than that during the 2008 deployment. Findings during the 2008 deployment also show similar results; however, the trend during a significant portion of the deployment period in winter 2008 is characterized by higher

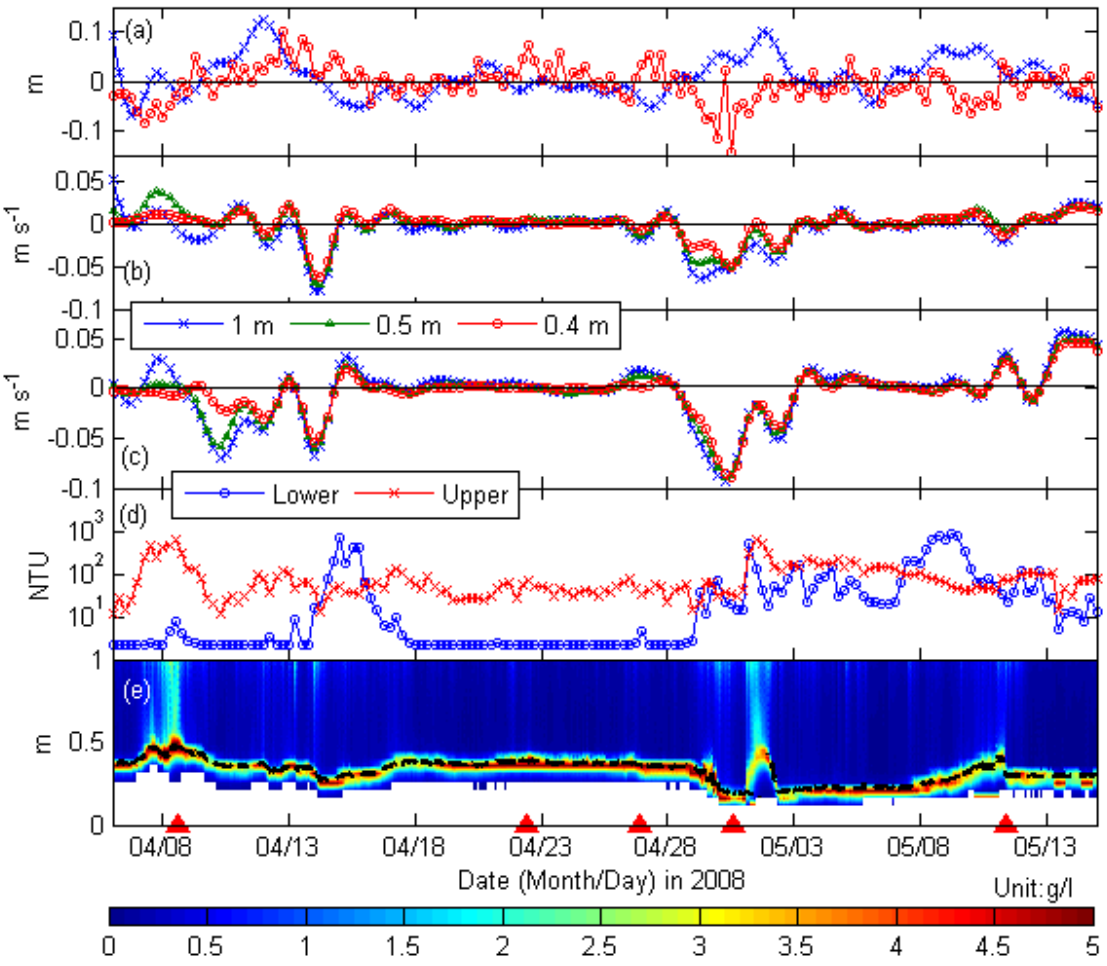

Figure 4.9 Time series of (a) adjusted water level and cross-shore sea surface slope, (b) alongshore current, (c) cross-shore current, (d) OBS (0.3 m and 0.61 m above the bottom) and (e) SSC profile (2006 deployment)

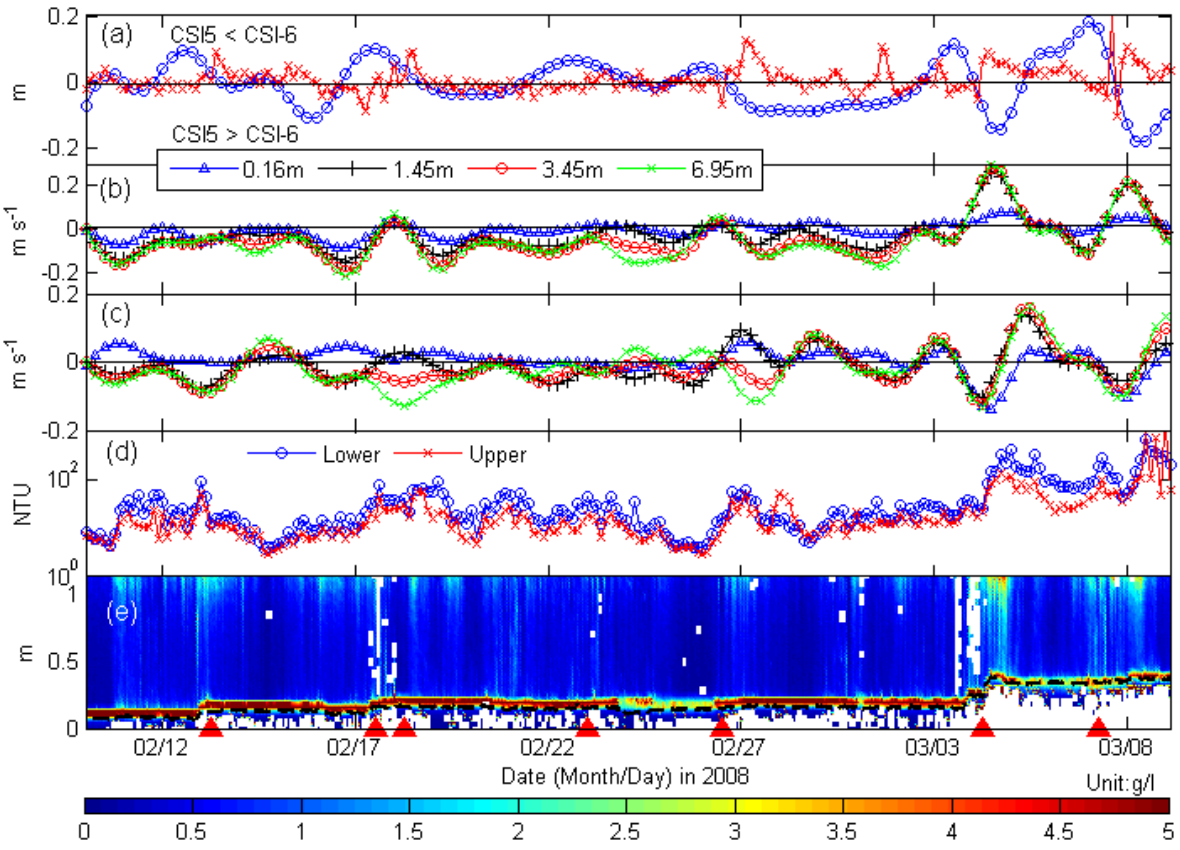

Figure 4.10 Time series of (a) adjusted water level and cross-shore sea surface slope, (b) alongshore current, (c) cross-shore current, (d) OBS (0.35 m and 0.74 m above the bottom) and (e) turbidity profile (2008 deployment)

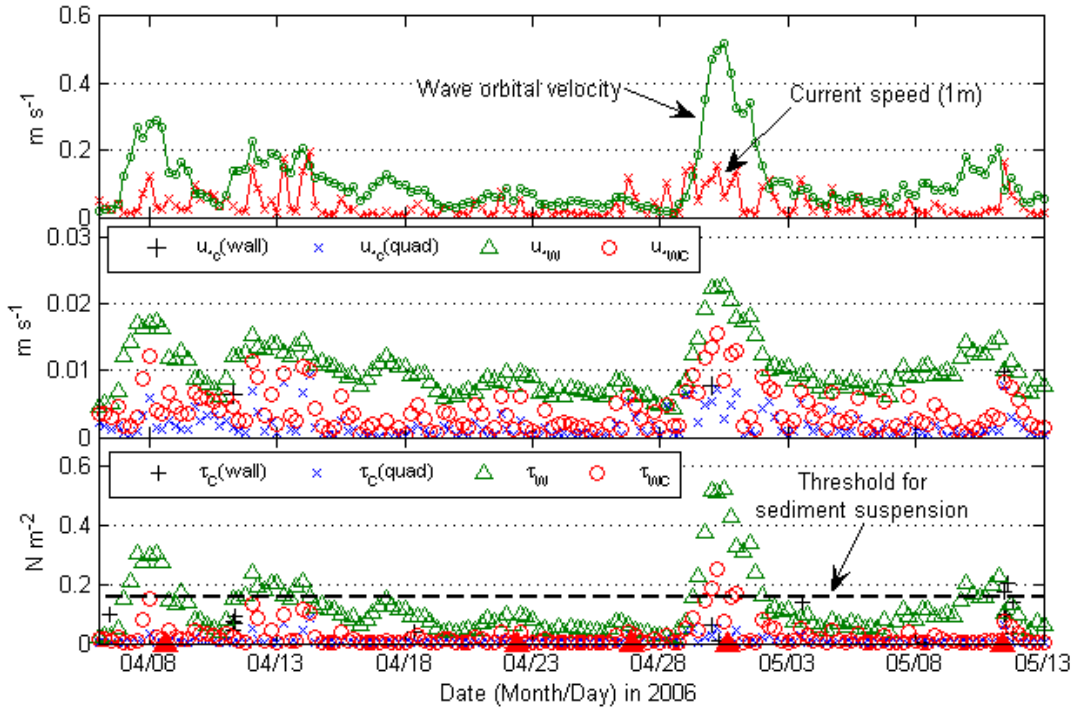

Figure 4.11 Time series of (a) wave orbital velocity and current speed (1m), (b) shear velocity, and (c) shear stress. The dashed line on the bottom figure shows the threshold for sediment suspension. Passage of winter storms is shown as shaded triangle on the bottom figure (2006 deployment)

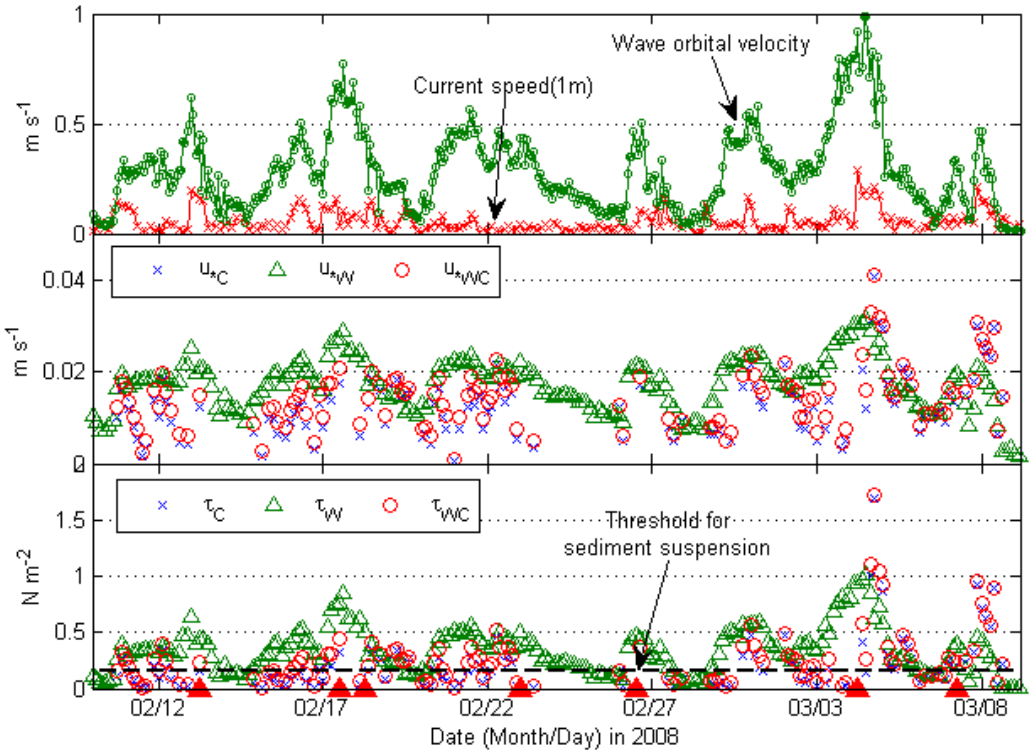

Figure 4.12 Time series of (a) wave orbital velocity and current speed (1m), (b) shear velocity, and (c) shear stress. The dashed line on the bottom figure shows the threshold for sediment suspension. Passage of winter storms is shown as shaded triangle on the bottom figure (2008 deployment)

wave shear stress than the threshold, even during non-storm conditions. A noticeable difference between results of both deployments is that shear stress was higher than the threshold value only during storms during the 2006 deployment; shear stress data obtained from the 2008 deployment was conspicuously higher than the threshold during most of the deployment. The reason for the difference is discussed in section 4.6.2.

4.6. Discussion

4.6.1. Sediment Heterogeneity due to Fluvial Fine Sediments and Winter Storms

Results of grain size analysis in spring 2006 and winter 2008 indicate conspicuous difference in bed characteristics between the two deployments (Figure 4.5). A satellite image during a pre-frontal phase, on April 4th, 2006 (Figure 4.13a), captured westward transport of fluvial sediments. On April 8th, 2006, during a post-frontal phase (Figure 4.13b), the transport trend had shifted from the west to southeast due to the post-frontal wind fields, which generated wind-induced southeast currents that pushed water and sediment offshore and eventually the plumes reached the shoal. During this period ((1) in Figure 4.13d), the PCADP measured approximately a 15 cm increase in the bed elevation and 2.5 g/l of SSC at SS06_2. A similar situation occurred in mid May, during which approximately a 15 cm increase in the bed elevation and 0.5 g/l of SSC were recorded ((3) in Figure 4.13d&e). Both shifts corresponded to high river discharge at Simmesport, LA, upstream of the Atchafalaya River (Figure 4.13c) following the peak discharge. In late April when a cold front passed over south-central Louisiana ((2) in Figure 4.13), a distinct characteristic was detected; strong winds blew from the southeast, in contrast to the aforementioned two storms resulting in insubstantial fluvial sediment supply as detected by the satellite imagery (not shown). However, during this period, substantial bottom sediment reworking during the pre-frontal phase followed by significant accumulation of the sediment (i.e.

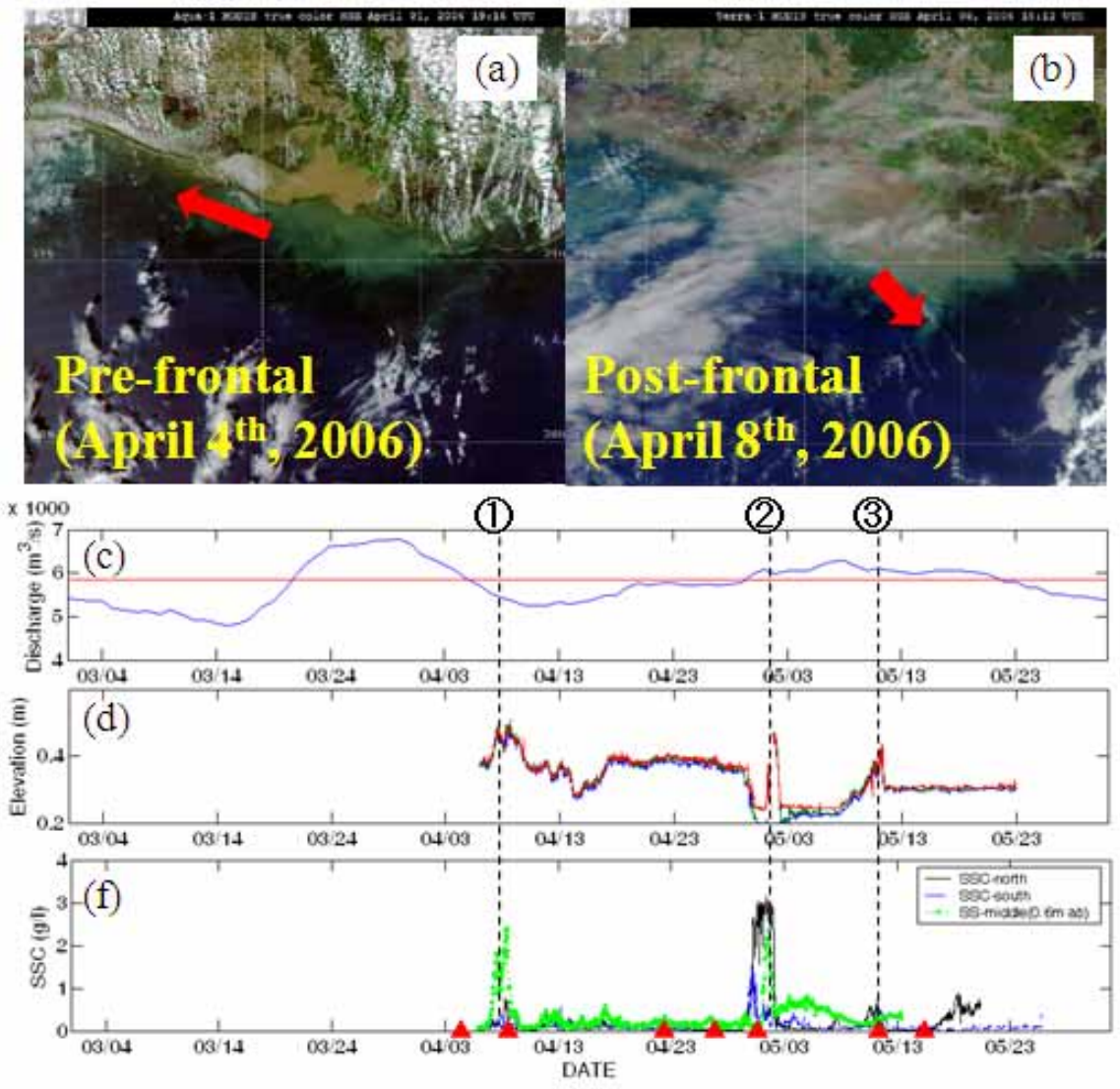

Figure 4.13 Satellite images during a pre-frontal phase (a) and a post-frontal phase (b) along with river discharge (c), bottom elevation at the SS06_2 (d), and SSC (f). Red line in (c) shows the border between high and low discharge suggested by Walker and Hammack (2000). The numbers, (1) and (3) represent passages of winter storms that accompany sediment supply from the Atchafalaya River. The number, (2) represent a passage of winter storms that does not accompany sediment supply from the river.

fluid mud) during the post-frontal phase occurred. More detailed mechanisms are addressed in section 4.6.2.

This pattern of sediment supply was further corroborated by Kobashi et al (In review, 2008a) which investigates the dispersal shifts associated with winter storms using prolonged *in-situ* data collected from the vicinity of the Atchafalaya River and using satellite imagery. The study concluded that post-frontal wind induces strong southeast currents in concert with an enhanced bottom sediment re-suspension, transporting the fluvially-derived sediments further southeast. All aforementioned evidence clearly supports that the post-frontal wind and high river discharge contribute to the sediment heterogeneity on the shoal. During the spring 2006 deployment, a total of five storms passed over the study area and eventually two of them yielded the dispersal shifts which reached the shoal. During the deployment in winter 2008, a total of 11 storms passed over the study area and approximately five of them caused dispersal shifts which eventually reached the shoal. However, during the winter 2008, bottom sediments were predominantly sandy during most of the deployment period given strong meteorological forcing and a shallower water depth except around March 5th when fluid mud accumulation was evident. This likely happened because of strong downwelling currents (not shown) which seems to enforce the accumulation rather than fluid mud settling (see Figure 4.10e).

Fine sediment transport from offshore is another possible factor that has to be addressed here; however, the sediment supply from offshore is not thought as significant as the fluvial sediment supply from the Atchafalaya because sediment re-suspension on the outer shelf is thought to be significant only during severe storms, given the fact that the depth of the surrounding shelf is much deeper than that of the shoal and thus sediment re-suspension offshore is less significant than that on the shoal. We computed sediment re-suspension intensity (RI),

defined as the wave shear stress minus the critical shear stress, at CSI-15 off Ship Shoal (17 m isobath) and CSI-6 located southeast of Ship Shoal (20 m isobath); the intensity was *on average* 70 and 81 percent lower than that on the shoal crest (SS08_2), respectively. The RI was positive during severe storms; net cross-shore sediment flux during winter storms are largely offshore; however, a small portion of fine sediment may have been transported to the shoal during pre-frontal phases, but is not considered to yield significant changes in bed characteristics. This is further corroborated by a numerical model analysis conducted by Kobashi et al (In preparation, 2008b). Thus, it is concluded that sediment supply from the mid-/outer shelf is limited during severe extra- and tropical storms (off-shoal wave height > 4 m according to Kobashi et al., in preparation, 2008b).

Spatial distributions of fluid mud on the shoal are highly complicated given the following reasons; (1) bottom sediment types during the 2006 deployment changed drastically as already mentioned; however, we also found evidence of fluid mud on the proximity of the deployment area during the retrieval cruise. In winter 2008, we also sampled small amounts of fluid mud on the other side of the platform from our tripod on the crest, which is roughly less than 50 meter apart; (2) During our collaborative biological cruises, any evidence of fluid mud from box cores were not found from the shoal bottom although there is a possibility that the box cores did not capture unconsolidated fluid mud (Winans, W., personal communication, 2007); (3) frequencies of winter storms are higher than the frequency of dispersal shifts which eventually reached the shoal (Kobashi et al, in prep., 2008a). The above reasons suggest that the spatial distribution of fluid mud on the shoal is patchy possibly due to complex shoal bathymetry (i.e. irregularity of the shoal bottom).

4.6.2. Wave-Current-Bottom Sediment Interactions over the Shoal during a Storm

As mentioned in the previous sections, shoal bed characteristics and associated bottom boundary layer dynamics are remarkably different depending on the predominant sediment regime. Those differences create two distinct morphodynamic characteristics over the shoal, and which are discussed in the following sub-sections.

4.6.2.1. Fluid Mud Bottom (2006)

In spring 2006, the instrument arrays and satellite images captured the signal that fluvial fine sediments debouched from the Atchafalaya River, in a form of fluid mud, were accumulated onto the shoal in the wake of storms. The accumulated fluid mud further interacted with hydrodynamic forcing associated with winter storms. In late April, 2006, a strong winter storm passed over the study area and the arrays captured a unique wave-current-fluid mud interaction scenario (Figure 4.14 (a)-(k)).

Prior to the storm passage, a thin layer of fluid mud likely existed on the shoal with an approximate thickness of 30 cm and 15 cm for partially consolidated (brown shaded area in Figure 4.14i) and the least consolidated (gray shaded area in Figure 4.14i) fluid mud layer, respectively. This thickness is in general agreement with the report from a diver during the instrument deployment (Depew, D. personal communication, 2006). When the next cold front approached, wave height increased and sediments were re-suspended from the sea floor once the shear stress exceeded the critical value above which bottom sediment was suspended (Fig 4.14e); this was consistent with an increase in the bottom turbidity shown by the OBS sensors (Figure 4.14f).

Sediment transport rates integrated from bottom to the sensor height, approximately 1 m, were then elevated due to increased high storm-induced currents and sediment re-suspension

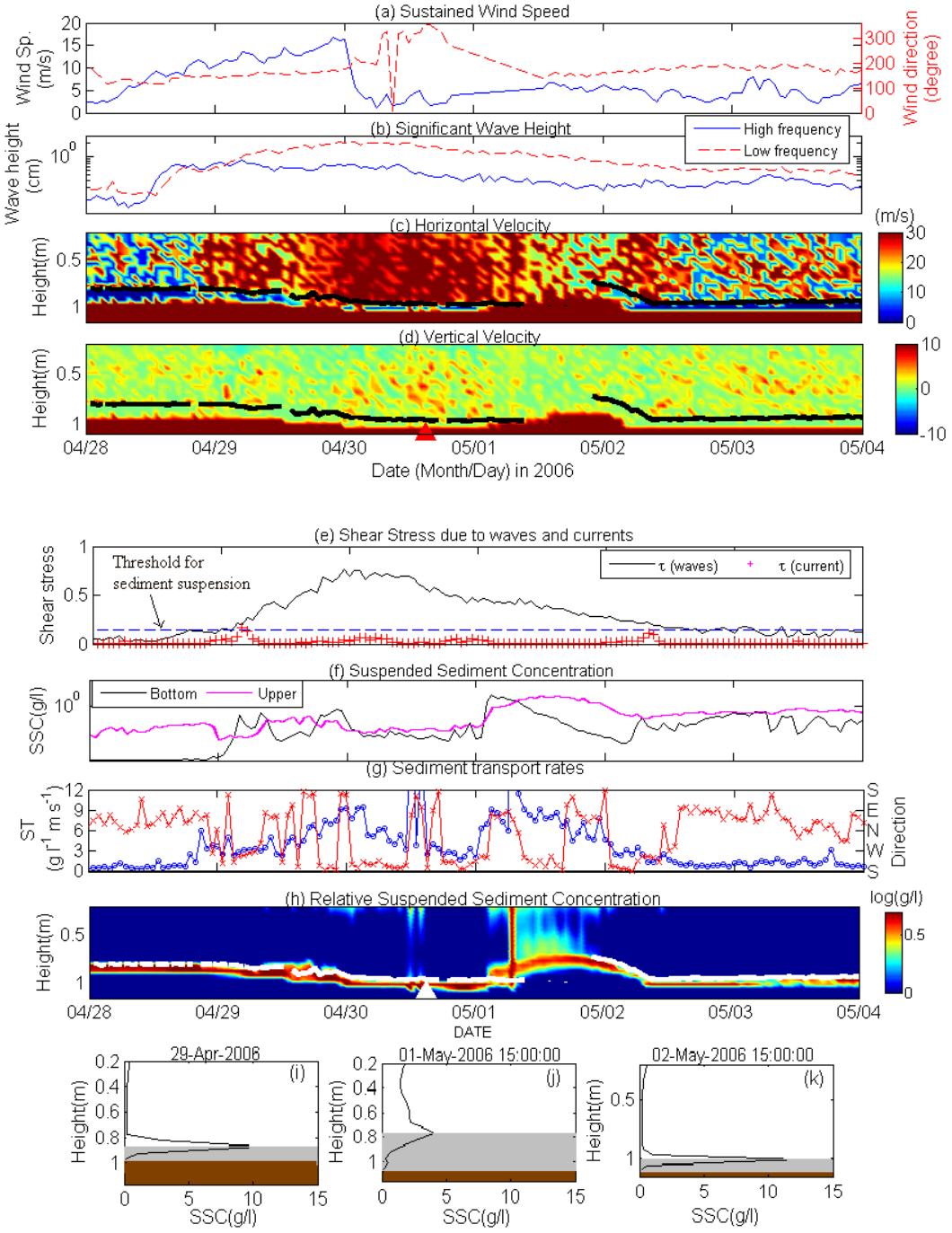

Figure 4.14 Time series of (a) wind speed and direction, (b) wave height, (c) horizontal current profile (d) vertical current profile (e) shear stress, (f) upper and lower SSC (g) sediment transport rates, (h) SSC profile (log scale), and (i)-(k) SSC profiles

(Figure 4.14c and g), reaching approximately 9.0 kg m^{-1} s^{-1}, more than an order of magnitude higher than numerically-derived sand transport rates (~0.1 kg m^{-1} s^{-1}) when the bottom sediment is fine sand and ripple steepness is 0.33. Such high sediment transport rates resulted in a 20 cm reduction in the bed elevation (i.e. sediment reworking). When the front passed, strong vertical mixing occurred and suspended sediments were mixed vertically upward due to a positive vertical velocity, resulting in shifting the SSC maxima upward (Figure 4.14d and j) and lowering the upper and bottom SSCs (Fig 4.14f) and consequent transport rates (Figure 4.14g). During the post-frontal phase, the mixed sediment was gradually re-settled out in the wake of the storm as the wave height and current velocity decreased; however, the upper turbidity remained high in spite of a reduction in the lower turbidity; this is probably because settling was significantly hindered due to the formation of large flocs that interfere each other (Figure 4.14f). During this time, the sediment transport rates were high (~10 kg m^{-1} s^{-1}) given the high SSC in spite of weak currents. Despite such high transport rates, a portion of the mixed sediments were re-deposited on the bottom with a reduction in thickness of the fluid mud layer than was apparent during the pre-frontal phase (brown and grey areas in Figure 4.14i and k) because a portion of the reworked sediments was likely transported outside of the shoal as indicated by high sediment transport rates during the post-frontal phase (Figure 4.14g). Net fluid mud flux was directed offshore during the storm.

4.6.2.2. Sandy Bottom (2008)

In contrast to results obtained in spring 2006, bed type on the shoal in winter 2008 was predominantly sandy (Figures 4.5 bottom and 4.6 top). Basic hydrodynamic characteristics were similar to those during the spring 2006 deployment, as illustrated in Figure 4.15. Wave-current-bottom interaction over the sandy bottom was conspicuously different from those in spring 2006.

From a limited number of underwater camera images, wave ripples were likely formed on the shoal when the bottom was dominated by sand. In mid February, 2008, when a cold front approached the study area, wave height and current speed increased. Shear stress also increased and finally exceeded the threshold for sediment suspension (see also Figure 4.15e), the sign of incipient bottom sediment suspension. Turbidity values increased as wave height (and shear stress) increased (Figure 4.15b&f). Vertical velocity was highest when the storm passed (Figure 4.15d), and the suspended sediments were vertically mixed, consistent with increases in the upper and lower turbidities (Figure 4.15e&f). Sediment transport rates were high because of high horizontal current speeds and high turbidity; and net transport flux was directed offshore (i.e. south) during the storm (Figure 4.15g). When storms passed the study area, ripples are often washed out due to strong waves and currents (i.e. sheet flow). Soulsby (1997) addressed a ripple washout criterion and estimated that the ripples can be washed out when the mobility number exceeds approximately 150. Taking this into account for the 2008 deployment, the ripples were possibly washed out when near-bottom wave orbital velocity exceeded 0.6 m s^{-1} on the middle shoal crest.

There were four events during which the orbital velocity exceeded the threshold value, all being consistent with winter storms. In the waning phase of the storm, the re-suspended sediments were re-deposited due to decreasing wave height and current velocities attributable to post-frontal conditions. The ripples that were washed out during the storm were likely reformed during this phase. Grain settling for sand is remarkably different from that for cohesive sediments that undergo three stages: free settling, flocculation and hindered settling (Mehta, 1991; Sheremet et al., 2005; McAnally et al., 2007). Grain settling of sand follows Stokes law and the settling velocity is approximately 0.015 m s^{-1} (i.e. 1.5 cm s^{-1}, approximately 100 cm

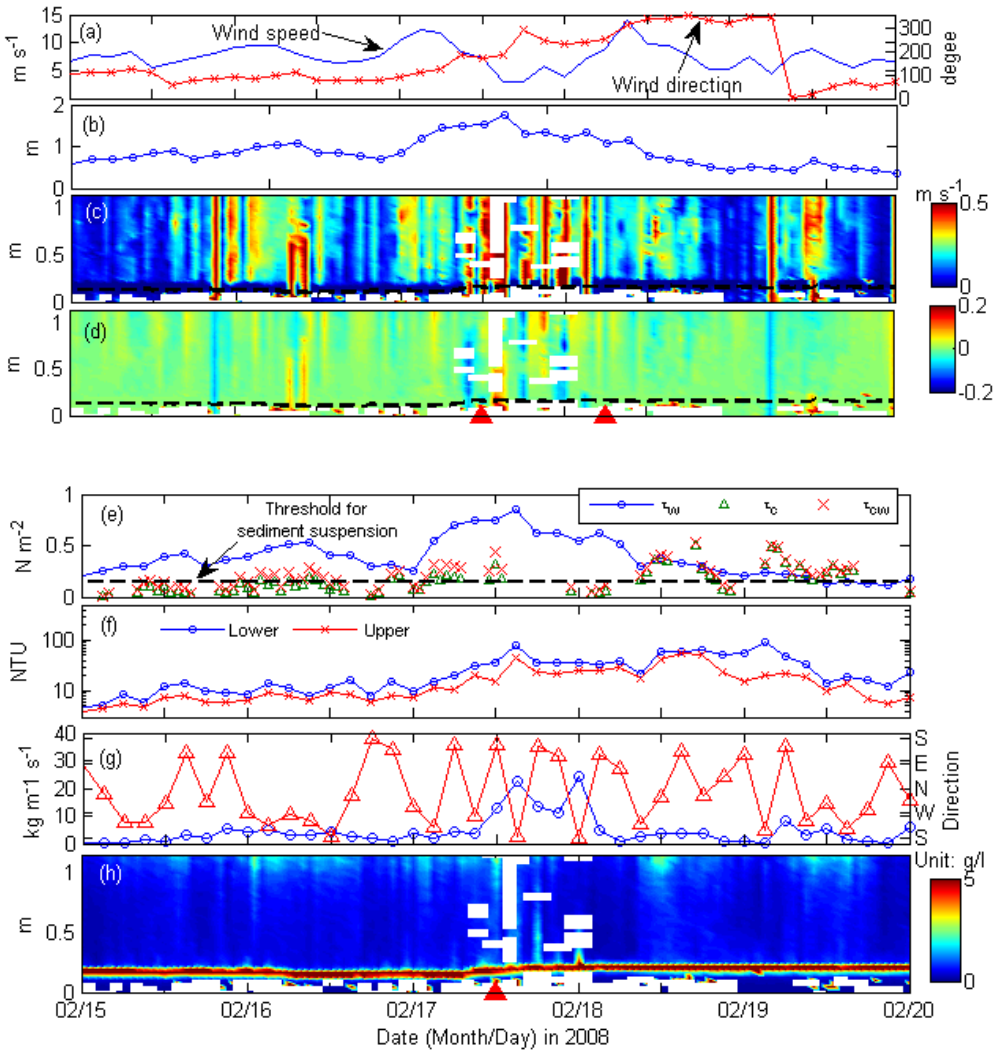

Figure 4.15 Time series of (a) wind speed and direction, (b) wave height, (c) horizontal current profile (d) vertical current profile (e) shear stress, (f) upper and lower SSC (g) sediment transport rates, and (h) SSC profile (log scale)

minute^{-1}) based on sediments sampled for the 2008 deployment, which is, as a first-order approximation, at least two orders higher than the maximum settling velocity for fluid mud (in the form of flocculation from Sheremet et al, 2005). Pepper and Stone (2004) estimated 0.6 kg m^{-1} s^{-1} (AC storms) and 1.0 kg m^{-1} s^{-1} (MC storms) of numerically-derived sand transport rates (Grant-Madsen-Rouse algorithm) based on their deployment on the western flank of Ship Shoal in 1998. In winter 2008, maximum sand transport rates (Engelund-Hansen total transport equation) of 0.015 kg m^{-1} s^{-1} were computed on March, 4th, 2008.

4.6.3. Sediment Exchange and Implication for Potential Sand Mining Impacts

Ship Shoal is exposed to recurring sandy and muddy bottoms and shows two contrasting sediment exchange scenarios depending upon predominant bed characteristics, as illustrated in Figures 4.16 and 4.17. Such unique sediment exchange processes are summarized below.

Whether the sea bed is fluid mud or not is dependent upon the balance between sediment supply and sediment loss (i.e. sediment reworking). Sediment supply, as already discussed above, is associated with fluvial sediment discharge from the Atchafalaya River and winter storm conditions. When the sediment influx from the Atchafalaya River occurs in tandem with the post-frontal phase of the winter storms, sediments are transported further southeast and are occasionally accumulated on the shoal in the wake of the storms. Given the frequency of winter storms, the fluid mud is not likely to get enough time to become permanently consolidated mud and resistant to re-suspension and transport by waves and currents. When another winter storm approaches and then passes over the study area, bottom sediments undergo re-suspension, mixing, hindered settling and re-distribution (Figure 4.16). Settling undergoes three stages: free settling, flocculation and hindered settling depending on sediment concentration (Mehta, 1991; McAnally et al, 2007).

The morphodynamic processes are dominated by the prevailing waves, bottom currents and the water depth. Measured data suggest that even if waves are not strong enough to suspend fluid mud, weak currents can potentially transport a portion of upper-layer unconsolidated fluid mud during weak storms.

When the sediments are predominantly sandy, shoal bottom undergoes sediment re-suspension, vertical mixing, and settling; the BBLDs follow conventional approaches (cf. Grant and Madsen, 1986), though the sediments may contain a small portion of fine-grained materials. Settling follows conventional Stokes settling and the settling velocity is much faster than the fluid mud settling. Another survey data set suggests that wave ripples are formed with an approximate dimension of 5 cm high and 15 cm long on the shoal. Those ripples are disturbed by storm waves and currents and eventually washed out when orbital velocities become high under sheet flow conditions (bottom orbital velocity reached greater than 0.6 m s^{-1} during the 2008 deployment).

The above discussion gives some insight regarding environmental impacts of future potential sand mining from the shoal; especially on the physical processes. As we have discussed above, alteration in water depth is considered to be an important factor for shoal morphodynamics. If large scale dredging is authorized and thus substantially alters the shoal bathymetry, the changes may eventually enhance fluid mud accumulation on the shoal, increasing bottom turbidity and changing bed characteristics and consequently become detrimental for the benthic communities. This is discussed in greater detail in Kobashi et al. (In preparation, 2008b) by means of a-state-of-the-art numerical model implementation and the preliminary results support the above hypothesis. Therefore, it is suggested that sand dredging needs to be carefully planned to minimize physical and biological impacts,

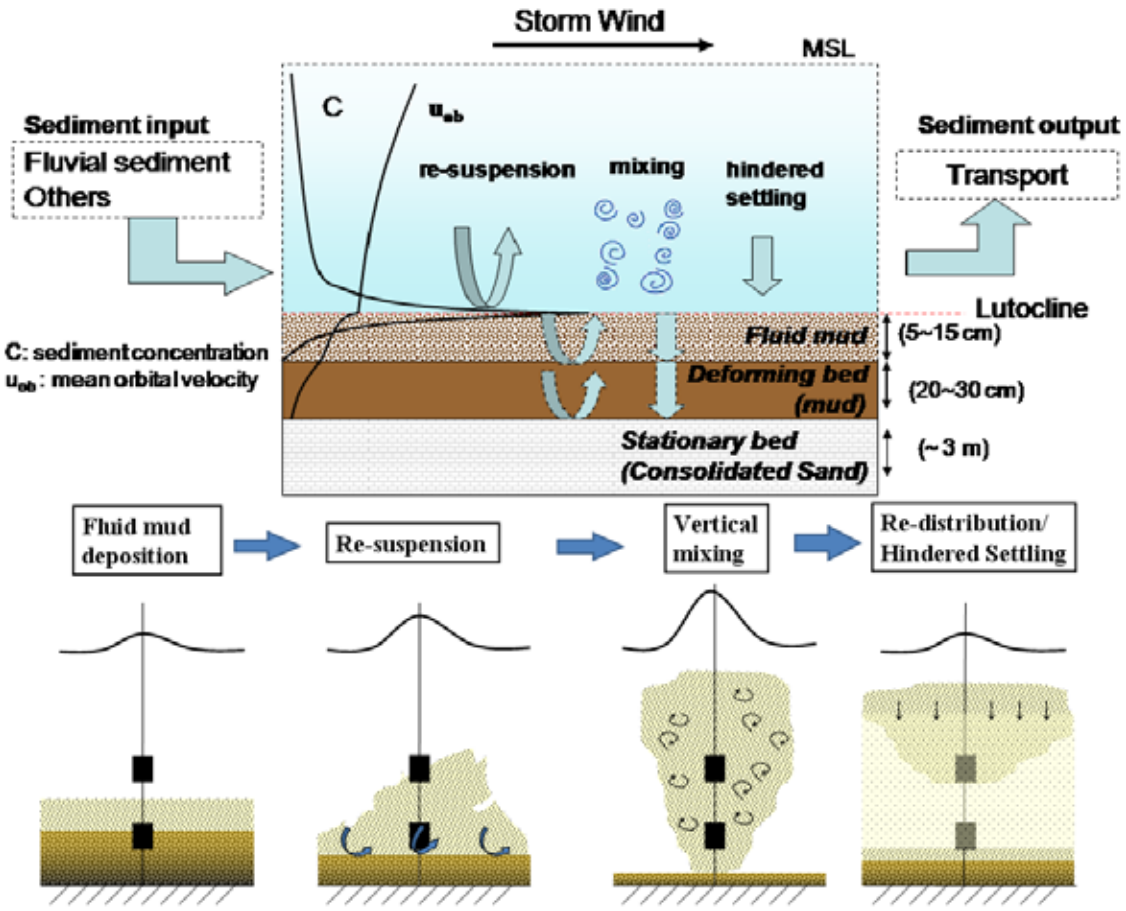

Figure 4.16 Schematic illustration of sediment exchange on Ship Shoal during fluid mud regime

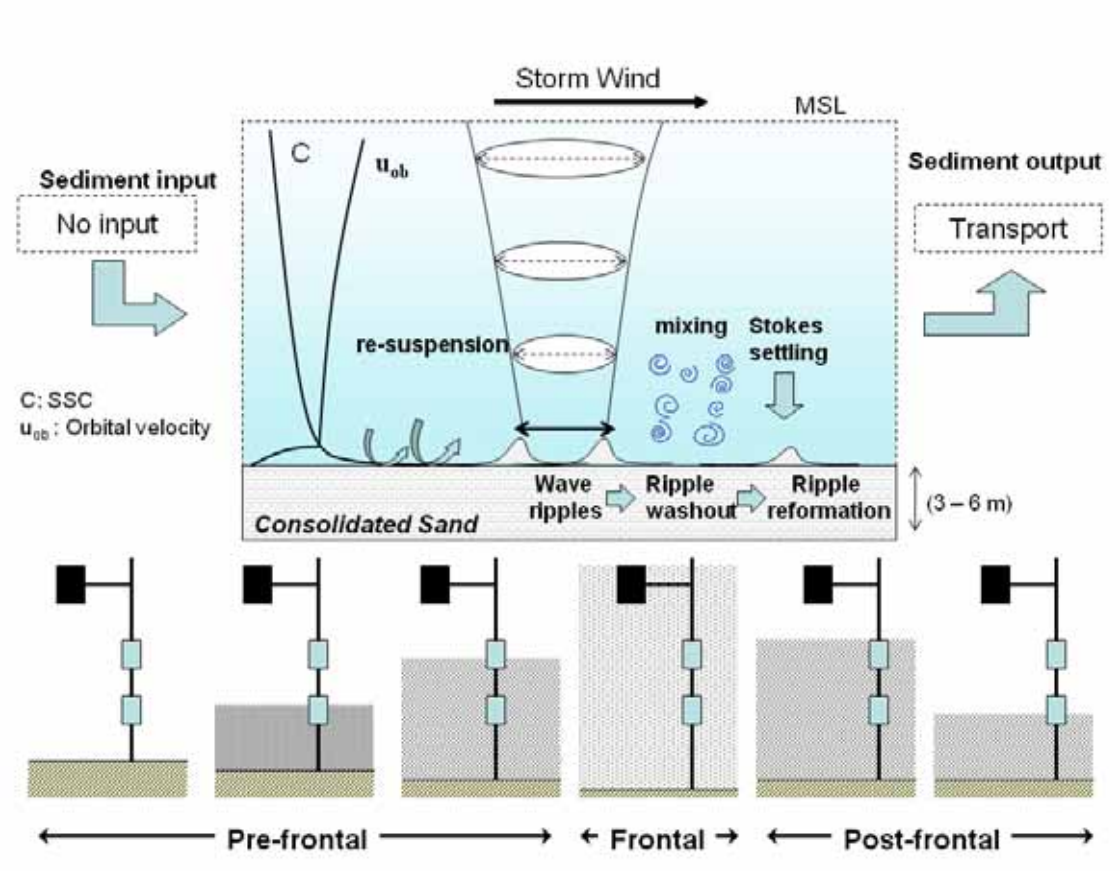

Figure 4.17 Schematic illustration of sediment exchange on Ship Shoal during sand regime

particularly in terms of protecting the endemic shoal benthic habitats. The shoal has been recently recognized as a biological hotspot for blue crabs and also an oxygen refugee for benthic organisms, particularly during the summer hypoxia season (Condrey and Gelpi, 2008; Grippo et al. submitted).

4.7. References in Chapter 4

Adams, C. E., Swift, D.J., Coleman, J.M. ,1987. Bottom currents and fluviomarine sedimentation on the Mississippi prodelta shelf: February-May 1984, *Journal of Geophysical Research*, Vol.92(C.13),14,595-14,609.

Allison, M.A., Sheremet, A., Goñi, M.A., Stone, G.W., 2005. Storm layer deposition on the Mississippi-Atchafalaya subaqueous delta generated by Hurricane LILI. *Continental Shelf Research*, 25, 2213-2232.

Cacchoine, D.A., Grant, W.D., Drake, D.E., Glenn, S. 1987. Storm-Dominated Bottom Boundary Layer Dynamics on the Northern California Continental Shelf: Measurements and Predictions, Journal of Geophysical Research, VOL. 92, NO. C2, 1817–1827.

Cacchoine D.A., Sternberg, R.W., Ogston, A.S. 2006. Bottom instrumented tripods: History, Application and Impacts. Continental Shelf Research, 26, 2319-2334.

Chuang, W-S., and Wiseman, W.J., Jr. 1983. Coastal Sea Level Response to Frontal Passages on the Louisiana-Texas Shelf. *Journal of Geophysical Research*, 88 (C4), 2615–2620.

Cipriani, L.E., Stone, G.W. 2001. Net longshore sediment transport and textural changes in beach sediments along the southwest Alabama and Mississippi barrier islands, U.S.A. *Journal of Coastal Research*, 17 (2), 443-458.

Cochrane and Kelly, 1986. Low-frequency circulation on the Texas-Louisiana continental shelf. *Journal of Geophysical Research*, 91 (C9), 10645-10659.

Condrey, R. and Gelpi, C. 2008. Blue crab (*Callinectes sapidus*) use of the Ship/Trinity/Tiger Shoal Complex as a nationally important spawning/hatching/foraging ground: Discovery, evaluation, and sand mining recommendations. MMS final report. 41pp.

Cragg, J., Mitchum, G., and Sturges, W. 1983. Wind-induced sea surface slopes on the west Florida shelf. *Journal of Physical Oceanography*, 13, 2201-2212.

DiMego, G.J., Bosart, L.F., and Endersen, G.W., 1976. An examination of the frequency and mean conditions surrounding frontal incursions into the Gulf of Mexico and Caribbean Sea. *Monthly Weather Review*, 104,709-718.

Drake, E. D. and Cacchione, D. A., 1992, Wave-Current interaction in the bottom boundary layer during storm and non-storm conditions: observations and model predictions, *Continental shelf research*, Vol.12, No.12, 1331-1352.

Friedrichs, C.T., Wright, L.D., Hopworth, D.A. and Kim, S.C., 2000, Bottom-boundary-layer processes associated with find sediment accumulation in coastal sea and bays, *Continental Shelf Research*, 20, 807-841.

Gartner, J.W., 2002. Estimation of suspended solids concentrations based on acoustic backscatter intensity: theoretical background, Turbidity and Other Sediment Surrogates Workshop, April 30 – May 2, 2002, Reno, NV. 4p.

Georgiou, I.Y., FitzGerald, D.M., and Stone, G.W., 2005. Impact of physical processes along Louisiana coast. *Journal of Coastal Research*, SI 44, 72-89.

Gordon, L. and Lohmann, A. 2001. Near-shore Doppler current meter wave spectra. Proceeding of *Waves 2001*, San Francisco, USA.

Glenn, S.M. and W.D. Grant, 1987. A Suspended Sediment Stratification Correction for Combined Wave and Current Flows. *J. Geophysical Res.* 92(C8): 8244-8264.

Grant, G.D. and Madsen, O.S., 1986. The continental-shelf bottom boundary layer. *Annual review of fluid mechanics*. 18, 265-305.

Green, M.O.,1992. Spectral Estimates of Bed Shear Stress at Subcritical Reynolds Numbers in a Tidal Boundary Layer. J. Phys. Oc. 22: 903-917.

Green, M. O., Vincent, C. E., McCave, I. N., Dickson, R. R., Rees, J. M., and Pearson, N. D. 1995. Storm sediment transport: observations from the British North Sea shelf. *Continental Shelf Research*. 15: (8) 889-912.

Grippo, M., Fleeger, J.W., Condrey, R. and Carman, K.C. High Benthic Microalgal Biomass Found on Ship Shoal, North-central Gulf of Mexico. Submitted.

Hsu, S.A., 1988. Coastal Meteorology, Academic Press, 260pp.

Jose, F., Kobashi, D., and Stone, G.W., 2007. Spectral Wave Transformation over an Elongated Sand Shoal off South-Central Louisiana, U.S.A., *Journal of Coastal Research*, SI 50. 757-761.

Keim, BD, Muller, RA,, and Stone GW. 2007. Spatiotemporal Patterns and Return Periods of Tropical Storm and Hurricane Strikes from Texas to Maine. *Journal of Climate*, 20(14): 3498.

Khalil, S.M., Finkl, C., Andrew, J.,Knotts, C.P., 2007. Restoration-quality sand from Ship Shoal, Louisiana: Geotechnical investigation for sand on a drowned barrier island. Proceeding of *Coastal Sediments '07.* New Orleans, Louisiana, 685-698.

Kobashi, D., Jose, F., and G. W. Stone, 2005. Hydrodynamics and sedimentary responses within bottom boundary layer: Sabine Bank, western Louisiana, Transaction*, Gulf Coast Association of Geological Societies*, v.55, 392-399.

Kobashi, D., Jose, F., and Stone, G.W., 2007a. Impacts of fluvial fine sediments and winter storms on a transgressive shoal, off south-central Louisiana, U.S.A., *Journal of Coastal Research*, SI 50, 858-862.

Kobashi, D., Jose, F., and Stone, G.W., 2007b. Heterogeneity and dynamics of sediments on a shoal during spring-winter storm season, south-central Louisiana, USA. Proceedings of *Coastal Sediments* '07, 921-934.

Kobashi, D, Stone, G.W., Jose, F., Spaziani, A.L. 2008. Dynamics of sediments within the bottom boundary layer over a transgressive shoal influenced by fluvial sediments and winter storms: south–central Louisiana. Abstract, *Ocean Science Meeting*, Orlando, Florida, USA.

Kobashi, D. and Stone, G.W. 2008a. Response of fluvial sediment dispersal to storm wind-current effects on a Holocene transgressive sand shoal, Atchafalaya Shelf, Louisiana, U.S.A.: A numerical simulation. *In review*.

Kobashi, D., and Stone, G.W. 2008b. Variability of Surface Water Level and Current Profiles associated with Varying Storm Winds over the Louisiana Inner Shelf and a Holocene Transgressive Shoal, Louisiana, USA: *In-Situ* Observations and Numerical Model Analyses. *In prepatation*.

Kobashi, D., Jose, F, Luo, Y., and Stone, G.W. 2008a. Wind-driven dispersal of fluvial fine sediments for two contrasting storms: extra-tropical and tropical storms, Atchafalaya Bay-Shelf, Louisiana. *In review*.

Kobashi, D., Stone, G.W., Khalil, S.M., Kerper, D. 2008b. Impacts of Sand Removal from a Shore-Parallel Holocene Transgressive Shoal on Hydrodynamics over the Shoal and Shoreface of Barrier Islands, South-Central Louisiana, U.S.A. *In preparation*.

Kulp, M., Penland, S., and Ramsey K., 2001, Ship Shoal: Sand Resource Synthesis Report, Coastal Research Laboratory, Dept. of Geology and Geophysics, Univ. of New Orleans, 70 p.

Li, M.Z., Amos, C.L., Heffler, D.E. 1997. Bottom boundary layer dynamics and sediment transport under storm and non-storm conditions on the Scotian shelf. *Marine Geology*, 141, 157-181.

Li, M.Z. and Gust, G. 2000. Boundary layer dynamics and drag reduction in flows of high cohesive sediment suspensions. *Sedimentology* 47, 71-86.

McAnally, W. H., Friedrichs C., Hamilton, D., Hayter, E. Shrestha, P., Rodriguez, H., Sheremet, A., and Teeter, A., 2007. Management of fluid mud in estuaries, bays and lakes. I: Present state of understanding on character and behavior. *Journal of Hydraulic Engineering*, 133 (1), 9-22.

Mehta, A.J., 1991. Understanding fluid mud in a dynamic environment. *Geo-Marine Letters*, 11:113-118.

Michel, J., Nairn, R., Johnson, J.A., and Hardin, D., 2001. Development and design of biological and physical monitoring protocols to evaluate the long-term impacts of offshore dredging operations on the marine environment: U.S. Department of Interior, Minerals Management Service, OCS Report MMS 2001-089, 116p.

Mossa, J., 1996. Sediment dynamics in the lowermost Mississippi River, *Engineering Geology*, 45, 457-479.

Murray, S., 1997. An observational study of the Mississippi-Atchafalaya coastal plume: Final report. OCS Study MMS 98-0040 U.S. Dept. of the Interior, Minerals Mtmt. Service, Gulf of Mexico OCS Region, New Orleans, LA. 513pp.

Palmer, T.A., Montagna, P.A., and Nairn, R.B. 2008. The effects of a dredged excavation pit on benthic macrofauna in offshore Louisiana. *Environmental Management*, 41: 573-583.

Penland, S., Suter, J.R., and Moslow, T. F., 1986. Inner-shelf shoal sedimentary facies and sequences: Ship Shoal, Northern Gulf of Mexico, SEPM Core Workshop No.9, Modern and Ancient Shelf Clastics, 73-123.

Penland, S., R. Boyd, and J. R. Suter, 1988, Transgressive depositional systems of the Mississippi delta plain: A model for barrier shoreline and shelf sand development: *Journal of Sedimentary Petrology*, v. 58, no. 6, p. 932-949.

Pepper, D.A. and Stone, G.W., 2002. Atmospheric forcing of fine sand transport on a low energy inner shelf: south-central Louisiana, USA. *Geo-Marine Letters*: 33-41.

Pepper, D.A. and Stone, G.W., 2004, Hydrodynamics and sedimentary responses to two contracting winter storms on the inner shelf of the northern Gulf of Mexico, *Marine Geology*, 210, 43-62.

Rabalais, N. N., Turner, R.E., and Scavia, D., 2002. Beyond science into policy: Gulf of Mexico Hypoxia and the Mississippi River. *Bioscience*, vol.52, no.2, 129-142.

Rabalais, N.N. Wiseman, W., Turner, E. 1994. Comparison of Continuous records of Near-Bottom. Dissolved Oxygen From the Hypoxia Zone Along the Louisiana Coast. *Estuaries*. 17 (4), 850-861.

Roberts, H. H., 1997, Dynamic changes of the Holocene Mississippi River delta plain: The delta cycle: *Journal of Coastal Research*, v. 13, no. 3, p. 605-627.

Sheremet, A, and Stone, G. W., 2003, Observations of nearshore wave dissipation over muddy sea bed, *J. Geophys. Res.*, 108(C11), 2257, doi: 10.1029/2003JC001885, 2003.

Sheremet, A., A.J. Mehta, B. Liu, G.W. Stone, 2005, Wave–sediment interaction on a muddy inner shelf during Hurricane Claudette, *Estuarine, Coastal and Shelf Science*, v.63, p.225–233.

SonTek Inc., 1997a. SonTek Doppler Current Meters – Using Signal Strength Data to monitor Suspended Sediment Concentration, SonTek Application Notes, San Diego, California, 7p.

SonTek, 1997b. Pulse-coherent Doppler processing and the ADV correlation coefficient. SonTek Technical Notes, San Diego, 5pp.

SonTek Inc., 2004. PC-ADP - Read Me First!, SonTek PC-ADP manual, San Diego, California, 28p.

Soulsby, R., 1997. Dynamics of marine sands, Thomas Telford Ltd, 272p.

Stone, G.W. and Xu, J.P., 1996. Wave climate modling and evaluation relative to sand mining on Ship Shoal, offshore Louisiana, for coastal and barrier island restoration, MMS OCS Study MMS96-0059. 170p.

Stone, G. W., 2000, Wave climate and bottom boundary layer dynamics with implications for offshore sand mining and barrier island replenishment in south-central Louisiana. *OCS Study MMS 2000-53*. U.S. Dept. of the Interior, Minerals Mgmt. Service, Gulf of Mexico OCS region, New Orleans, LA, 90pp.

Stone, G.W., Liu, B., Pepper, D. A., and Wang, P., 2004, The importance of extratropical and tropical cyclones on the short-term evolution of barrier islands along the northern Gulf of Mexico, *Marine Geology*, 210, 64-78.

Stone, G.W., Kumar, B.P., Sheremet, A., and Watzke, D.A., 2005a, Complex morpho-hydrodynamic response of estuaries and bays to winter storms: North-central Gulf of Mexico, U.S.A. *In* Fizgerald, D.M. and Knight, J. (eds.) *High Resolution Morphodynamics and Sedimentary Evolution of Estuaries*. Springer, 243-267.

Stone, G.W., Condrey, R., and Fleeger, J. 2005b. Environmental investigation of long-term use of Ship Shoal sand resources, Year 1 annual report submitted to U.S. Minerals Management Service/Louisiana Department of Natural Resources, 39pp.

Stone, G.W., Condrey, R., Fleeger, J., 2006. Environmental investigation of long-term use of Ship Shoal sand resources. Year 2 annual report submitted to U.S. Minerals Management Service/Louisiana Department of Natural Resources, 62pp.

Thompson, C.E.L., Amos, C.L., Angelaki, M., Jones, T.E.R, and Binks, C.E., 2006. An evaluation of bed shear stress under turbid flows, *J. of Geophys. Res.*, 111, C04008, doi:10.1029/2005JC003287.

Walker, N.D. and Hammack, A. B., 2000. Impacts of Winter Storms on Circulation and Sediment Transport: Atchafalaya-Vermilion Bay Region, Louisiana, U.S.A., *Journal of Coastal Research*, 16(4), 996-1010. West Palm Beach (Florida), ISSN 0749-0208.

Walker, N.D., Jarosz, R., Murray, S.P. 2001. An investigation of pressure and pressure gradients along the Louisiana/Texas inner shelf and their relationships to wind forcing and current variability. OCS Study MMS2001-057. U.S. Dept. of the Interior, Minerals Management Service, Gulf of Mexico OCS region, New Orleans, LA, 40pp.

Wells, J.T. and Kemp, P., 1981. Atchafalaya mud stream and recent mudflat progradation: Louisiana chenier plain. *Transaction, Gulf Coast Association of Geological Society*, v.31, 409-416.

Whitehouse, R.J.S., Soulsby, R., Roberts, W., Mitchener, H., 2000. Dynamics of Estuarine Muds. Thomas Telfort Ltd. and HR Wallingford.

Wiseman, W. J., JR., Turner, R. E., Kelly, F. J., Rouse, L. J. JR., AND Shaw, R. F. 1986. Analysis of biological and chemical associations near a turbid coastal front during winter 1982. *Contributions in Marine Science* 29:141-151.

Wright, L.D., Xu, J.P., Madsen, O.S. 1994. Across-shelf benthic transports on the inner shelf of the middle Atlantic Bight during the "Halloween Storm" of 1991. *Marine Geology*, 118(1/2), 61-77.

Wright, L.D., Sherwood, C.R. and Sternberg, R.W., 1997. Field measurements of fair-weather bottom boundary layer processes and sediment suspension on the Louisiana inner continental shelf, *Marine Geology*, 140, 329-345.

CHAPTER 5

IMPACTS OF SAND REMOVAL FROM A SHORE-PARALLEL HOLOCENE TRANSGRESSIVE SHOAL ON HYDRODYNAMICS AND SEDIMENT TRANSPORT, SOUTH-CENTRAL LOUISIANA, U.S.A.

5.1. Introduction

Irregular bottom topography in shallow waters such as sand banks and shoals has been known to influence coastal hydrodynamics and bottom boundary layer dynamics (Stone and Xu, 1996; Pepper and Stone, 2004). Those offshore sand bodies have been given particular attention as viable sand resources as more sand becomes necessary for large-scale coastal restoration, particularly along the northern Gulf coast (Byrnes et al., 1999; Michel et al., 2001; Maa et al., 2004; Pepper and Stone, 2004; Khalil et al., 2007). Inner-shelf shoal bathymetry generates unique hydrodynamics which may have a profound influence on the endemic biological and sedimentary environments. (Swift, 1985; Snedden et al. 1999; Palmer et al., 2007; Condrey and Gelpi, 2008). For instance, such bathymetric highs act as submerged breakwaters, mitigating wave energy and hence changing wave refraction, flow patterns, and consequent sediment transport patterns (cf. Stone and Xu, 1996; Pepper and Stone, 2004; Stone et al., 2004; Jose et al., 2007).

Wave transformation studies in shallow waters have been mostly limited to numerical model analysis and laboratory experiments, given the complex nature of dynamics (e.g. Stone and Xu, 1996; Byrnes et al. 2004; Maa et al., 2004; Johnson et al., 2006). Stone and Xu (1996) in greater detail investigated wave transformation over a shore-parallel sand body, Ship Shoal, located approximately 20 km off the coast in south-central Louisiana on the approximate 10 m

isobath. The authors implemented a spectral wave model, STWAVE (Smith et al., 2001), with constant input parameters (i.e. deepwater wave height/directions, wind speeds/directions), based on wave-climate analysis, along with the hypothetical post-dredging bathymetric configuration in which the entire shoal was removed. This work concluded that prevailing southeast waves were impacted the most in terms of wave refraction and dissipation, particularly along the western flank of the shoal; whereas, the ultimate impact of sand removal on the shoreface of barrier islands was insignificant for all model cases. STWAVE is, however, a "half-plane" wave model and this study was limited to waves (both swells and seas) from the southern quadrant, and hence detailed mechanisms of waves, particularly associated with post-frontal winds as well as current variability and sediment transport associated with sand removal, are not fully understood. While Jose et al (2007) implemented a "full-plane" third generation spectral wave model, MIKE21 SW to investigate wave transformation over a shallow shoal and qualitatively addressed the importance of wave dissipation and wave-wave interaction associated with winter cold fronts. There are a growing number of publications which examine hydrodynamics associated with sand mining, particularly waves and their impacts on longshore transport along beaches and barriers (cf. Stone and Xu, 1996; Byrnes et al. 2004); however little has been discussed regarding the alteration in hydrodynamic and sediment transport over the sand bodies as a consequence to targeted mining.

Ship Shoal, the largest sand body off the Louisiana shelf, was recently recognized as being unique from a sediment dynamic perspective in addition to its biological habitat, and likely has important implications for commercial fisheries (Kobashi et al., 2007a; Condrey and Gelpi, 2008; Grippo et al., submitted; Kobashi et al., in preparation. 2008a). The sand resources from the shoal can be a viable alternative for restoring the rapidly disintegrating Louisiana barriers and

beaches (Kulp et al. 2001). Without such large-scale intervention Louisiana's barrier islands and marshlands are projected to be lost within the next 50 years or so (Kulp et al. 2001; Khalil et al. 2007).

Sand mining may cause a profound impact on the local physical and biological environments and hence understanding the prevailing hydrodynamics plays a key role to assess the impacts, given the lack of available scientific literature (Michel et al., 2001). Using a state-of-the-art numerical model, an attempt has been made to compare the hydrodynamics of the region corresponding to two contrasting bathymetric configurations: one with shoal and the other with the shoal completely and partially removed. It should be noted that complete sand removal from the shoal is not a realistic mining scenario even if the impacts were minimal, given the fact that there are numerous pipelines underneath the shoal. However, the extreme hypothetical comparison would provide an excellent opportunity to unveil the impact of shoal on the regional hydrodynamics.

We have implemented a coastal ocean model package, MIKE developed by DHI^{TM} Water and Environment to investigate wave transformation and current variations on Ship Shoal (Figure 5.1); the wave model outputs were further used to discuss sediment re-suspension and transport. We also examined wave, current variability, and sediment transport over the shoal with respect to the bathymetry modification that was based on the proposed barrier island restoration scenarios (Table 5.1) (Khalil et al. 2007). Two representative energetic events were considered for the computations, namely, winter storms and tropical cyclones. We implemented the models during a winter storm in mid February, 2008 and a tropical cyclone Lili in 2002. Three mining areas on Ship Shoal are currently being proposed: South Pelto 12/13 (area A in Figure5.1), Ship Shoal block 88/89 (area B in Figure5.1), and Ship Shoal blocks 84/85/98/99 (area C in

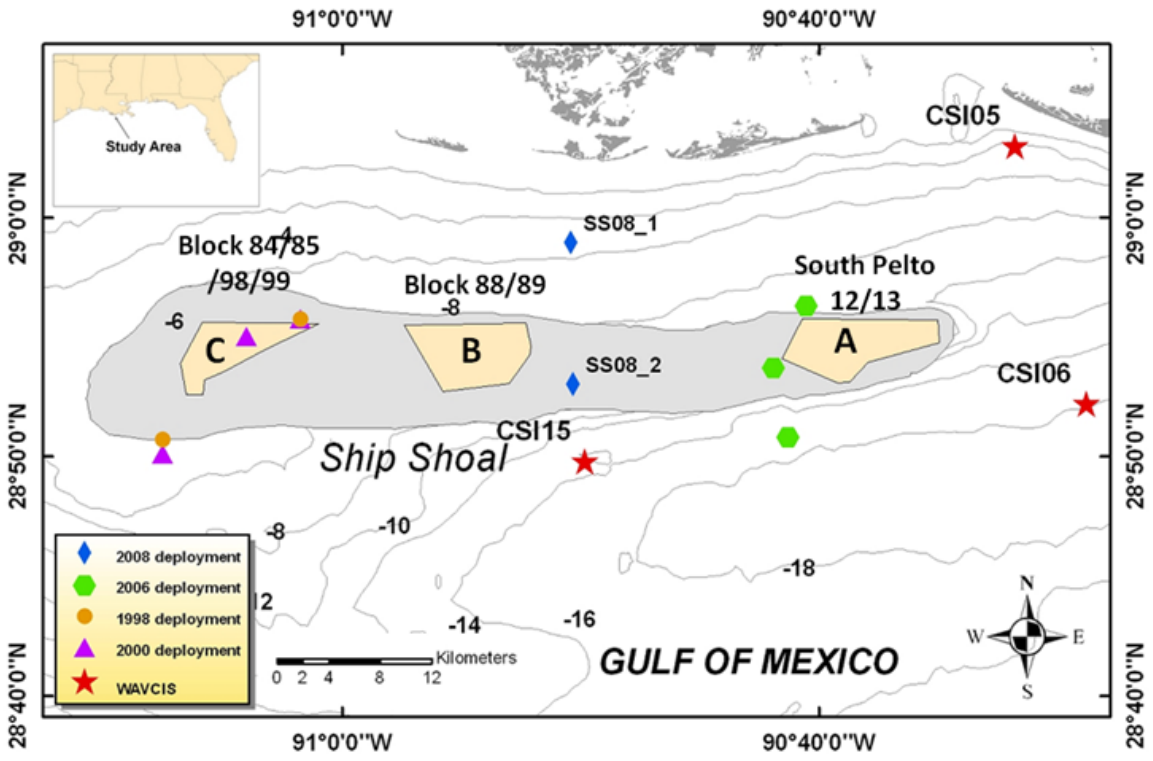

Figure 5.1 Proposed sand mining area: (A) South Pelto 13, (B) Ship Shoal Blocks 88/89, (C) Ship Shoal Blocks 84/85/98/99. Source: Khalil et al (2007)

Table 5.1 Louisiana barrier islands and restoration plans

Area	Restoration area	Rate of shoreline change (ft/yr)	Volume needed ($yard^3$)
Caminada headland	Caminada headland	-8.6 *[1]	8.0-10.0 x 10^6
Whisley Island	Isles Dernieres	-89.0 *[1]	4.0 x 10^6 *[2]
Trinity Island	Isles Dernieres	-62.5 *[1]	4.0 x 10^6 *[2]
Entire Isles Dernieres	Isles Dernieres	-61.9 *[1]	15.2 x 10^6 *[3]

*[1]Source: Penland et al (2005)
*[2]Source: Khalil et al. (2007)
*[3]Source: van Heeden et al. (1992)

Table 5.2 Ship Shoal Sand resources

Area	Restoration area	Volume ($yard^3$)	Total area (m^2)	Sand thickness (ft)
South Pelto (A)	Caminada Headland	28.3 x 10^6	11.6 x 10^6	13-20 ft
Blocks 88/89 (B)	Whiskey/Trinity Islands	>17.3 x 10^6	13.4 x 10^6	12-18 ft
Blocks 84 (C)	Whiskey/Trinity Islands	11.2 x 10^6	24.7 x 10^6	13 ft

Source: Khalil et al. (2007)

Figure 5.1). Those three areas are relatively free of pipelines (Khalil, S., personal communication; see also Figure 5.1 and Table 5.2).

Geological and physical settings pertinent to our study area commonly exist for wide-continental shelves worldwide (e.g. U.S. east coast); hence, our findings and inferences can be extended to such similar environments.

5.2. Wave-Climate and Current Variability over the Inner Shelf

Wave-climate and regional current variability were analyzed using *in-situ* data from various parts of the shoal and inner shelf prior to the model implementation. Data sources included instrument tripods deployed on the shoal and WAVCIS stations, CSIs-6 and 15 (Zhang, 2003). The wave-climate for the study area is characterized by low-energy (e.g, Georgiou et al., 2005). The *in-situ* data from WAVCIS CSI-15 (2007/01/01-2008/10/01, 639 days) showed that approximately 89 percent of time (568.7 days) wind speed was less than 10 m s^{-1}, 11 percent (70.3 days) between 10 and 20 m s^{-1}, 0.13 percent (8.3 days) above 20 m s^{-1} (severe storms). Wind predominantly blew from the northeast to the southeast (39 percent), but its direction was variable (Figure 5.2). Significant wave height (hereafter wave height) was mostly less than 1.0 m (68.3 percent) and only 2.0 percent of the wave height exceeded 1.5 m. Wave direction was mostly between the east and south (67.8 percent). The direction from the northern quadrant was associated with winter storms and to some extent with sea and land breeze interaction (Hsu, 1988; Kobashi et al., 2005; Stone et al., 2005). Current velocity was more spatially variable than waves and winds. Bottom and surface currents from the WAVCIS CSI-6 (2004/06/03-2008/09/01) was directed predominantly westward; the near bottom currents (1.5 m above the bottom) were varying directionally rapidly when compared to the surface currents (Figure5.3c&d). Near bottom currents on Ship Shoal were more dynamic than the current fields

off-shoal. The bottom current direction on the western flank of the shoal during winter 1998, directed predominantly north/south (cross-shore); the bottom currents on the eastern flank during spring 2006 prevailed to the north. For the near bottom currents on the middle shoal during winter 2008, predominant bottom current direction was westward.

The observations indicate that current fields associated with the shoal are highly complicated, depending on the coastal boundary, wind conditions (speed, direction, storm intensity and duration), Coriolis force, and bottom topography (Csanady, 1982; Swift and Niedoroda, 1985; Kobashi and Stone, in preparation, 2008b). Detailed discussion on three-dimensional current variability over the inner shelf and the shoal is made in Kobashi and Stone (In prep., 2008b).

5.3. Model Experiment

A third-generation spectral wave model, MIKE21 SW (hereafter SW) and a three-dimensional hydrodynamic model, MIKE3 HD (hereafter HD) were implemented in this study. Both models have been developed by DHI^{TM} Water and Environment. The SW model has been successfully implemented for the Gulf of Mexico and the Louisiana shelf (Jose and Stone, 2006; Jose et al., 2007), as part of a wave forecasting study. The HD model has not been utilized for the Louisiana shelf to date. Detailed model descriptions including the models, domain, and input parameters as well as initial conditions are briefly described in the following sections.

5.3.1. SW Module

SW is a third-generation spectral wind wave model based on unstructured meshes. The unstructured mesh approach gives the model high degree of flexibility. The model solves the wave action balance equation, the spatial discretization of which is performed using an unstructured finite volume method. The integration over time is based on a fractional step

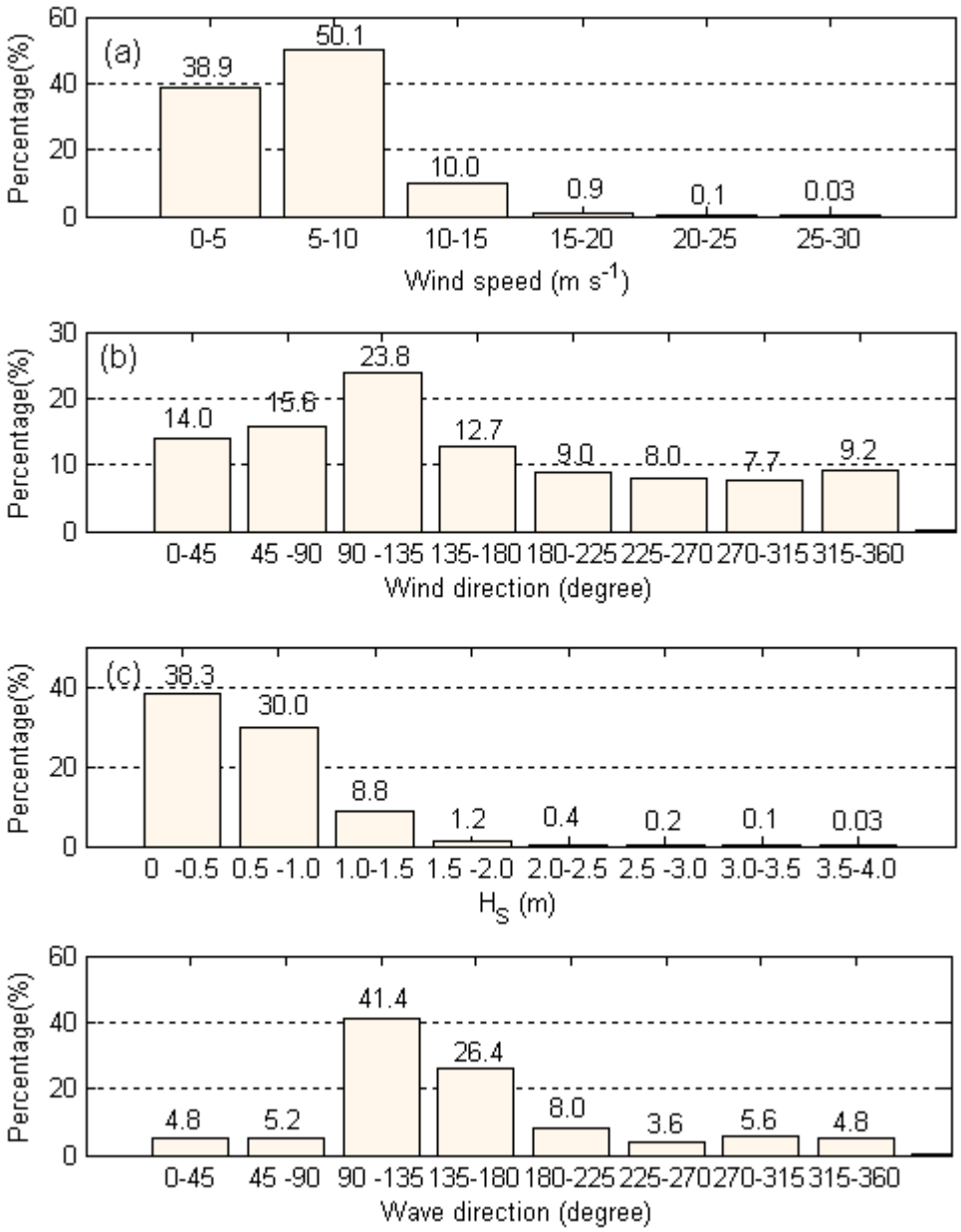

Figure 5.2 Histogram of wave-climate parameters: (a) Wind speed, (b) Wind direction, (c) Wave height, and (d) Wave directions between 2007/01/01 and 2008/10/01, 639 days. The numbers in the figure show percentages.

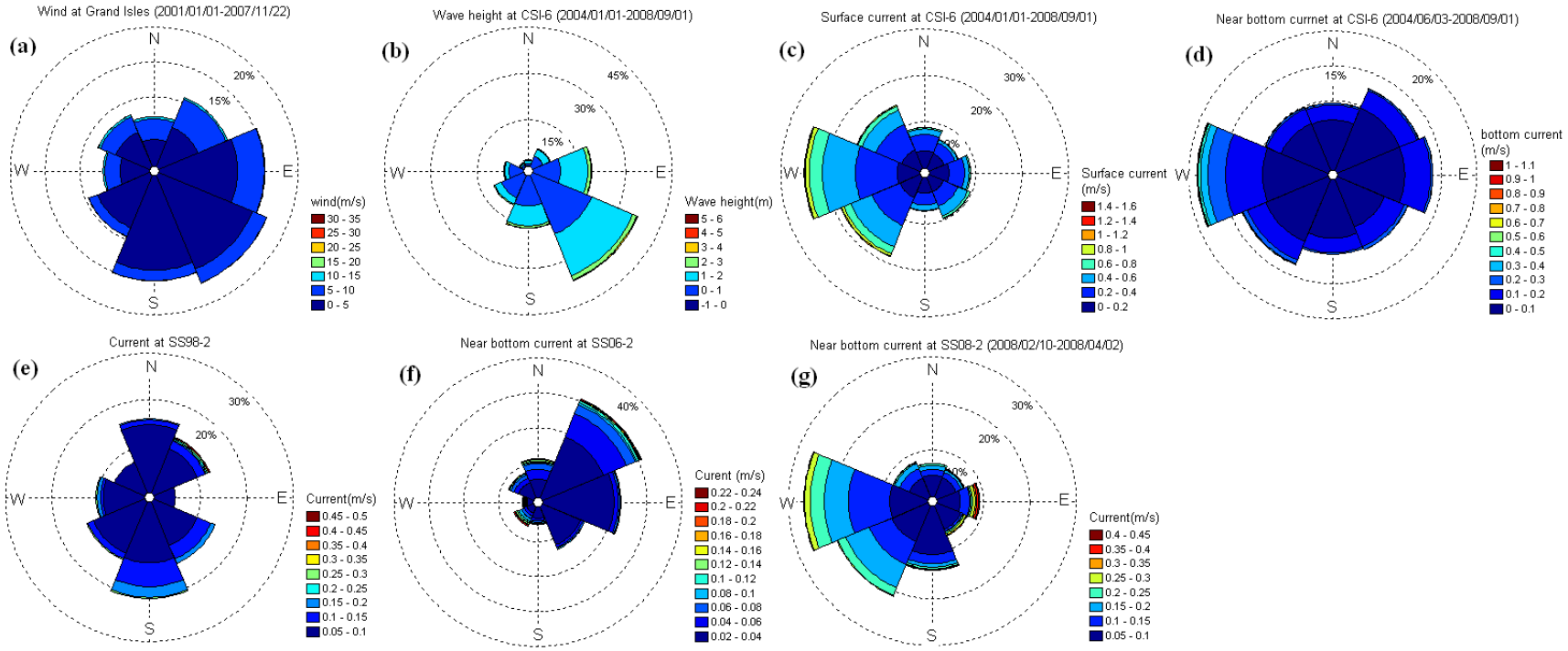

Figure 5.3 Polar plots pertaining to (a) winds at Grand Isle, (b) waves at CSI-6, (c) surface currents at CSI-6, (d) near bottom currents at CSI-6, (e) near bottom currents at SS98_2, (f) near bottom currents at SS06_2, (g) near bottom currents at SS08_2

approach, where the propagation steps are solved using an explicit method (Sorensen et al., 2004). The wind input, the main source function in the equation, is based on Janssen's quasi-linear theory of wind-wave generation (Janssen, 1989; 1991) and implemented as in WAM Cycle 4. The non-linear energy transfer through the four-wave interaction is represented by the discrete interaction approximation (DIA) proposed by Hasselmann et al. (1985) (see also Komen et al., 1994). The dissipation due to white capping is implemented according to Hasselmann (1974) and further tuned according to Janssen (1989). Detailed description of all the source functions and the numerical methods used in the model are discussed in Sorensen et al. (2004).

5.3.2. HD Module

The HD module simulates water level variations and flows in response to a wide variety of forcing in lakes, estuaries, bay and coastal areas (DHI, 2005b). The module solves three dimensional incompressible Reynolds-averaged Navier-Stokes equation. The model consists of momentum and continuity equations. The model solves horizontal terms explicitly and vertical term implicitly (DHI, 2005b). Horizontal and vertical eddy viscosities were based on Smagorinsky formulation and k-ε equation, respectively (DHI, 2005b). Bed resistance is computed based on the quadratic stress law. Vertical discretization can be selected from either equidistant, layer thickness, or variable grids, which consists of a uniform distribution, user specified distribution, and stretched and top/bottom specified distribution, respectively (DHI, 2005b). In the study, the equidistant discretization was used. More detailed model information is elaborated on in DHI (2005b).

5.3.3. Model Domains

The model domain (origin: -91.25º W, 28.75º N) covered Ship Shoal, south of the Isles Dernieres barrier island chain, and three ocean observing stations (Figure 5.4). Two bathymetries

were used: one with Ship Shoal (Figure 5.5 top) and the other without the shoal (Figure 5.5 bottom). The bathymetry without the shoal was developed based on the linear interpolation between the north and south edges of the shoal. The computational grids were unstructured triangular mesh grids with an embedded high resolution mesh grid encompassing the shoal boundary (Figure 5.4). The mesh size was based on the volume of grid each with maximal size of 2.0×10^{-5} degree^2 (2.5×10^5 m^2) over the shoal and 2.0×10^{-4} degree^2 (2.5×10^6 m^2) for the surrounding areas. For the HD, offshore mesh size was selected as 2.0×10^{-3} degree^2 (2.5×10^7 m^2). In addition, a fine-resolution mesh was created for another case study embedded with finer resolution grids over the three proposed mining areas, with a maximal area of 5.0×10^{-6} deg^2 (6.2×10^4 m^2) (not shown in Figure 5.4).

For the case study A (Table 5.3), deep water boundary conditions were applied along the southern boundary and all three other boundaries (North, East, West) were selected as radiative boundaries for the SW model. The HD model had all four boundaries treated as closed boundaries (Table 5.4). The coastal wave model was nested with the Gulf of Mexico (GOM) regional model for the additional case studies (Case B1-B5 in Table 5.5). A detailed description of the regional wave model is addressed in Jose and Stone (2006). Although all boundaries were assigned as closed, for HD Model, the computational domain for HD model was selected much larger than the wave model (origin: -92.0º W, 28.0º N) in order to avoid vortex effects near the closed boundaries; however, we only used the same area as the wave model domain to discuss current variability over the shoal.

5.3.4. Input Parameters and Initial Conditions

Input parameters were carefully selected from various data sources. For both GOM regional and high resolution coastal models, wind data from a re-analyzed hindcast model by

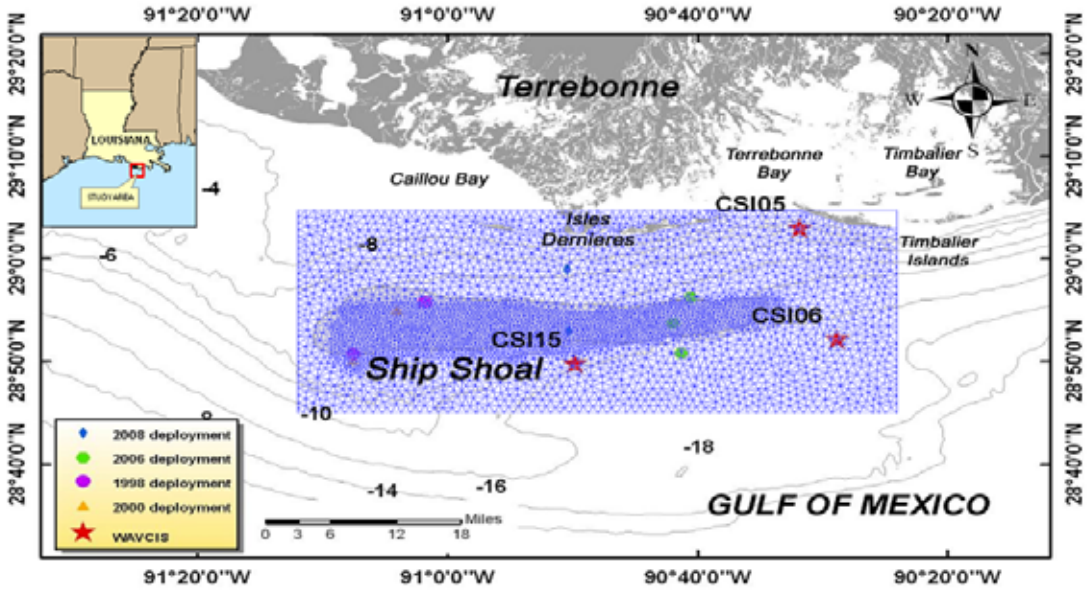

Figure 5.4 Map and computational grids

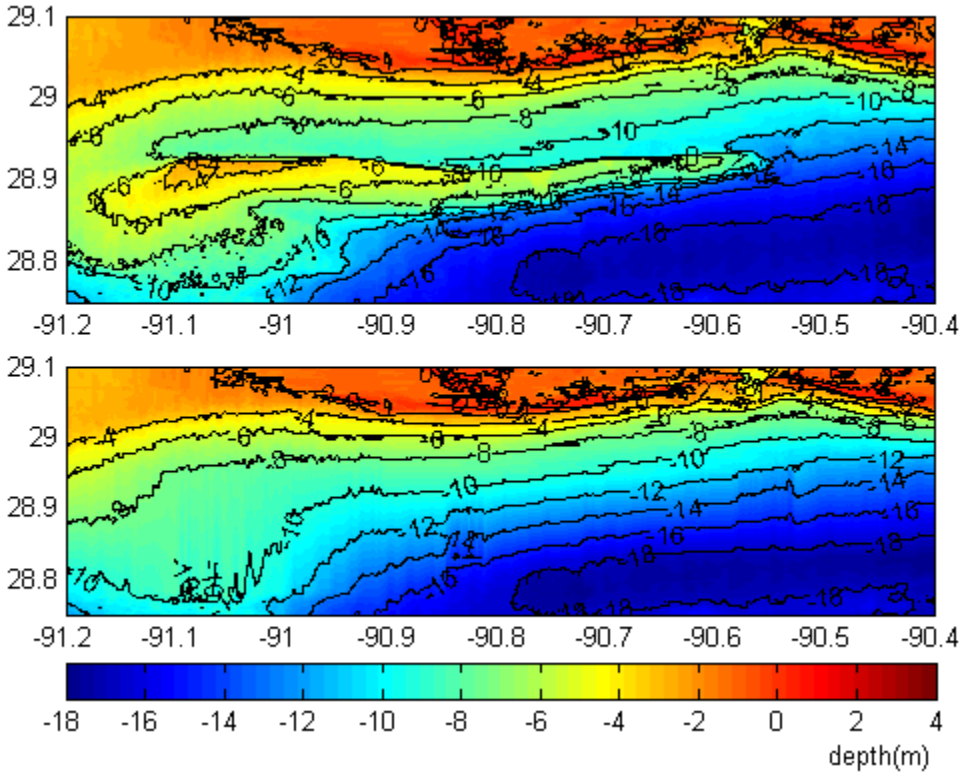

Figure 5.5 Bathymetry of model domain: with shoal (upper) and without shoal (lower)

NOAA NCEP (North America Regional Reanalysis: NARR) were used (cf. Mesinger et al 2006). The wind friction coefficient was selected as the constant value of 0.003 rather than linearly varying coefficients based on a calibration study. Bathymetry data from the NGDC (National Geophysical Data Center) coastal relief model (Divins and Metzger, 2008) were initially used; however, the preliminary results indicate that the bathymetry over the domain has significantly changed with the maximum difference is in the order of meters in magnitude with a mean difference of approximately 0.5 m. We corrected the bathymetry by krigging the difference in the bathymetry between the NGDC data and *in-situ* data from ocean observing stations as well as the bathymetry data obtained from the Louisiana Department of Natural Resources (LDNR); the adjusted NGDC data were used as the offshore bathymetry. For the GOM model, ETOPO2 bathymetry was also used. For keeping initial conditions of all model cases to be consistent, bottom friction for the SW model was estimated from a constant Nikraudse roughness height of 0.04 m rather than that from grain diameters based on Nielsen (1979); results of our preliminary model implementation showed little difference in the result between the two friction factors. For HD, the bottom friction was estimated from quadratic stress law using bottom drag coefficient. Water level was obtained from GOM regional modeling for each boundary (east, west, north, and south). The HD was implemented as a barotropic mode and density changes (e.g. stratification) were not considered (i.e. wind-induced currents). Also, for simplicity, the effects of waves on currents were not included. The time step was selected as 150 seconds for the SW and 10 seconds for the HD. It should be noted that the MIKE 21 SW wave model is not capable of simulating waves over a muddy seabed, which is the case for the Louisiana shelf (e.g. Sheremet and Stone, 2003). Therefore, wave dissipation over muddy bottoms is not discussed in this paper.

Table 5.3 Case study A: Wind condition (Constant in domain)

Case	Speed (m/s)	Direction (degree)
A1	20	NE(45), SE(135), SW(225), NW(315)
A2	15	NE(45), SE(135), SW(225), NW(315)
A3	12	NE(45), SE(135), SW(225), NW(315)
A4	10	NE(45), SE(135), SW(225), NW(315)
A5	5	NE(45), SE(135), SW(225), NW(315)

Table 5.4 Case study A: Offshore wave boundary condition (South boundary)

Case	H_S (m)	T_P (sec)	Direction (degree)
A1	6	11	135
A2	4	9	135
A3	3	7	135
A4	2	6	135
A5	1	5	135

Table 5.5 Ship Shoal sand mining scenarios

Case	Sand volume (x 10^6 m^3)	Mining area	Excavation depth (m)	Restoration target
B-1	7.65	A	0.24 m	Caminada
B-2	13.76	A	0.43 m	Caminada, Whiskey/Trinity
B-3	6.12	B	0.21 m	Wiskey/Trinity Islands
B-4	9.18	B	0.31 m	Entire Isles Dernieres
B-5	9.18	C	0.37 m	Entire Isles Dernieres

5.3.5. Case Studies

Various wave-climate conditions, mainly following Stone and Xu (1996), were selected to implement the wave and hydrodynamic models for two bathymetric configurations: one with the shoal and one without the shoal in the computational grids. For both models, five wind conditions, namely, severe storms (case A1), strong storms (case A2), moderate storms (case A3), weak storms (case A4), and fair weather (case A5) were selected (see Table 5.3). Stone and Xu (1996) concluded from their case study, which consists of offshore waves propagating from three different directions along the southern boundary, that the waves from the southeast along with predominant southeast winds yielded maximal changes in wave refraction and the highest dissipation rates. In this study, deepwater wave boundary conditions were selected as the southeast waves (i.e. 135 degrees) along the southern boundary (Figure 5.4 and Table 5.4). Constant winds in the domain were incorporated for varying wind speeds and directions listed in Table 5.4. In general, currents over the inner shelf and shoal are highly associated with persistent winds during storms given the fact that tidal currents are generally weak. In this study, four wind directions were selected based on wave climate results as shown in Figures 5.4&5.5 and Table 5.3. Wave model results were further analyzed to estimate sediment re-suspension intensity (RI).

In addition, another case study that was based on proposed restoration scenarios (Table 5.5) was implemented. Two representative storms were selected: winter storms (2008/02/25-2008/03/07) and tropical cyclones Isidore and Lili (2002/09/23-2002/10/06). Four scenarios based on different bathymetries were carried out in order to examine impacts of potential sand mining on waves and currents (see Table 5.5).

5.3.6. Skill Assessment of the Models

Model validation was conducted using various *in-situ* data from deployed instruments

(SS08_2 in Figure 5.1), and an *in-situ* observing station, WAVCIS CSI-15 (see the location in Figure 5.1). The validation included visual comparison of both time series data (Figures 5.6) as well as statistical analysis (Table 5.6). It is reported that the widely-used correlation coefficient often cannot evaluate the model well and a small difference between model results and measured data can result in a substantial change in the coefficient (Wilmott, 1982). Therefore, instead of the correlation coefficient, the following statistical parameter (*Iw* in equation 5-1) proposed by Wilmott (1982), and an error function (ε in equation 5-2, see also Johnson et al. 2005) in addition to the linear regression coefficient (r^2) were used to evaluate the model performance.

$$Iw = 1 - \frac{\sum_{k=1}^{N} (V_{model} - V_{measured})^2}{\sum_{k=1}^{N} [|V_{model} - \overline{V}_{measured}| + |V_{measured} - \overline{V}_{measured}|]^2} \quad \text{..... (5-1)}$$

Where V_{model}, $V_{measured}$, and $\overline{V}$ are simulated, measured, and mean values, respectively. N is the number of data. If the two parameters are correlated well, Iw becomes close to 1. The error function was computed based on the following equation. If the values are well correlated, the value approaches 0.

$$\varepsilon = \left[\frac{\sum_{k=1}^{N} (V_{model} - V_{measured})^2}{\sum_{k=1}^{N} (V_{measured})^2} \right] \quad \text{..... (5-2)}$$

Figures 5.6a and 5.6b show comparisons between the measured and the simulated values of various parameters including wave height, peak period and mean wave direction as well as wind speed, wind direction, water level and surface and bottom currents at the shoal crest (SS08_2) and CSI-15 (see locations in Figure 5.1). Wind data from the *in-situ* data and the

NARR wind data were in good agreement except during storm peaks when the NARR wind speed was often lower than the *in-situ* data as also reported by Jose et al. (2007) (Figure 5.6). The model result provided high I_W values (i.e. the values close to 1) and low ε values (i.e. the values close to 0) for wind parameters.

For the spectral wave model, all measured and simulated wave parameters agreed reasonably well (Table 5.6). The model result provided high I_W values and low ε values for bulk wave parameters. Considering the fact that the model cannot simulate waves over muddy bottoms, it is reasonable to say that the wave model performs well for the study area. For the HD model, simulated surface current and water level were in general agreement with the measured data (Table 5.6) also supported by high I_W values and low ε values; however, simulated bottom cross-shore current showed a low correlation (I_W=0.33, ε=3.34, r^2=0.0035) with in-situ data probably due to inaccuracy of the bathymetry despite its correction. Simulated sea surface slope for cross-shore and alongshore both agreed well with measured data. Overall, the HD model performed well even if the density changes were not considered.

5.4. Results and Discussion

5.4.1. Wave Transformation over the Shoal

Incoming deep water waves significantly transformed as they propagated over complex coastal bathymetry (Figure 5.7). Spatial differences in wave transformation were similar for all cases although having differences in magnitude (Table 5.7). Particular attention was paid to spatially-varying wave dissipation and refraction for different bathymetries. The wave model results provided similar results as given in Stone and Xu (1996). In Figure 5.7, wave height and wave vector distributions with shoal (Figure 5.7 top), and without shoal (Figure 5.7 bottom) were

Table 5.6 Skill assessment of model results at CSI-15

Parameters	**Station**	$\mathbf{I_W}$	**ε**	$\mathbf{r^2}$
Wind speed	CSI-15	0.8837	0.0697	0.7291
Wind direction	CSI-15	0.9092	0.0917	0.7192
Significant wave height	SS08_2	0.9343	0.0567	0.7695
Peak wave period	SS08_2	0.7968	0.0462	0.4638
Wave direction	SS08_2	0.6363	0.1637	0.1168
Surface east current	SS08_2	0.7653	0.4426	0.4154
Surface north current	SS08_2	0.7773	0.5338	0.5225
Bottom east current	SS08_2	0.4696	4.5675	0.1032
Bottom north current	SS08_2	0.3283	3.3434	0.0035
Water level	SS08_2	0.8788	0.3549	0.6650
	CSI-15	0.9616	0.1504	0.8944
Sea surface slope	CSI-6 – CSI-15	0.6687	0.7195	0.2683
	CSI-5 – CSI-6	0.7723	0.6783	0.3843

presented. When the wave height was high (Case A1 in Figure 5.7a&b), substantial wave refraction on the western flank of the shoal was clearly evident compared to that without the shoal. As the deep water wave height decreased, the difference became less evident. On the middle and eastern flank of the shoal the difference in the refraction with and without the shoal was minimal (Figure 5.7). The wave height on the western flank of the shoal was significantly smaller than that on the eastern shoal (up to 32 percent difference between the east and west). When the shoal existed, the difference was up to 9 percent higher than the difference without the shoal. The difference decreased as the deep water wave height decreased (Table 5.7). Wave height and wave energy dissipation between south and north of the shoal, as a general trend, decreased from the west toward east except during case 1 for which the dissipation was minimum due to wave dissipation along the seaward boundary of the western shoal, which was significantly shallower than the middle and eastern flank of the shoal. For case A1, the difference in wave height was approximately 34 percent higher on the middle shoal than the eastern flank of the shoal. The dissipation in wave height along the western flank of the shoal was approximately 70 percent higher than that on the eastern flank; while, for the model result without the shoal, the difference in the height was significantly smaller (Table 5.7). Wave energy dissipation showed similar results and maximal difference was 52 percent for the bathymetry with shoal and 9 percent for that without shoal (Table 5.7). The above results indicate that the shoal has significant influence on wave dissipation. The above results further influenced sediment re-suspension on the shoal and which is discussed in the section 5.4.3.

5.4.2. Variability of Currents over the Shoal

Simulated current fields varied primarily with wind speeds and directions (Figures 5.8a-d); however the current pattern was more associated with the wind direction than the wind speed.

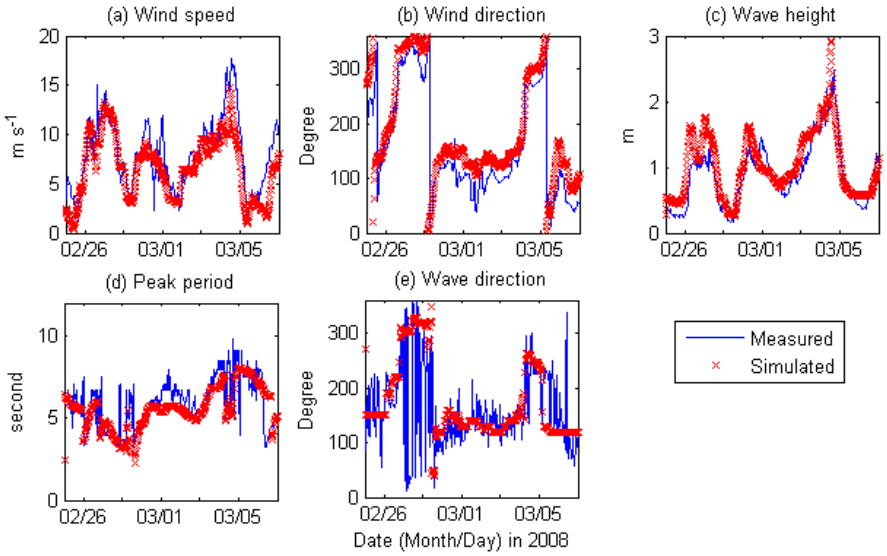

Figure 5.6a Model validation of (a) wind speed, (b) wind direction, (c) wave height, (d) peak wave period, and (e) wave direction (MIKE 21 SW).

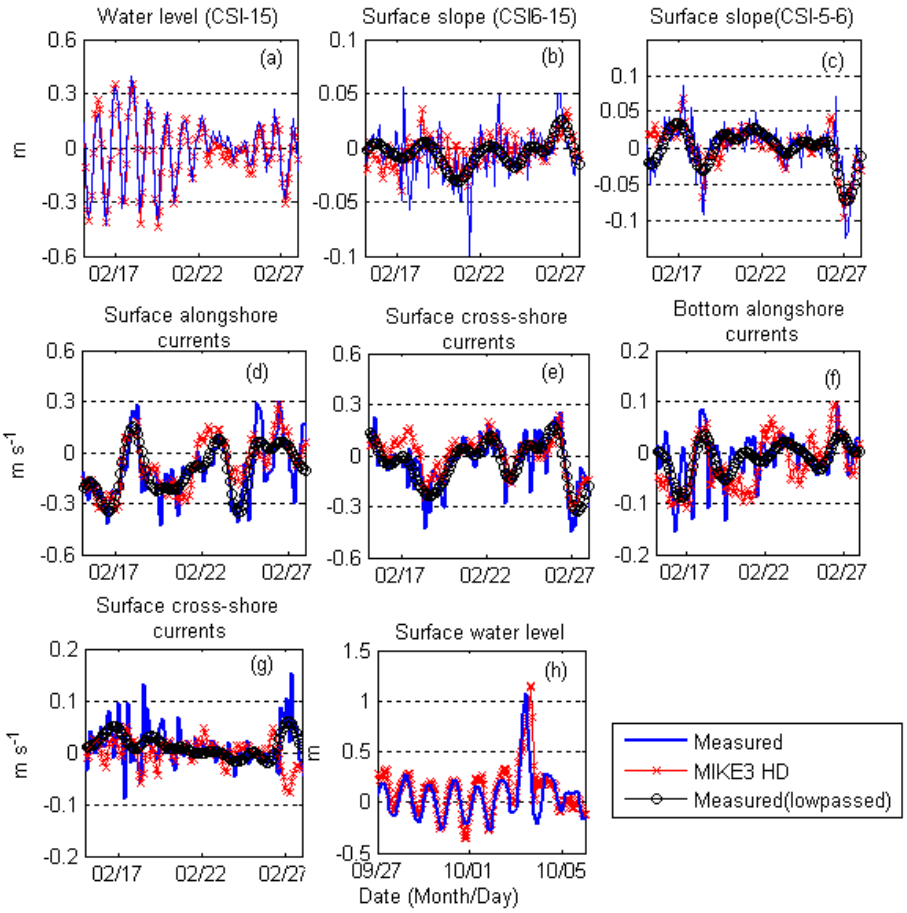

Figure 5.6b Model validation of (a) water level, (b) alongshore surface slope, (c) cross-shore surface slope, (d) alongshore current (surface), (e) cross-shore current (surface), (f)alongshore current (bottom), (g) cross-shore current (bottom), (h) water level during hurricane Lili (MIKE21/3 HD)

Surface currents generally followed prevailing wind regardless of their speed (Figures 5.8a and 8d). For instance, when northeast winds blew, southwest currents on the eastern flank of the shoal and westward currents on the western flank of the shoal prevailed at the surface (Figure 5.8). The surface currents tend to move toward isobaths; such characteristics were also reported over the northern Gulf coasts (e.g. Adams et al. (1987) off the southwest pass; Byrnes et al. (2004) off the Alabama coast; Marmorino (1983) over the western Florida shelf). Bottom currents were more variable and strongly influenced by the shoal bathymetry particularly on the western shoal. Both surface and bottom currents were stronger over the shallower shoal than the surrounding shoal because of flow acceleration due to the shoal topography, to satisfy continuity despite increases in bottom friction (Table 5.8) (cf. Swift, 1985; Snedden et al. 1999). Data indicate that without the shoal, general spatial patterns of both surface and bottom currents were similar. The surface currents on the western portion of the shoal were higher than those on the eastern flank of the shoal as with the result with the shoal in the computational grid; however, the flow acceleration over the shoal was not evident as seen from the model result with the shoal. Modification of the bottom currents with respect to the inner shelf topography was also not evident.

Water fluxes for both u-component (P flux on Table 5.8) and v-component (Q flux on Table 5.8) were high on the western shoal and during high winds; they decreased from the west to east and as the wind speeds decreased (Table 5.8). The alongshore flux was high when the winds blew from the northeast and southwest. In addition, the alongshore flux was significantly higher than cross-shore flux, suggesting the importance of alongshore component of the winds on current variability over the shoal. This can be attributed to the isobaths which trend northeast-southwest, since the currents tend to flow toward the isobaths as a result of geostrophic

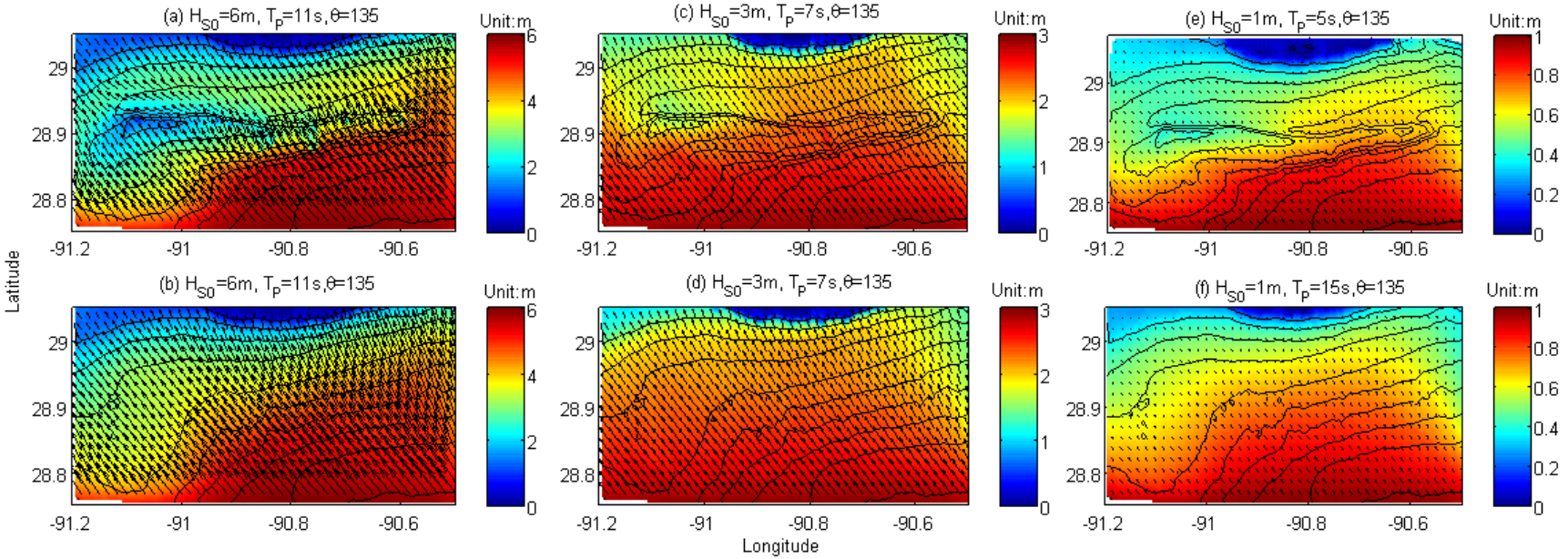

Figure 5.7 Wave height and vector distributions for case A study: (a, b) H_S=6m, T_P=11 s, Wave direction=135 (degree). (c, d) H_S=3 m, T_P=7s, Wave direction=135 (degree), (e, f) H_S=1m, T_P=5 s, Wave direction=135 (degree). Top figures represent the result with shoal and bottom figures the result without shoal.

Table 5.7 MIKE21 SW model result with shoal (left) and without shoal (right)

Parameter	Case	West	Middle	East	Outside
H_S (m)	A1	1.93 (3.32)	2.75 (4.46)	3.85 (4.70)	5.20 (5.17)
	A2	2.15 (3.03)	2.91 (3.41)	3.23 (3.29)	3.66 (3.59)
	A3	2.01 (2.31)	2.34 (2.35)	2.21 (2.22)	2.55 (2.52)
	A4	1.36 (1.43)	1.47 (1.41)	1.38 (1.41)	1.70 (1.67)
	A5	0.49 (0.63)	0.64 (0.77)	0.70 (0.73)	0.87 (0.85)
PWD (degree)	A1	140.0 (140.0)	150.0 (140.0)	150.0 (126.3)	140.0 (130.0)
	A2	140.4 (140.0)	150.0 (140.0)	150.0 (124.2)	140.0 (130.0)
	A3	150.0 (130.0)	150.0 (140.0)	150.0 (122.1)	140.0 (130.0)
	A4	140.7 (140.0)	140.0 (140.0)	150 9 (110.8)	140.0 (138.0)
	A5	140.0 (140.0)	140.0 (140.0)	150.0 (109.1)	140.0 (139.0)
ΔHs Upper: ΔHs/Hs, Lower: ΔHs (m)	A1	0.21 (0.08) 0.63 (0.27)	0.37 (0.32) 1.90 (1.64)	0.25 (0.17) 1.26 (0.86)	-
	A2	0.42 (0.13) 1.32 (0.41)	0.23 (0.13) 0.84 (0.46)	0.12 (0.11) 0.41 (0.37)	-
	A3	0.35 (0.13) 0.89 (0.33)	0.16 (0.13) 0.41 (0.32)	0.14 (0.16) 0.33 (0.39)	-
	A4	0.20 (0.15) 0.31 (0.23)	0.19 (0.22) 0.32 (0.36)	0.24 (0.23) 0.40 (0.36)	-
	A5	0.37 (0.18) 0.26 (0.12)	0.31 (0.23) 0.27 (0.20)	0.23 (0.21) 0.19 (0.18)	-
RI ($N\ m^{-2}$)	A1	0.97 (1.31)	1.20 (1.42)	1.50 (1.40)	1.39 (1.40)
	A2	1.03 (1.13)	1.27 (0.95)	1.18 (0.75)	0.73 (0.78)
	A3	0.90 (0.60)	0.92 (0.27)	0.45 (0.10)	0.14 (0.18)
	A4	0.16 (-0.05)	0.03 (-0.14)	-0.14 (-0.18)	-0.14 (-0.13)
	A5	-0.11 (-0.11)	-0.15 (-0.15)	-0.19 (-0.19)	-0.15 (-0.15)

H_S: Significant wave height, PWD: peak wave period, ΔH_S: wave dissipation, RI: Re-suspension intensity

adjustments (cf. Swift, 1985; Csanady, 1982; Unoki, 1994). Whereas, cross-shore flux was significantly smaller, but much more variable than the alongshore flux (Table 5.8). Overall, the results with and without the shoal had similar variability in terms of the current variations and the fluxes; the difference in the fluxes for two bathymetries was small. The result suggests that neither large-scale nor small-scale sand mining should give rise to abrupt changes in current patterns, but the large-scale sand mining can change the magnitude of the velocity and therefore, fluxes. This current variability has further implications for sediment transport over the shoal.

5.4.3 Re-suspension of Bottom Sediments

Changes in sediment re-suspension have strong implications for sediment transport and bed characteristics. We estimated sediment re-suspension (RI) from the computed bulk wave parameters defined as wave-induced shear stress subtracted by critical shear stress. Wave shear stress was estimated from Madsen (1976) and the critical shear stress for sand bottoms (grain diameter coarser than 63 microns (63×10^{-6} m)) were estimated based on Li et al. (1997). The critical stress for sediments finer than 63 microns was chosen as a constant value of 0.15 ($N\ m^{-2}$) (Kobashi and Stone, in review, 2008b). Results are summarized in Table 5.7 and also illustrated in Figure 5.9.

The RI corresponds to wave height, wave period, and water depth; generally speaking, the higher the wave height and the shallower the depth, the higher the RI. When storms were strong (i.e. case A1 and A2), the RI was high across the domain, but was higher on the middle and eastern shoal than on the western shoal due to wave dissipation on the western shoal. As wave energy decreased, in general trend, the RI on the shoal decreased from the west to east following the change in the shoal bathymetry. For the case A3 (moderate storms), the RI on the western shoal was twice as high as that on the eastern shoal and approximately six times as high

as that outside of the shoal. For case A4 (weak storm conditions), the RI was positive on the western and middle shoal and was negative on the eastern flank of the shoal and outside of the shoal. The negative values are in favor of sediment deposition. For the case A5 (fair weather conditions), the RI was negative across the domain, suggesting no sediment re-suspension during fair weather conditions. The results were corroborated by *in-situ* measurements (e.g. Pepper, 2000; Kobashi et al., 2007a; Kobashi et al., in review, 2008b). Recent studies revealed unique sediment dynamics on predominantly a fluid mud bottom on the deeper eastern flank of the shoal during spring 2006 and on predominantly a sandy bottom on shallower middle and western flank of the shoal during winter 1998 and 2008 (Pepper and Stone, 2004; Kobashi et al., 2007a; Kobashi et al, in review, 2008b). Our results suggest that the deeper eastern portion of the shoal, seems to be suitable for the accumulation of fine sediment supplied from the Atchafalaya River during moderate to weak storms, typically during spring. On the western and middle portions of the shoal, re-suspension is prone to outweigh sediment accumulation in spite of its closer location to the Atchafalaya River as in greater detail discussed in Kobashi and Stone (in review, 2008a).

Results of the RI without the shoal showed that sediment re-suspension was high on the western flank of the shoal during strong storms because of lower wave dissipation rates despite deeper depth (Table 5.7). However, for most of the model results, the RI without shoal was significantly lower than the re-suspension with shoal, particularly when wave energy was moderate to weak (Figure 5.9). This suggests that a large portion of the shoal sand excavations enhance accumulation of fluid mud on the shoal when sediment is deposited on the shoal (Kobashi et al., in review, 2008a). The result has further strong implication for benthic organisms.

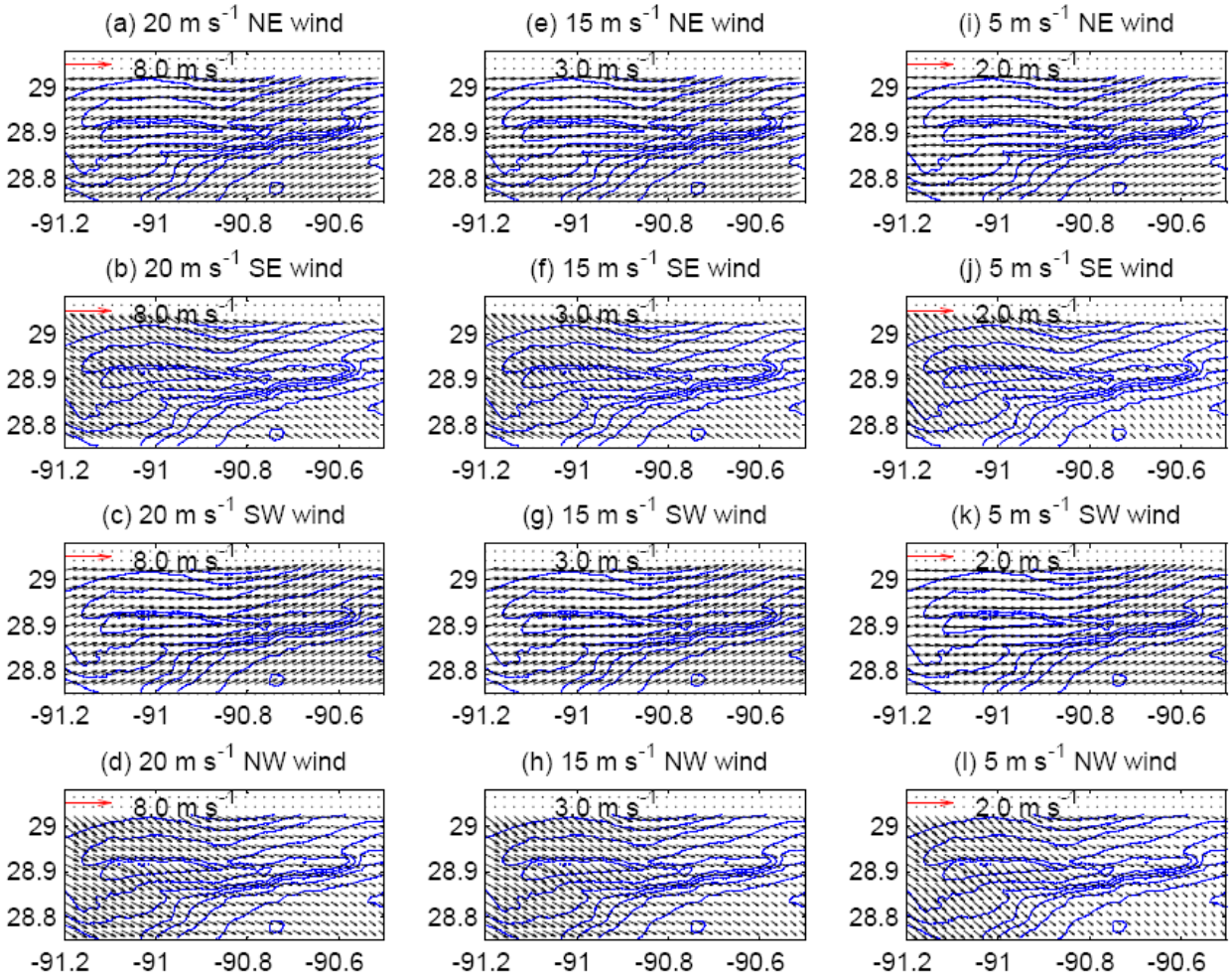

Figure 5.8a Surface currents with shoal for various wind speeds and directions

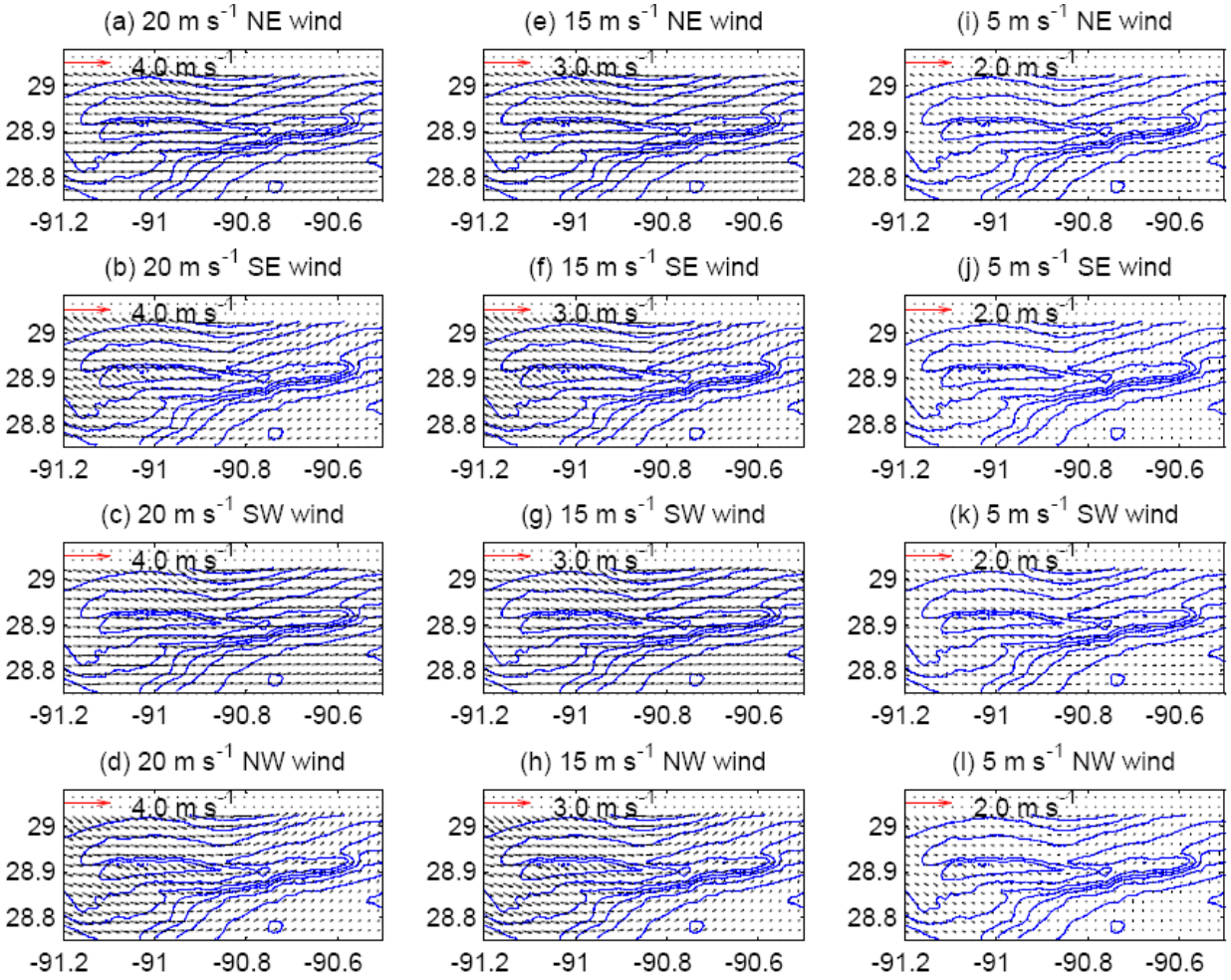

Figure 5.8b Bottom currents with shoal for various wind speeds and directions

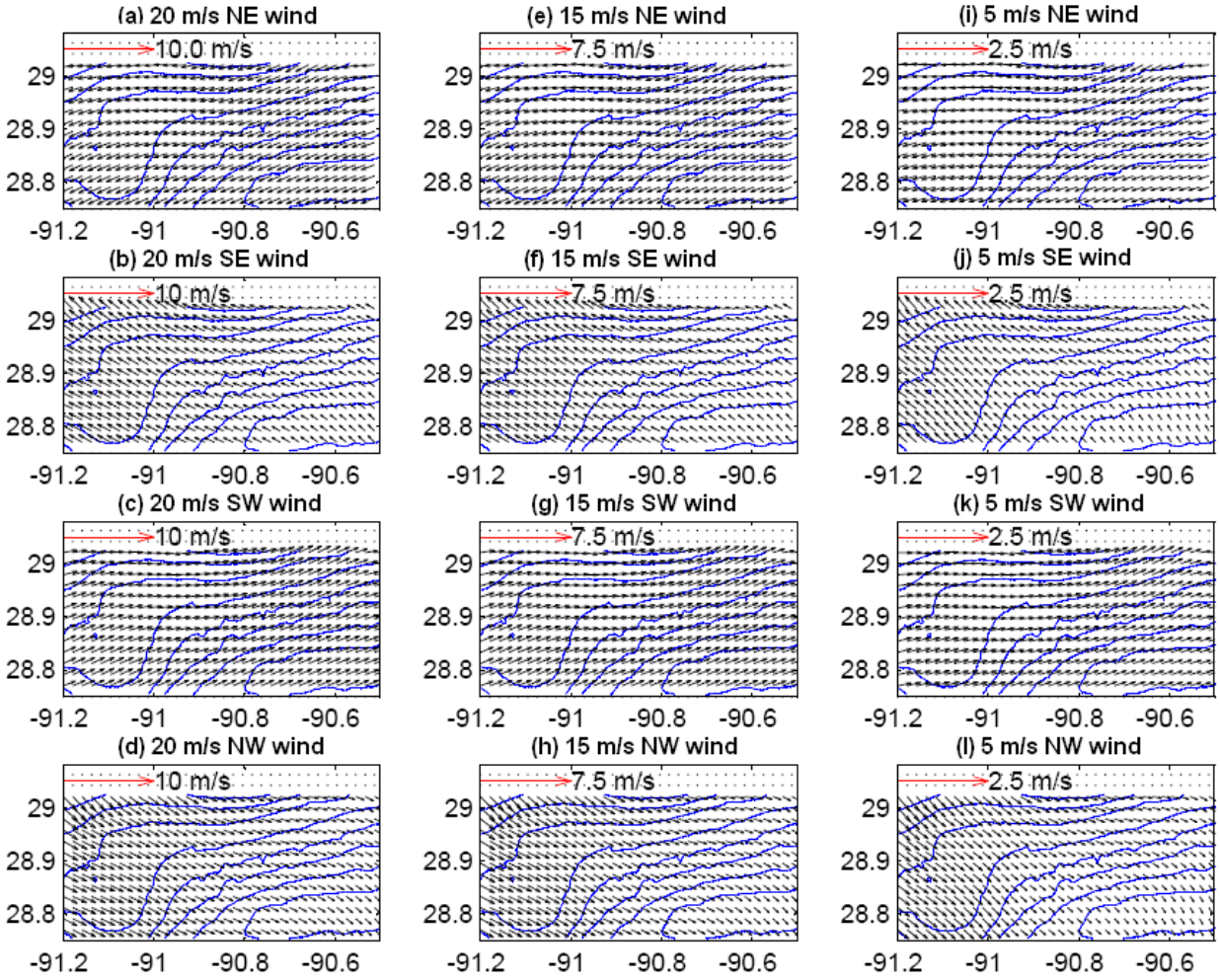

Figure 5.8c Surface currents without shoal for various wind speeds and directions

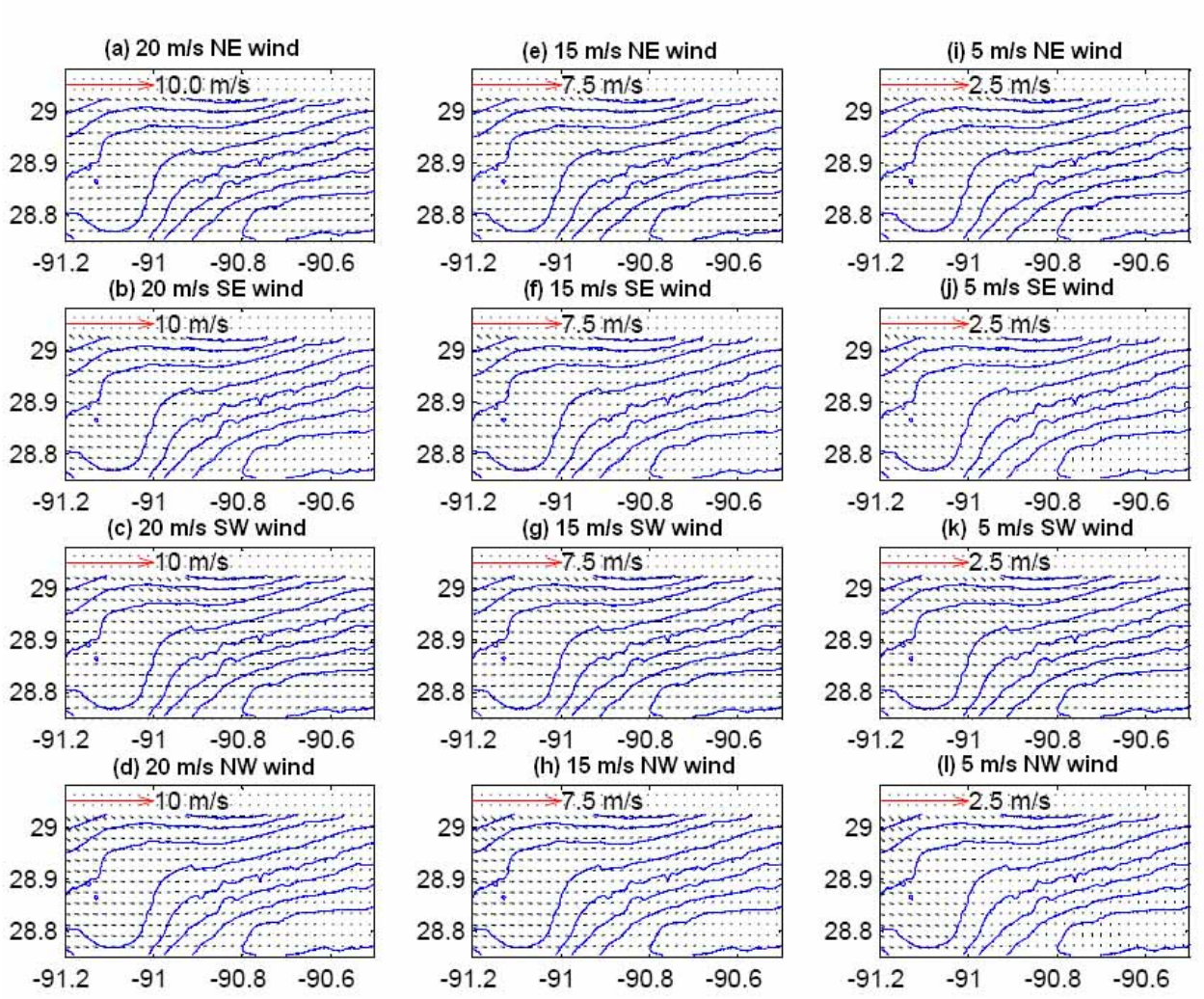

Figure 5.8d Bottom currents without shoal for various wind speeds and directions

Table 5.8 M3 HD model result with shoal (left) and without shoal (right)

Parameter	Wind Speed	Wind direction	Western shoal	Middle shoal	Eastern shoal	Outside (offshore)
P flux (u-component) (m^2s^{-1})	20 m s^{-1}	NE	-6.36, -6.08	-3.86, -5.04	-2.69, -4.53	-2.12, -3.50
		SE	-1.81, -2.09	-2.58, -2.97	-2.12, -3.06	-1.90, -3.17
		SW	6.44, 6.15	4.00, 5.21	2.71, 4.71	2.17, 3.51
		NW	1.85, 2.10	2.36, 2.84	1.96, 2.79	1.75, 3.06
	15 m s^{-1}	NE	-4.62, -4.44	-2.89, -3.76	-2.03, -3.40	-1.60, -2.65
		SE	-1.22, -1.43	-1.86, -2.10	-1.53, -2.16	-1.37, -2.29
		SW	4.68, 4.49	2.97, 3.85	2.01, 3.50	1.62, 2.65
		NW	1.28, 1.46	1.72, 2.03	1.45, 2.01	1.30, 2.26
	10 m s^{-1}	NE	-2.89, -2.79	-1.90, -2.45	-1.34, -2.24	-1.08, -1.78
		SE	-0.67, -0.81	-1.16, -1.25	-0.96, -1.29	-0.86, -1.43
		SW	2.91, 2.81	1.93, 2.49	1.32, 2.28	1.07, 1.78
		NW	0.73, 0.84	1.08, 1.23	0.92, 1.21	0.83, 1.43
	5 m s^{-1}	NE	-1.18, -1.16	-0.89, -1.10	-0.64, -1.03	-0.52, -0.87
		SE	-0.20, -0.26	-0.50, -0.49	-0.42, -0.47	-0.34, -0.56
		SW	1.18, 1.16	0.89, 1.10	0.62, 1.03	0.52, 0.87
		NW	0.23, 0.28	0.47, 0.49	0.41, 0.44	0.34, 0.57
Q flux (v-component) (m^2s^{-1})	20 m s^{-1}	NE	-0.77, -0.59	-1.02, -0.96	-0.33, -0.20	0.06, -0.20
		SE	-0.13, 0.46	-0.13, -0.18	0.55, 0.27	1.40, 1.03
		SW	0.85, 0.63	0.91, 0.93	0.25, 0.13	-0.13, 0.05
		NW	0.38, -0.27	0.40, 0.29	-0.56, 0.29	-1.30, -0.81
	15 m s^{-1}	NE	-0.50, -0.38	-0.73, -0.69	-0.21, -0.12	0.11, -0.07
		SE	-0.14, 0.29	-0.11, -0.15	0.40, 0.18	1.05, 0.77
		SW	0.57, 0.40	0.67, 0.67	0.18, 0.09	-0.13, 0.02
		NW	0.29, -0.18	0.30, 0.22	-0.44, -0.23	-1.01, -0.66
	10 m s^{-1}	NE	-0.26, -0.18	-0.45, -0.43	-0.11, -0.06	0.12, 0.01
		SE	-0.10, 0.17	-0.09, -0.11	0.26, 0.09	0.70, 0.52
		SW	0.29, 0.20	0.43, 0.42	0.10, 0.05	-0.13, -0.01
		NW	0.19, -0.12	0.21, 0.15	-0.30, 0.14	-0.70, -0.48
	5 m s^{-1}	NE	-0.07, -0.04	-0.19, -0.18	-0.03, -0.02	0.11, 0.06
		SE	-0.04, 0.09	-0.05, -0.06	0.11, 0.003	0.35, 0.28
		SW	0.07, 0.04	0.19, 0.18	0.02, 0.007	-0.11, -0.05
		NW	0.08, -0.07	0.11, 0.08	-0.13, -0.03	-0.36, -0.26

5.4.4 Impacts of Sand Dredging for Proposed Restoration Scenarios on Waves, Current, and Sediment Suspension

An additional case study was implemented (case B1-B5) to examine changes in physical conditions for various sand mining scenarios from B1 to B5. Two contrasting storms were selected: a winter storm in mid February 2008 (equivalent to moderate storms (case A3)) and a tropical cyclone, Lili (equivalent to severe weather (case A1)). Here results of the cases B2, B4, and B5 were presented (Table 5.9). The results of the cases B2 and B4 were more extensive mining scenarios than B1 and B3 (Table 5.5).

During tropical cyclone Lili, the maximum difference in wave height over the mining area A, was 0.07 m for scenario B2, 0.04 m over area B for scenario B4, and 0.07 m over area C for scenario B5, respectively (Table 5.9). The difference in current velocity at the surface and bottom showed less than 0.15 m s^{-1} and 0.07 m s^{-1} for all cases (B2, B4, and B5). RI changed in magnitude of less than 0.08 N m^{-1} for all cases.

During a winter cold front in mid-February, 2008, the difference in wave height on each mining area was 0.09 m for the scenario B2 and 0.04 m for the scenario B4, respectively (Table 5.9). Maximal differences in magnitude of surface currents were 0.17 m s^{-1} over area A during, 0.11 m s^{-1} over area B, and 0.16 m s^{-1} over area C (Table 5.9). RI changed in magnitude of 0.02 N m^{-2} for the cases B2 and B4, and B5 (Table 5.9). Compared to maximal values during model duration as listed in Table 5.9, the above values are significantly small and thus, small-scale sand mining is not expected to have profound impacts on hydrodynamics and sediment transport over the shoal.

5.5 References in Chapter 5

Adams, C. E., Swift, D.J., Coleman, J.M., 1987. Bottom currents and fluviomarine sedimentation on the Mississippi prodelta shelf: February-May 1984, J. Geophys. Res., Vol.92(C.13),14,595-14,609.

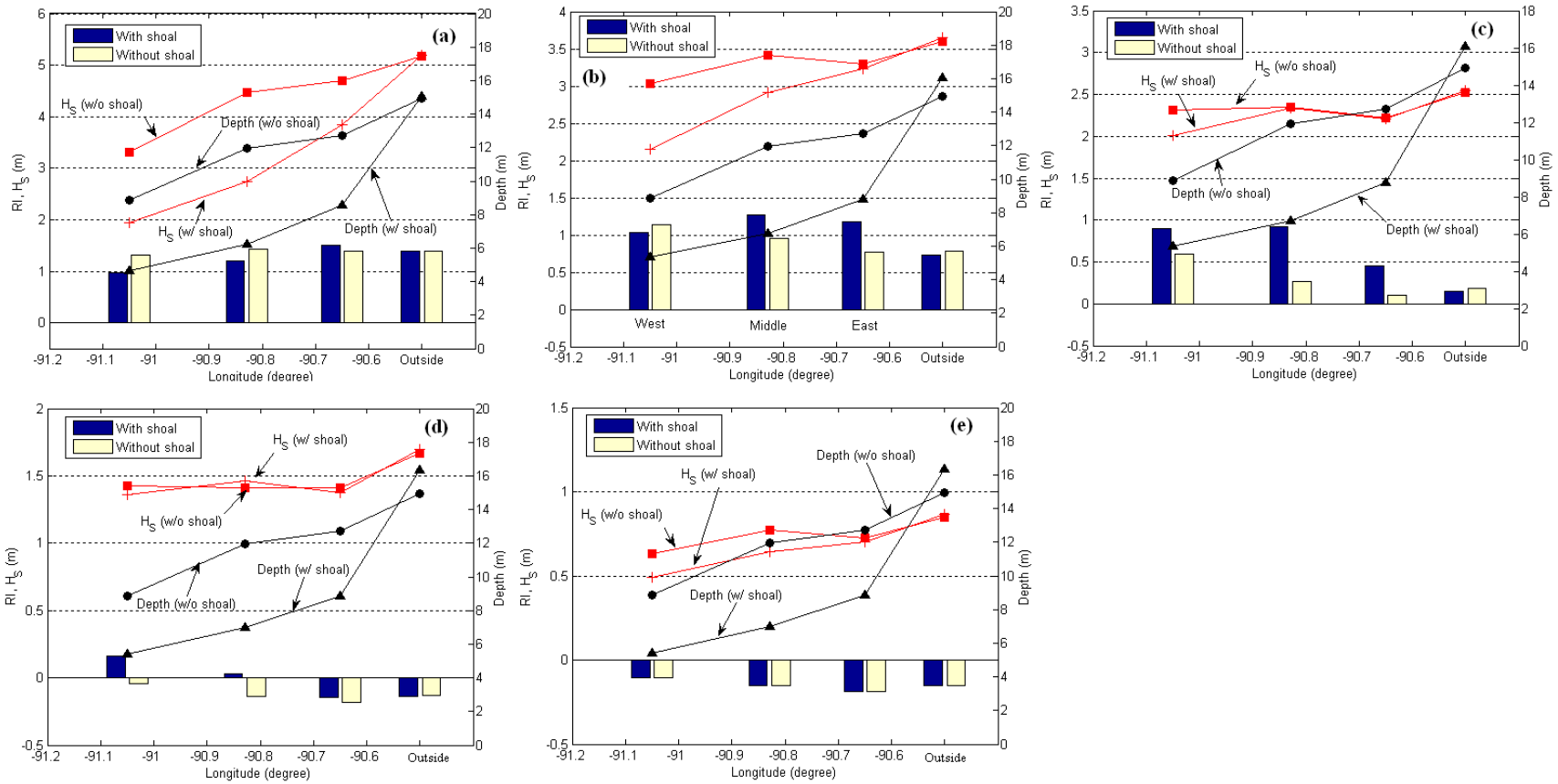

Figure 5.9 Wave re-suspension Intensity (RI) for various cases. (a) Case A1, (b) Case A2, (c) Case A3, (d) Case A4, (e) Case A5

Table 5.9 Maximal difference in magnitude of hydrodynamic parameters between actual bathymetry and hypothetical bathymetry. Top low; Maximal difference in absolute magnitude of each parameter. Bottom low: Maximal values in magnitude of each parameter during model duration

Storm	**Case**	**Wave height m**	**Surface currents m s^{-1}**	**Bottom currents m s^{-1}**	**RI N m^{-2}**
Winter storms	B2	0.09	0.17	0.03	0.02
		1.19	0.59	0.20	0.82
	B4	0.04	0.11	0.06	0.02
		1.30	0.49	0.15	0.62
	B5	0.03	0.16	0.06	0.02
		1.67	0.10	0.10	0.60
Hurricane Lili	B2	0.07	0.09	0.04	0.01
		1.52	0.97	0.33	1.10
	B4	0.04	0.15	0.07	0.08
		2.06	0.75	0.22	1.16
	B5	0.07	0.05	0.03	0.04
		3.47	0.06	0.15	1.39

Andersen, O.B., 1995. Global ocean tide from ESR-1 and TOPEX/POSEIDON altimetry. *Journal of Geophysical Research*, 100 (C12), 25,249-25,259.

Buczkowski, B.J., Reid, J.A., Jenkins, C.J., Reid, J.M., Williams, S.J., and Flocks, J.G., 2006. usSEABED: Gulf of Mexico and Caribbean (Puerto Rico and U.S. Virgin Islands) offshore surficial sediment data release, U.S. Geological Survey Data Series 146 2006. Version 1.0, 50pp.

Byrnes, M.R., R.M. Hammer, B.A. Vittor, J.S. Ramsey, D.B. Snyder, K.F. Bosma, J.D. Wood, T.D. Thibaut, N.W. Phillips, 1999. Environmental Survey of Identified Sand Resource Areas Offshore Alabama: Volume I: Main Text, Volume II: Appendices. U.S. Department of Interior, Minerals Management Service, International Activities and Marine Minerals Division (INTERMAR), Herndon, VA. OCS Report MMS 99-0052, 326 pp. + 132 pp. appendices

Condrey, R. and Gelpi, C. 2008. Blue crab use of the Ship/Trinity/Tiger shoal complex as a nationally important spawning/hatching/foraging ground: Discovery, evaluation, and sand mining recommendations. Final report submitted to U.S. Minerals Management Service, 34pp.

Csanady, G.T. 1983. Circulation in the coastal ocean, D. Reidel, Hingham, MA. 279pp.

Divins, D.L., and D. Metzger, 2008. NGDC Coastal Relief Model, 2008/06/01, *http://www.ngdc.noaa.gov/mgg/coastal/coastal.html*

Mesinger, F., DiMego, G., Kalnay, E., Mitchell, K., Shafran, P. C., Ebisuzaki, W., Jović, D., Woolen, J., Rogers, E., Berbery, E. H., EK, M. B., FAN, Y., Grumbine, R., Higgins, W., LI, H., Lin, Y., Manikin, G., Parrish, D., and Shi, W. 2006. North America Regional Reanalysis. *Bulletin of American Meteorological Society*, 87 (3), 343-360.

DHI, 2005a. MIKE21 Spectral wave model SW, Scientific Documentation, XXp.

DHI, 2005b. MIKE21&3 Flow Model FM. Hydrodynamics and Transport Module Scientific Documentation, 42p.

Hasselmann, K., 1974. On the spectral dissipation of ocean waves due to whitecapping, *Boundary. Layer Meteor.*, 6, 107-127.

Hasselmann, S., Hasselmann, K., Allender, J.H. and Barnett, T.P., 1985. Computations and parameterizations of the non-linear energy transfer in gravity wave spectrum. Part II: Parameterizations of non-linear energy transfer for applications in wave models, *J. Phys. Oceanog.*, **15**, 1369-1377.

Hsu, S.A., 1988. Coastal Meteorology, Academic Press, 260pp.

Komen, G.J., Cavaleri, L., Donelan, M., Hasselmann, K., Hasselmann, S., and Janssen, P.A.E.M.. 1994. Dynamics and modeling of ocean waves, Cambridge University Press, 532p.

Janssen, P.A.E.M., 1989. Wave-induced stress and the drag of airflow over sea waves, *J. Phys. Oceanogr.*, 19, 745-754.

Janssen, P.A.E.M., 1991. Quasi-linear theory of wind-wave generation applied to wave forecasting, *J. Phys. Oceanogr*., 21, 1631-1642.

Johnson, H. K., and H. Kofoed-Hansen, 2000: Influence of bottom friction on sea surface roughness and its impact on shallow water wind wave modeling. *J. Phys. Oceanogr.,* **30,** 1743–1756.

Johnson, H.K., Karambas, T.V., Avgeris, I., Zanuttigh, B., Gonzalez-Marco, D., and Caceres, I., 2005. Modelling of waves and currents around submerged breakwaters. *Coastal Engineering*, 52, 949-969.

Jose, F and Stone, G.W., 2006. Forecast of nearshore wave parameters using MIKE 21 spectral wave model, *Transactions*, Gulf Coast Assn. of Geological Societies, 56, 323-327.

Jose, F., Kobashi, D., Stone, G.W., 2007. Spectral wave transformation over an elongated sand shoal off south central Louisiana, USA. *Journal of Coastal Research*, SI 50. 757-761.

Khalil, S.M., Finkl, C., Andrew, J.,Knotts, C.P., 2007. Restoration-quality sand from Ship Shoal, Louisiana: Geotechnical investigation for sand on a drowned barrier island. Proceeding of *Coastal Sediments '07.* New Orleans, Louisiana, 685-698.

Kobashi, D., Jose, F., and G. W. Stone, 2005. Hydrodynamics and sedimentary responses within bottom boundary layer: Sabine Bank, western Louisiana, Transaction*, Gulf Coast Association of Geological Societies*, v.55, 392-399.

Kobashi, D., Jose, F., and Stone, G.W., 2007a. Impacts of fluvial sediments and winter storms on a transgressive shoal off south-central Louisiana, U.S.A., *Journal of Coastal Research*, SI 50, 858-862.

Kobashi, D. and Stone, G.W., 2008a. Two contrasting morpho-hydrodynamics over recurring sandy and muddy bottoms of a shore-parallel Holocene transgressive shoal, south-central Louisiana, USA. Submitted to *Continental Shelf Research.*

Kobashi, D., and Stone, G.W. 2008b. Variability of Surface Water Level and Current Profiles associated with Varying Storm Winds over the Louisiana Inner Shelf and a Holocene Transgressive Shoal, Louisiana, USA: *In-Situ* Observations and Numerical Model Analyses. *In preparation*.

Kobashi, D., Jose, F, Luo, Y., and Stone, G.W. 2008a. Wind-driven dispersal of fluvial fine sediments for two contrasting storms: extra-tropical and tropical storms, Atchafalaya Bay-Shelf, Louisiana. Submitted to *Marine Geology*.

Kulp, M., Penland, S., and Ramsey K., 2001, Ship Shoal: Sand Resource Synthesis Report, Coastal Research Laboratory, Dept. of Geology and Geophysics, Univ. of New Orleans, 70 p.

Li, M.Z., Amos, C.L., Heffler, D.E. 1997. Bottom boundary layer dynamics and sediment transport under storm and non-storm conditions on the Scotian shelf. *Marine Geology*, 141, 157-181.

Maa, J., Hobbs, C., Kim, S. C., and Wei, Y. 2004. Potential Impacts of Sand Mining Offshore of Maryland and Delaware: Part 1—Impacts on Physical Oceanographic Processes. Journal of Coastal Research, 20(1), 44-60.

Madsen, O.S., 1976, Wave climate of the continental margin: Elements of its mathematical description., In: Stanley and Swift, eds, Chapter 6, Marine Sediment Transport and Environmental Management, 65-87.

Michel, J., Nairn, R., Johnson, J.A., and Hardin, D., 2001. Development and design of biological and physical monitoring protocols to evaluate the long-term impacts of offshore dredging operations on the marine environment: U.S. Department of Interior, Minerals Management Service, OCS Report MMS 2001-089, 116p.

Nielsen, P. 1979. Some basic concepts of wave sediment transport. *Series paper 20* Institute of Hydrodynamics and Hydraulic Engineering, Technical University of Denmark, 160pp.

Penland S, Connor PF Jr, Beall A, Fearnley S, Williams SJ. 2005. Changes in Louisiana's shoreline: 1855–2002. Journal of Coastal Research 44:7–39.

Pepper, D.A. and Stone, G.W., 2004, Hydrodynamics and sedimentary responses to two contracting winter storms on the inner shelf of the northern Gulf of Mexico, *Marine Geology*, 210, 43-62.

Sheremet, A, and Stone, G. W., 2003, Observations of nearshore wave dissipation over muddy sea bed, *J. Geophys. Res.*, 108(C11), 2257, doi: 10.1029/2003JC001885, 2003.

Smith, J.M., Sherlock, A.R., and Resio, D.T., 2001. STWAVE: Steady-state spectral wave model. User's manual for STWAVE, version 3.0. ERDC/CHL SR-01-1. Coastal and Hydraulic Laboratory, US Army Corps of Engineers. 81p.

Snedden, J.W., Dalrymple, R.W., 1999. Modern shelf sand ridges: From historical perspective to unified hydrodynamic and evolutionary model. SEPM Special Publication, 64,13-28

Sorensen, O.R., H. Kofoed-Hansen, M. Rugbjerg, and L.S., Sorensen, 2004, A third-generation spectral wave model using an unstructured finite volume technique: International Conference on *Coastal Engineering Proceedings*, v. 29, p. 894-906.

Stone, G.W. and Xu, J.P., 1996. Wave climate modling and evaluation relative to sand mining on Ship Shoal, offshore Louisiana, for coastal and barrier island restoration, MMS OCS Study MMS96-0059. 170p.

Stone, G.W., Pepper, D.A., Xu, J. and Zhang, X., 2004. Ship Shoal as a Prospective Borrow site for barrier island restoration, Coastal south-central Louisiana, USA: Numerical wave modeling and field measurements of hydrodynamics and sediment transport. *Journal of*

Coastal Research, 20(1), 70-89.

Unoki, S., 1994. Phyiscal oceanography of coastal waters, Tokai University Press. 672pp., Tokyo (in Japanese).

van Heerden, Li, I., Suhayda, J.N., Kemp, G. P. 1993. The importance and role of barrier islands to coastal wetlands in Terrebonne Parish. Report submitted to the Terrebonne Parish Consolidated Government, Houma, LA.

Walker, N.D., Jarosz, R., Murray, S.P. 2001. An investigation of pressure and pressure gradients along the Louisiana/Texas inner shelf and their relationships to wind forcing and current variability. OCS Study MMS2001-057. U.S. Dept. of the Interior, Minerals Management Service, Gulf of Mexico OCS region, New Orleans, LA, 40pp.

Wilmott, C.J., 1982: Some Comments on the Evaluation of Model Performance. *Bulletin of the American Meteorological Society* 63 (11), 1309 – 1313.

CHAPTER 6

SYNTHESIS AND CONCLUSIONS

In order to examine the bottom boundary layer dynamics (BBLD) and sediment transport over Ship Shoal, a shore-parallel transgressive sand shoal identified as a potential sand resource for future large-scale coastal restoration, field measurements and numerical modeling were conducted. Particular attention was paid to examine (1) fluvial sediment dispersal and its influences on the shoal's bed characteristics, (2) bottom boundary layer dynamics and sediment transport over the shoal for two contrasting bed regimes: fluid mud and fine sand, and (3) potential impacts of sand removal from the shoal on hydrodynamics, using state-of-the-art numerical models. Research efforts allowed for the following conclusions.

6.1. Fluvial Sediment Dispersal and Its Influence on Ship Shoal

(1) Strong wind speed and directionality of tropical and extra-tropical storms ostensibly influenced the fluvial sediment dispersal and transport on the inner shelf and on Ship Shoal. The excess debouchments of the sediment from the Atchafalaya River occasionally coincided with post-frontal events so that material being deposited onto the inner shelf and also onto the shoals, further south, occurred during the waning phase of the storm;

(2) A prevailing westward dispersal pattern during the winter-spring season shifted to the southeast following strong post-frontal northwesterly wind, which in turn generated southeastward currents and further transport of fluvially-derived fine sediments from both the Atchafalaya River and the Atchafalaya Bay to the southeast; these eventually blanketed Ship Shoal, located approximately 50 km southeast from the river mouth. Sediment transport occurred coincident with high fluvial sediment discharge during spring floods and local sediment re-suspension. While, during tropical cyclones, fluvially-derived sediment transport occurred based on strong local sediment re-suspension and mixing, and was possibly in part based on high SSC from both the lower Atchafalaya River and the Wax Lake Outlet, being redistributed onto the Atchafalaya Shelf and to adjacent transgressive shoals;

(3) Our preliminary modeling efforts to link the Atchafalaya River sediment plume structure to storm winds and its consequent effects on the offshore shoal, corroborated the results of *in-situ* measurements by demonstrating a strong response of the dispersal

to various wind conditions, illustrating conspicuous shifts in sediment dispersal patterns during post-frontal wind conditions. For the model case with northwest winds, sediments transported southeastward did not reach the shoal after 20 days of the model duration under all storm wind conditions; while, the case with combined no wind and northwest wind provided that sediment plumes transported further southeastward and blanketed the shoal within 3 days of post-frontal winds;

(4) Results from numerical model studies suggest that sediment supply from offshore may not be significant except during strong storms, given the fact that sediment re-suspension off the shoal is much lower than that on the shoal (on average 70-80 percents);

(5) Frequencies of the dispersal shifts (once every 8 days) and the sediment plume that reached the shoal (once every 19 days) had no correlation with monthly mean river discharge; however the latter was strongly correlated with monthly mean wind stress, suggesting the importance of storm winds regarding the dispersal shifts rather than river discharge, although increased river discharge likely contributes high fluvial sediment supply onto the Atchafalaya Bay and farther inner shelf;

6.2. Wave-Current-Bottom Sediment Interaction

(6) A sediment plume shift from the Atchafalaya River/Bay to the southeast results in accumulation of a thin fluid mud layer on the shoal with a maximal thickness of approximately 15 cm and 30 cm for unconsolidated and partially consolidated fluid mud in the waning phase of storms as measured during the 2006 deployment;

(7) The accumulated fluid mud layer strongly interacted with bottom sediment through the process of sediment re-suspension, vertical mixing, hindered settling, and re-distribution, resulting in a maximum of 20 cm of erosion followed by 30 cm of accumulation. Ship Shoal, although comprised primarily of sediment in the sand range, appears to undergo significant changes in sediment type in the bottom boundary layer with surficial sediments being comprised of predominantly fine silts and clays during the spring flood season;

(8) The data during the 2008 deployment showed that the bottom sediments were comprised primarily in the sandy range and hence the bottom boundary layer dynamics followed conventional approaches;

(9) Wave ripples, based on underwater camera images, were formed when the shoal bottom was exposed to sand, and the ripples were likely washed out during severe storms when wave orbital velocities exceeded approximately 0.6 m s^{-1}. The washed-out ripples were likely re-formed in the wake of the storms;

(10) The rate of transport for cohesive sediment was more than an order of magnitude higher than those numerically derived non-cohesive sediment transport as calculated for fine sand sampled during the retrieval cruise in 2006, suggesting the importance of fluid mud transport;

(11) The accumulation of fluid mud may be temporary and non-uniform on the shoal given the frequencies of the dispersal shifts (once every 19 days) and sediment re-working associated with winter storms (once every 6.05 days).

6.3. Numerical Modeling

(12) Results obtained from numerical modeling of waves, currents and sediment transport, were in general agreement with *in-situ* observational data and satellite images except during peak storm conditions. Simulated currents also agreed with *in-situ* currents; however, bottom cross-shore currents were poorly correlated with *in-situ* bottom currents and are probably due to the inaccuracy of shoal bathymetry despite its depth correction;

(13) In spite of the influences on freshwater and fluvial sediments from the Atchafalaya River, a barotropic hydrodynamic model performed reasonably well on examining currents over the shoal and the surrounding inner shelf;

(14) Waves and wave-induced sediment re-suspension significantly changed with and without shoal scenarios. While the result for the partial shoal removal, the differences were minimal;

(15) Although there are differences in magnitudes for the model results with and without the shoal, large-scale targeted sand mining did not result in abrupt changes in current patterns;

(16) Sediment re-suspension intensity (RI) was high across the inner shelf and the shoal during severe and strong storms; in general, it was spatially different and dependent upon physical forcing (i.e. wind and deep water waves). The RI decreased from the shallowest western portion of the shoal to the deepest eastern flank of the shoal; the RI off the shoal was significantly lower than that on the shoal. The results suggest that deeper eastern flank of the shoal is in favor of fluid mud accumulation. This suggestion was supported by in-situ measurements;

The data presented here demonstrated that Ship Shoal, recently recognized as having a unique physical and biological environment, is exposed to recurring sandy and muddy bottoms and provided conspicuously different BBLD for the 2006 deployment on the eastern shoal and the 2008 deployment on the middle shoal. This uniqueness was caused by fluvial sediment supply from the Atchafalaya River and sediment re-working associated with winter storms on the shoal. The distribution of fluid mud, based on the repeated sediment sampling and in-situ measurements, may be patchy and temporary. The patchiness of the fluid mud

distribution is extremely hard to be resolved within the scope of this study, given the unavailability of seasonal sediment data from the entire shoal environment. The data also suggest that as storm intensity varies, strongest in January and decreases toward spring, the eastern portion of the shoal tends to be more susceptible for the accumulation of fluid mud than the middle and western portions of the shoal; moreover, sediment re-working tends to outweigh the sediment supply in spring and results in the formation of a sandy surface layer on the shoal by the end of the winter storm season in May. Numerical modeling suggests that large-scale sand dredging would have spatially profound impacts on waves and sediment suspension on the shoal, however, no abrupt changes in current patterns. The changes in wave transformation and sediment suspension suggest that large-scale sand dredging may enhance fluid mud accumulation on the shoal.

The above findings have further important implications for benthic biological communities on the shoal which was recently found to be a biological "hotspot" and an oxygen refuge compared to the surrounding inner shelf. There is still an information gap regarding the unique change in the bed characteristics and our collaborative biological study results although the shoal bottom sediments likely influence the shoal benthic communities. However, both studies agreed that large-scale sand mining would have profound impacts on both shoal physical and biological environments and thus, is not recommended. Targeted small-scale mining should have minimal impacts and the impacts are expected to be mitigated through natural processes within several years after the termination of sand extraction.

VITA

Daijiro Kobashi was born in Kuwait City in Kuwait in 1975, the younger son of Nobuyuki Kobashi and Nagisa Kobashi. He spent three years in Kuwait since he was born and came back to Japan. He grew up in Ichikawa City, Chiba Prefecture, during his elementary, junior high and high schools. He enrolled at Tokai University, School of Marine Science and Technology, in 1994. He obtained his Bachelor of Science in marine science in 1999 and continued to study specializing mangrove hydrodynamics in Tokai University to complete his master degree in physical oceanography in 2001. He was accepted to Louisiana State University, Department of Oceanography and Coastal Sciences, as a doctoral student in 2004. He was awarded the Joint Japan/World Bank scholarship for a part of his doctoral study. He became a candidate for the degree of Doctor of Philosophy in September, 2007. On December, 12, 2008, he was awarded the John A. Knauss Marine Policy Fellowship offered by the National Sea Grant Office, National Oceanic and Atmospheric Administration. He was also awarded the Theodore Ford Memorial Scholarship Award in December, 2008.